# MINDeSEA

## Seabed Mineral Deposits in European Seas: Metallogeny and Geological Potential for Strategic and Critical Raw Materials

## Deliverable 3.3: Metallogeny of hydrothermal deposits in European waters


| WP3 lead:<br>Geological Survey of Norway (NGU) - Norway | | |
|---|---|---|
| GEOLOGICAL SURVEY OF NORWAY<br>- NGU - | **Address:**<br>Leiv Eirikssons vei 39<br>PB 6315 Torgarden<br>7491 Trondheim<br>Norway | **Telephone:**<br>+47 990 91 747 (Henrik Schiellerup)<br><br>**E-mail:**<br>Henrik.schiellerup@ngu.no |
| **WP3: Geological Survey of Norway (NGU):**<br>Henrik Schiellerup (WP lead) | | |


*This project has been supported by the European Union's Horizon 2020 research and innovation programme, GeoERA (Grant Agreement Nº 731166, project GeoE.171.001).*

| Deliverable number | Short Title |
|---|---|
| 3.3 | Metallogeny of hydrothermal deposits in European waters |
| **Long Title** | |
| Deliverable 3.3. Metallogeny of hydrothermal deposits in European waters | |
| **Short Description** | |
| The current report provides a review of European marine exhalative deposits based on their metallogenic setting. Settings include mid ocean ridge spreading sites, sites related to intra-plate hotspots, and arc/back-arc spreading sites. | |
| **Keywords** | |
| GeoERA Raw Materials, SMS, Sulphides, Copper, Zinc, Lead, CRM, Metallogeny | |
| **Authors / Organisation(s)** | **Editor / Organisation** |
| Schiellerup, H. (NGU), Ferreira, P. (LNEG), González, F.J., Marino E., Somoza, L., Medialdea, T. (IGME) | Geological Survey of Norway (NGU) |
| **File name** | |
| MINDeSEA_D3-3_WP3-Hydrothermal.doc | |
| **Deliverable due date** | **Deliverable submitted date (WP leader)** |
| 30 December 2020 (M28) | 31 May 2021 (M35) |
| **Comments** | |
| | |

| History | | | | |
|---|---|---|---|---|
| **Version** | **Author(s)** | **Status** | **Date** | **Comments** |
| 01 | Schiellerup, H. (NGU), Ferreira, P. (LNEG), González, F.J., Marino E., Somoza, L., Medialdea, T. (IGME) | final | 31 May 2021 | |

| Dissemination level | | |
|---|---|---|
| **PU** | Public | X |
| **CO** | Confidential, for project partners, GeoERA and the European Commission only | |

*This project has been supported by the European Union's Horizon 2020 research and innovation programme, GeoERA (Grant Agreement Nº 731166, project GeoE.171.001).*

## ACKNOWLEDGEMENT & DISCLAIMER



This publication is part of a project that has received funding from the European Union's Horizon 2020 research and innovation programme under grant agreement No 731166.

How to cite this report: **Schiellerup, H., Ferreira, P., González, F.J., Marino E., Somoza, L., Medialdea, T. 2021. Deliverable 3.3: Metallogeny of hydrothermal deposits in European waters. GeoERA-MINDeSEA project. 66 pp. https://geoera.eu/projects/mindesea2/**

# D 3.3. METALLOGENY OF HYDROTHERMAL DEPOSITS IN EUROPEAN WATERS

## SUMMARY

**GeoERA** is a Co-Fund ERA-NET action under Horizon 2020, towards **"Establishing the European Geological Surveys Research Area to deliver a Geological Service for Europe"**. The main objective is to contribute to the optimal use and management of the subsurface.

The project **"Seabed Mineral Deposits in European Seas: Metallogeny and Geological Potential for Strategic and Critical Raw Materials" (MINDeSEA)"** was designed within the scope of the GeoERA Raw Materials Theme (Grant Agreement Nº 731166, project GeoE.171.001), and relies on the collaboration between eight GeoERA Partners and four Non-Funded Organizations with common interest in the exploration for, and investigation of, seafloor mineral deposits.

This document is a deliverable of the MINDeSEA Work Package 3 (WP3); "Seafloor Hydrothermal Deposits", led by the Geological Survey of Norway (NGU). The mineralisations discussed in this document are exhalative polymetallic mineral accumulations formed at or beneath the seabed through hydrothermal activity. The aim of MINDeSEA WP3 is to update and compile existing data on marine sulphides in European waters, including their mineralogy and geochemistry, with contained base, noble and special metals.

The current report gives a brief introduction to seabed hydrothermal mineralisations; how they are formed, where they are formed and their elemental and mineralogical composition. Through the project, data have been collected from 153 sites on European seabed under national jurisdiction. Data include positional and administrative data, deposit types and possible commodities, structural, morphological, and other geological data. Chemical data are unabundant but the MINDeSEA database includes chemical data from 25 sites presented as average numbers. The settings include mid ocean ridge spreading sites along the Mid-Atlantic Ridge, the Arctic Mid-Ocean Ridge, intra-plate hotspot influenced sites adjacent to the Canary Islands, and sites related to arc and back-arc settings within the Mediterranean Sea.

All data are submitted and are universally accessible through the EGDI information platform (http://www.europe-geology.eu/).

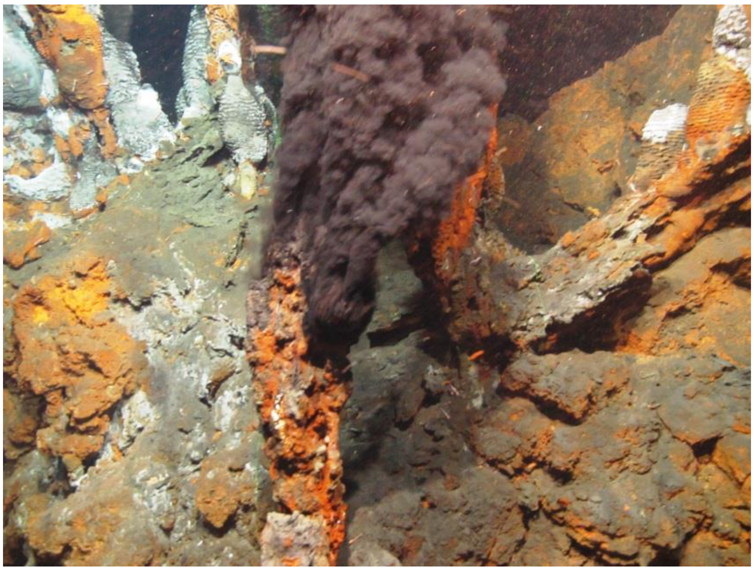

ROV "Luso" image of active black smokers and sulphide chimneys in Moytirra hydrothermal field (NE Atlantic Ocean). EXPLOSEA 2019 Expedition. Photo: IGME.

# 1. CONTENT



*This project has been supported by the European Union's Horizon 2020 research and innovation programme, GeoERA (Grant Agreement Nº 731166, project GeoE.171.001).*

# 2. INTRODUCTION

GeoERA is a Co-Fund ERA-NET action under Horizon 2020, towards "Establishing the European Geological Surveys Research Area to deliver a Geological Service for Europe". The main objective is to contribute to the optimal use and management of the subsurface.

The project MINDeSEA was designed within the scope of the GeoERA Raw Materials Theme (Grant Agreement Nº 731166, project GeoE.171.001), and relies on the collaboration between eight GeoERA Partners and four Non-Funded Organizations with common interest in the exploration for, and investigation of, seafloor mineral deposits.

This document is a deliverable of the MINDeSEA Work Package 3 (WP3); "Seafloor Hydrothermal Deposits", led by the Geological Survey of Norway (NGU). The mineralisations discussed in this document are exhalative polymetallic mineral accumulations formed at or beneath the seabed through hydrothermal activity. The aim of MINDeSEA WP3 is to update and compile existing data on marine sulphides in European waters, including their mineralogy and geochemistry, with contained base, noble and special metals.

For strategic evaluation of the European resource potential, and in particular for Europe's ability to improve its resilience towards supply shortages in critical and other necessary raw materials, the land-sea boundary is becoming increasingly irrelevant. Whereas almost all metals and minerals through history have been produced from mining operations on land, the quest for defining mineable targets in the oceans is continuously intensifying. As marine targets are slowly being identified and delineated, it is important to include both marine and onshore mineral potentials and identified resources in the European mineral resource inventory. One of the prime goals of GeoERA and MINDeSEA is therefore to expand and complement the European Geological Data Infrastructure (EGDI) with marine mineral resource information, for politicians, strategists, authorities, and stakeholders to make as informed analyses and decisions as possible. Some databases on marine mineral resources and vent sites do exist today and have provided important base data to the MINDeSEA library. It is, however, of the utmost importance to build a unified mineral resource database for all European resources, whether on land or on the seabed, for clever decision making.

The current report gives a brief introduction to seabed hydrothermal mineralisations; how they are formed, where they are formed and their elemental and mineralogical composition. Through the project, data have been collected from 153 sites under European national jurisdictions. Data include positional and administrative data, deposit types and possible commodities, structural, morphological, and other geological data. Chemical data are unabundant, but the MINDeSEA database includes data from around 600 samples representing 25 sites. Chemical data exist for around 450 of these samples. Only publicised data have been included, and whereas some data are based on individual samples, others have been published in aggregated form. The setting of hydrothermal deposits in European waters are diverse and include mid ocean ridge spreading sites along the Mid-Atlantic Ridge, the Arctic Mid-Ocean Ridge, intraplate hotspot influenced sites in Macaronesia around the Canary Islands, and sites related to arc/back-arc settings within the Mediterranean Sea.

*This project has been supported by the European Union's Horizon 2020 research and innovation programme, GeoERA (Grant Agreement Nº 731166, project GeoE.171.001).*

# 3. SEA FLOOR HYDROTHERMAL DEPOSITS

Seafloor hydrothermal deposits, most notably expressed as seafloor massive sulphides (SMS), are modern volcanogenic equivalents of onshore (fossil) deposits of volcanogenic massive sulphides (VMS). VMS deposits have constituted important mining targets through history in many regions of Europe and around the World, and still provide significant resources of copper, zinc, lead, silver, and gold (Singer 1995). Generally speaking, SMS deposits and the exhalative processes leading to their formation are well known to geologists after millennia of mining metals and sulphur from VMS deposits found on land.

Massive sulphide deposits, whether on land or on the seabed, are strata-bound accumulations of sulphide minerals that precipitated at or near the sea floor in spatial, temporal, and genetic association with contemporaneous volcanism (Franklin et al. 2005). On the sea floor, massive sulphide deposits form as a result of heated seawater interacting with oceanic crust through a convection process driven by magmatic activity at depth. During convection, cold seawater infiltrates the seafloor and percolates through the marine crust to reach depths of several kilometres, where the water is heated to temperatures above 400 °C.

Chemical reactions in the descending sea water will generate a fluid, which is hot, acidic, chemically reduced, and able to leach the surrounding rocks (Petersen et al. 2016; 2018). The resulting fluid will become enriched in metals, sulphur, and silica, and quickly rise to the sea floor where it will be expelled into the water column at a confined vent site. Sulphides, sulphates, silicates, and other minerals are precipitated from the hot vent fluids as they cool or come into contact with cold seawater. The associated metal-rich plumes are called black or white smokers depending on their temperature and metal lode. Most of the metals will disperse into the overlying water column, but the remainder will precipitate to form SMS deposits in the form of chimneys, mounds, and metalliferous sediments on and around the vent site (Petersen et al. 2016; 2018), or form veins or massive units below the surface. Base metal rich seafloor massive sulphide deposits generally form from high-temperature hydrothermal activity at black smoker vent sites located at water depths between < 500 to more than 4000 m.

## 3.1. Occurrence

Whereas mining of VMS deposits on land has been going on for more than two millennia, mapping the global seafloor and exploration for seafloor hosted ore deposits is a relatively recent development. The first massive sulphide sample was recovered from the East Pacific Rise in 1978, and in 1979 the first images of a chimney emanating black metal-rich hydrothermal water was observed from the Alvin submersible in the same area (Cherkashov 2017). New data are continuously being generated, and the knowledge of modern exhalative deposits is steadily growing to the benefit of our understanding also of VMS-type deposits. Mapping the sea floor has made it possible to directly observe and study how a VMS-type deposit is formed prior to tectonic transportation, metamorphosis, and structural dismemberment.

Most vent sites are located along constructive plate margins where active formation of oceanic crust takes place (Figure 1). Of more than 700 vent sites currently (May 2021) recorded in the InterRidge database (http://www.interridge.org) approximately 400 are classified as related to mid-ocean spreading ridges, and 150 as back-arc spreading sites. Arc volcanoes make up around 150 sites and only 10 are hosted by intraplate volcanoes.

This project has been supported by the European Union's Horizon 2020 research and innovation programme, GeoERA (Grant Agreement № 731166, project GeoE.171.001).

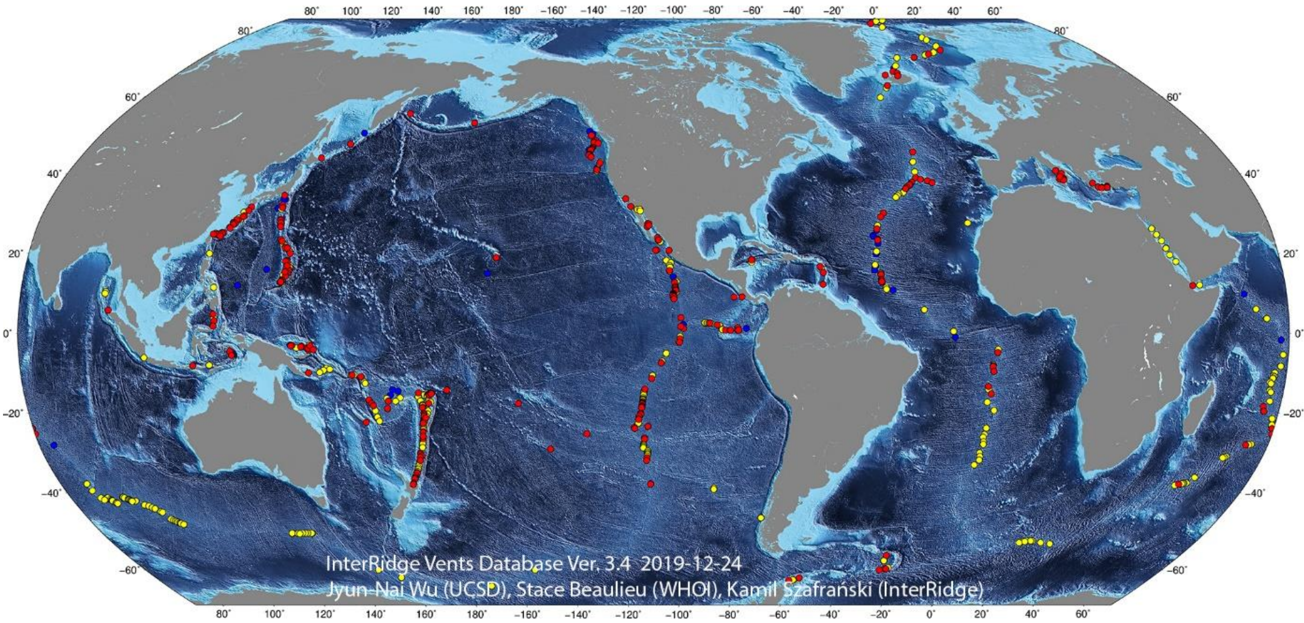


*Figure 1. Static map of the InterRidge database displaying more than 700 recorded vent sites. Confirmed active sites are shown with a red dot. Red colours designate confirmed active sites. Figure from InterRidge Global Database (Beaulieu et al. 2020)*

The discovery potential and the perspective for future mining on the sea floor remain key questions. Several attempts at quantifying the global resource potential have been published and arrive at very disparate results. Hannington et al. (2011) predicted around 30 Mt of copper + zinc in the global neovolcanic zones, and Singer (2014) arrived at a smaller figure of 18 Mt. Much more significant endowments have also been suggested (e.g., Cathles 2011). More than 300 deposits and black smoker sites have been identified since the first discovery of seafloor hydrothermal vents in 1979, but significant massive sulphide accumulations have only been found at 165 of these sites (Hannington and Petersen 2016).

## 3.2. Size

The perspective for sulphide mining on the sea floor remains uncertain, and the public does not seem to be less concerned about environmental impacts from active mining at sea than they are on land. Even though the World is not running out of mineral resources on land, the sea floor may host deposits of base and special metals of sufficient size and quality to support feasible mining projects.

Seafloor sulphide deposits range in size from a few thousand tonnes to several million tonnes, and massive sulphide deposits of significant size (> 5000 $m^{2)}$ have been found in most geodynamic settings (Hannington et al. 2010). However, most of the documented occurrences are very small and would be considered showings if found on land. The continuity of sulphide bodies on the sea floor is difficult to assess, and reliable estimation of size, even in two dimensions, is challenging (Hannington et al. 2010). Tonnage models most likely depend on the geodynamic setting, but Hannington (2010) gives a median tonnage value of less than 100 kt for SMS deposits, independent of tectonic setting. Median tonnage values for Cyprus-type VMS deposits on land are much higher

*This project has been supported by the European Union's Horizon 2020 research and innovation programme, GeoERA (Grant Agreement Nº 731166, project GeoE.171.001).*

at 2 Mt (Mosier et al. 1983), presumably because showings and very small VMS deposits on land are usually ignored.

Sulphide mounds in the Trans-Atlantic Geotraverse (TAG) hydrothermal area reach 200 m in diameter and 40–50 m in height (Cherkashov 2017), and recent seismic surveys indicate the presence of substantial resources below the mounds in the TAG area (Murton et al. 2019). Murton et al. (2019) gives an estimate of 26 Mt of sulphide ore in and below investigated mounds in the TAG area. However, so far, the only SMS deposit that has been thoroughly investigated and assessed as a mining target is the Solwara 1 deposit off the coast of Papua New Guinea, with an indicated and inferred resource base of 2.57 Mt (Lipton et al., 2018).

The size of SMS deposits depends on the spreading rates which also controls the incidence and longevity of hydrothermal venting. For instance, vent field frequency is positively correlated with the spreading rate (German et al. 2016), but various analyses show that there is a higher resource potential in slow and ultraslow ridges compared with faster spreading ridges (e.g., Hannington et al., 2011). Slow spreading ridges are characterised by a low magma supply or vent sites may not be associated with magmatic activity at all, and spreading is generally accommodated by detachment faults (German et al. 2016). Deep and sustained fault-controlled circulation of hydrothermal water is characteristic for slow or ultraslow ridges and explains why these systems are expected to host the largest hydrothermal systems on the sea floor (Hannington et al. 2005).

According to Hannington et al. (2005) the most productive sea-floor hydrothermal systems are likely to be found in extensional arc environments, where rifting of the arc crust provides the necessary heat for the generation of abundant deep crustal melts and large-scale hydrothermal convection. Sedimented rifts in epicontinental or continental margin arc environments may provide conditions for enhanced and prolonged sulphide accumulation.

## 3.3. Mineralogy and chemistry

The minerals forming chimneys and sulphide mounds are typically dominated by iron sulphides, mainly pyrite, with subordinate amounts of the copper sulphides chalcopyrite or isocubanite, and the zinc sulphide, sphalerite. Non-sulphide gangue minerals include sulphates, such as barite and anhydrite, and silicates, which are mainly chert. Most VMS deposits investigated on land show mineral and metal zonation caused by the changing physical and chemical environments of the circulating hydrothermal fluids in the oceanic crust. Ideally, massive sulphide deposits contain a core of massive pyrite and chalcopyrite, formed in the centre of the vent system, a feeder zone, and a halo of chalcopyrite-sphalerite-pyrite grading into a distal sphalerite-galena and galena-manganese-barite, and finally into chert-manganese-hematite facies. Lower temperature venting, such as observed at white smoker vent sites, will generally be dominated by a non-sulphide mineralogy.

The geochemistry of the seabed hosted massive sulphide deposits is of crucial importance to the possibility for future exploitation. The exhalative deposit type of main current interest is the high temperature sulphide dominated deposits exsolved from black smoker vents. Copper, zinc, gold, and to some extend lead and silver are the major commodities, which should form the base for an economically feasible mining operation on SMS deposits. Many of the metals on the current EU criticality list (https://eur-lex.europa.eu/legal-content/EN/TXT/?uri=CELEX:52020DC0474) are minor metals which may accompany the base metals into the seabed massive sulphides and add to

*This project has been supported by the European Union's Horizon 2020 research and innovation programme, GeoERA (Grant Agreement Nº 731166, project GeoE.171.001).*

the value. Metals such as gallium, germanium and indium are considered critical in the EU, and are wholly or partly derived as biproducts from zinc ores, including the land-based volcanogenic VMS deposits. Cobalt may be present in both VMS and SMS deposits, but usually in small amounts and partly hosted by iron sulphides. Marine crusts and nodules are the primary exploration target for cobalt.

The geochemistry of massive sulphide deposits depends on a range of factors, including the temperature of the vent systems, as observed in the mineralogical zonation on both deposit, chimney and hand specimen scale (Hannington et al. 2005). Both spreading rate and structural setting assert control on the leaching and carrying capacity of the hydrothermal system and the chemistry of the hydrothermal fluids. Phase separation processes, such as boiling, cause fractionation of the elemental lode and are also important.

The general geochemistry of high-temperature black smoker systems is primarily dependant on the tectonic setting in which they occur (Hannington et al. 2005). The geodynamic setting controls the lithostratigraphic environment of massive sulphide deposits which is generally used to classify VMS deposits on land into one of five categories: (1) bimodal-mafic; (2) mafic; (3) pelite-mafic; (4) bimodal-felsic; and (5) siliciclastic-felsic deposits (Franklin et al. 2005). A similar classification has been attempted in the MINDeSEA library.

The dependency of local chemistry on temperature, with continuous exsolution, dissolution, reprecipitation and zone refining makes it impossible to assess the quality of any given SMS deposit without thorough drilling. Sampling will be biased by overrepresentation of chimneys and surficial deposits, which tend to be richer in copper than the massive sulphides below. This results in a median copper content in SMS deposits of 4.3 % which is more than double the concentrations in for instance mafic hosted VMS deposits at 1.4 % copper. Samples from mid-ocean ridge hosted SMS deposits carry an average of 5.9 % copper (Hannington, 2010). Still, the Solwara deposit off the coast of PNG carries averages of 7.2 and 8.1 % copper in indicated and inferred resources respectively, with a 2.6 % Cu cut-off.

On mid-ocean ridges hydrothermal fluids dominantly leach mafic or ultramafic substrates which are the major sources of Fe, Mn, Zn, and Cu in mid-ocean ridge vent fluids (Hannington et al. 2005). The substrate may also influence the content of noble elements, such as gold and silver, and mafic rock hosted metals, such as nickel and cobalt. There are systematic differences between mafic and ultramafic hosted deposits with, for instance, higher copper and gold contents in ultramafic hosted deposits, and higher zinc and lead contents in mafic hosted deposits (Hannington et al. 2005). Deposits in arc and back-arc settings are generally richer in zinc, lead, and silver than deposits in mid ocean ridge settings. Trace elements, such as antimony, bismuth, cadmium, gallium, germanium, indium, tellurium, and thallium, can be significantly enriched in deposits forming at volcanic arcs (Petersen et al. 2016).

Toffolo et al (2019) investigated the first order controls on the geochemistry of mid ocean ridge hosted sulphide deposits through multivariate statistical analyses on a comprehensive chemical dataset. In a constrained geodynamic setting, Toffolo et al. concluded that temperature of deposition has the major impact on deposit chemistry, with spreading rate and secondary zone refining also impacting on the chemistry. Contributions from magmatic fluids to the hydrothermal systems are suspected in several SMS deposits (Hannington et al. 2005) but their importance was not substantiated by the study (Toffolo et al. 2019).

This project has been supported by the European Union's Horizon 2020 research and innovation programme, GeoERA (Grant Agreement № 731166, project GeoE.171.001).

# 4. THE GEODYNAMIC SETTING OF HYDROTHERMAL DEPOSITS IN EUROPEAN WATERS

In European waters vent sites are hosted by various geodynamic regimes. The settings include mid ocean ridge spreading sites along the Mid-Atlantic Ridge, intraplate hotspot influenced sites in Macaronesia around the Canary Islands, and sites related to arc/back-arc settings within the Mediterranean Sea (Figure 2).

## 4.1. The Mid-Atlantic Ridge

The Mid-Atlantic Ridge (MAR) is a constructive plate boundary, about 16 000 km long, that extends from the Bouvet triple junction in the South Atlantic Ocean to the Siberian Shelf in the Laptev Sea. The ridge separates the North and South American plates to the west from the Eurasian and African plates to the east. The ridge rises to more than 2 km above the ocean floor and is marked by a rift valley at its centre. The average full spreading rate is considered slow at 2.5 cm per year but varies along the strike of the ridge and slows towards north. In the Northern Atlantic (Figure 2), the MAR connects to the triple junction between the two American plates and the African plate east of the Caribbean Islands, and another triple junction at the Azores Islands, which separates the North American plate from the Eurasian and African plates. A major part of the Northern Mid-Atlantic Ridge lies within the territorial waters of European countries.

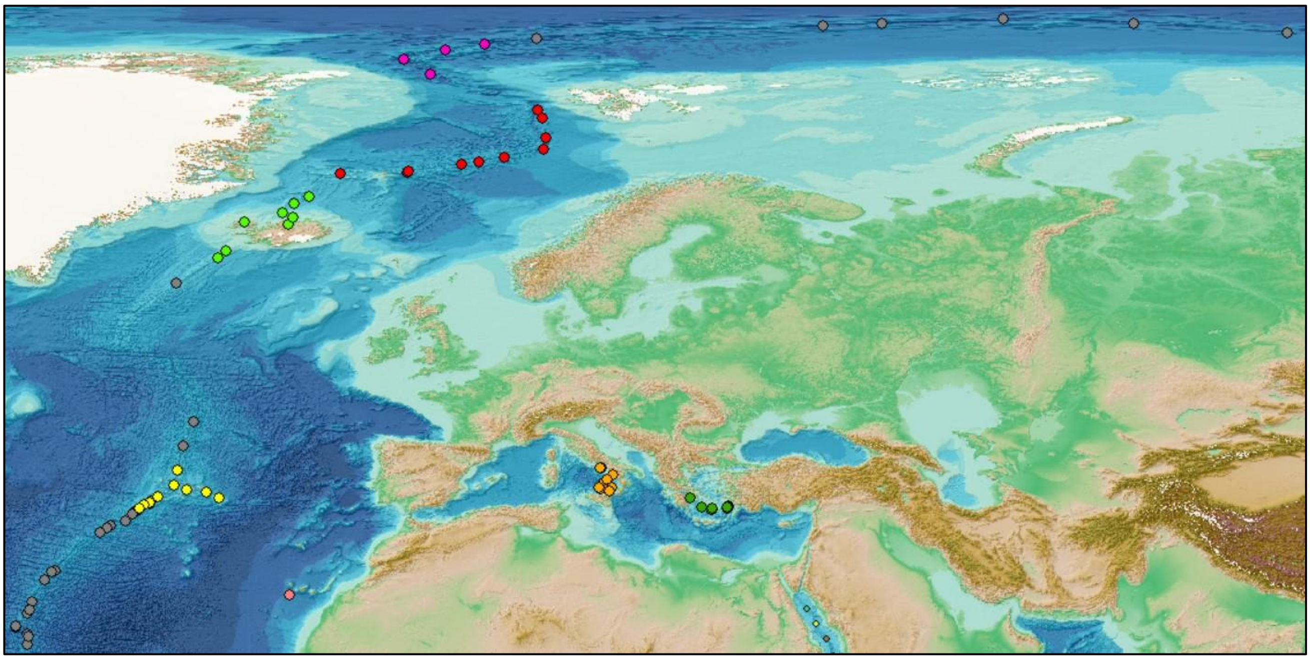

*Figure 2. Northern Hemisphere Atlantic and Mediterranean vent sites. The Mid-Atlantic Ridge is clearly marked by registered vent sites. Colours designate national jurisdictions with grey colours for high seas. Vent site data from the MINDeSEA library. Bathymetric imagery reproduced from the GEBCO_2020 Grid, GEBCO Compilation Group (2020) GEBCO 2020 Grid (doi:10.5285/a29c5465-b138-234d-e053-6c86abc040b9).*

This project has been supported by the European Union's Horizon 2020 research and innovation programme, GeoERA (Grant Agreement № 731166, project GeoE.171.001).

Since 1991, the MAR has been extensively surveyed between 33°N and the Azores Archipelago. Many cruises were conducted in order to establish bathymetric maps, study the segmentation, look for hydrothermal anomalies in the water column or sample basalts, massive sulphides, hydrothermal fluids or biological material (e.g., Detrick et al.,1995; Langmuir et al. 1997; Charlou et al. 2000, and references therein). The first bathymetric maps in this MAR region were obtained using the EM12 system during the FARA-SIGMA cruise in 1991 (Needham et al. 1992).

The MAR between 33 and 41°N exhibits a gradient in seafloor depth, from 3500 m just north of the Hayes Transform near 33°N to less than 1000 m near 39°N. Together with this depth gradient, the MAR is characterized by a broadening with a funnel shape best represented by the 2000 m bathymetric contour. This large bathymetric structure representing a volcanic topographic high is designated by Azores Platform.

The Azores platform is characterised by a high tectonic complexity due to the existence of a triple junction between the American, Eurasian and African Plates. The boundary between the Eurasian and African plates has always been contentious but, presently, is considered as represented by the NW-SE lineament of São Miguel-Terceira-Graciosa (Terceira rift). Several models have been proposed to describe the plate kinematics along this boundary: pure extension, pure strike-slip and a combination of both (e.g., Krause & Watkins 1970; Searl 1980; Madeira & Ribeiro 1990; Lourenço et al. 1998).

The maximum bathymetric expression of this platform is given by the emergence of a group of nine volcanic islands, forming the Azores archipelago. Seven islands (Santa Maria, São Miguel, Terceira, São Jorge, Graciosa, Pico, and Faial) are located East of the MAR (Eurasian plate) whereas the other two (Corvo and Flores) are located West of the ridge, on the North American plate. The islands form a broad WNW-ESE lineament between 31°W and 24°W, that crosses the MAR at 39°N, in the KP-2 segment.

The Azores hotspot corresponds to a broad (a few hundred kilometres in diameter) domain of anomalously low S-wave velocities in the 100 to 200 km depth range, centred somewhat to the east of the MAR (Zhang & Tanimoto 1992). The distribution of recent volcanism in the Azores archipelago suggests a similar location (100 to 200 km east of the ridge, near the island of Faial) for the hotspot centre (Schilling, 1985; Ito & Lin, 1995). However, the size, depth and the accurate location of this mantle anomaly are still a matter of debate.

Besides being characterised by a topographic high, the Azores platform has a crustal thickness 60 % higher than normal, according to seismic refraction studies (Searl 1980) as well as detailed modelling of the gravity field (Detrick et al. 1995). The morphology is also anomalous in the shallowest zones of the MAR platform, where the axial valley is less marked and the segments are swollen (e.g., Detrick et al. 1995). This situation is also present in the Reykjanes ridge by the segments closer to Iceland (e.g., Parson et al. 1993). These anomalies are visible in large-scale gravity maps (Cochran & Talwani 1978) with high residual gravity anomalies on the Azores platform.

The MAR in this region is segmented by four large discontinuities: Kurchatov (~40°N), the Pico (~ 38°N), the Oceanographer (~ 35°N), and the Hayes (~ 33.5°N) fracture zones, which delineate three main ridge sections (Figure 3). The Pico-Kurchatov section has a length of 325 km and six second-order segments, referred to as KP-0 to KP-5 (Detrick et al. 1995; Goslin 1999). The Pico to Oceanographer (PO) section is about 275 km long, and composed of eight second-order segments, referred to as PO1-PO8. Lastly, the Oceanographer to Hayes (OH) section is made up by five second-order segments (OH-1 to OH-5) and is about 220 km long. These segments have lengths

This project has been supported by the European Union's Horizon 2020 research and innovation programme, GeoERA (Grant Agreement № 731166, project GeoE.171.001).

between 10 and 100 km and are linked by a series of systematic left-lateral, non-transform offsets (NTOs, e.g., Parson et al. 2000). The NTOs are broad areas where a gradual transition between adjacent spreading segments involves no significant transform faulting. They are defined by spatial offsets of 15-30 km and age offsets of 1-3 Ma and have small segment length/offset ratio (e.g., Grindlay et al. 1991; Sempéré et al. 1993; Gràcia et al. 2000).

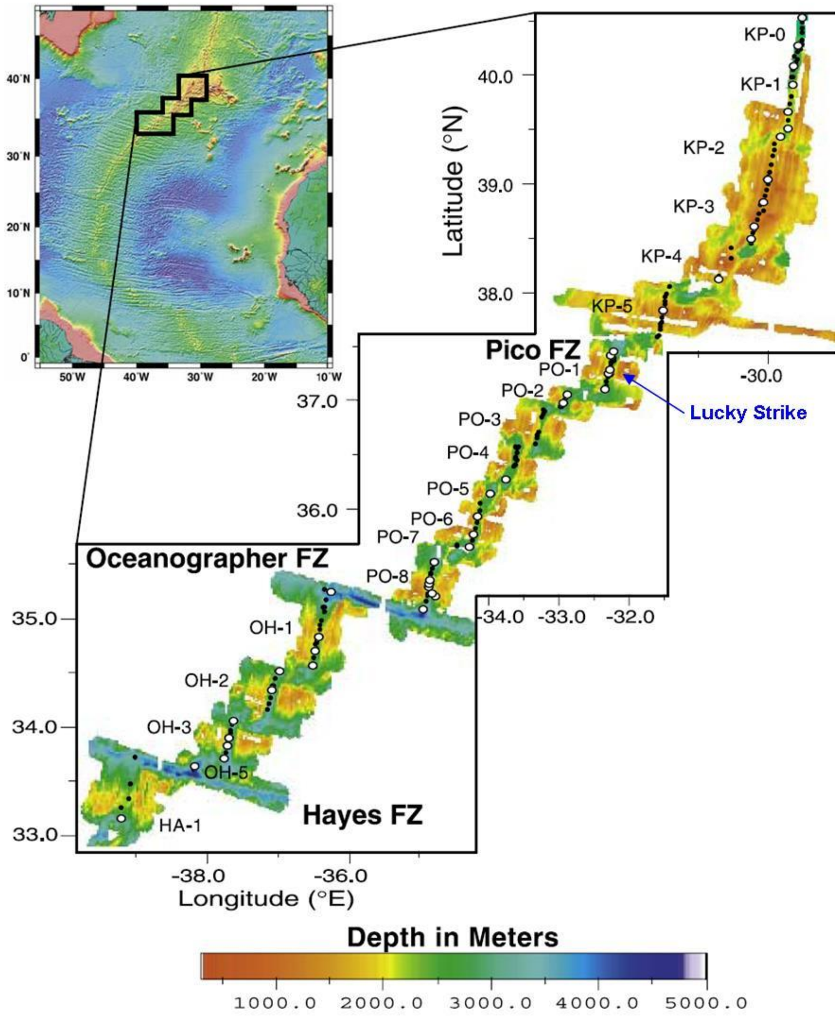


*Figure 3. Segments along the MAR between 33°N and 40.5°N (adapted from Asimow et al. 2004). Pico, Oceanographer and Hayes fracture zones referred to by their common names are also shown. Simplified bathymetry of the MAR section based on data from SIGMA cruise (Detrick et al. 1995; Bougault et al. 1997). Black and white dots represent sample locations where glass was recovered from the FAZAR cruise. Inset is shaded relief image of satellite-based bathymetry of Smith & Sandwell (1997).*

The NTOs at the MAR south of Azores are characterized by the presence of shallow, dome-like shaped massifs, oblique to parallel to the ridge, with complex structural fabrics accommodating the offset. Some of these massifs have been explored and sampled, revealing that they are composed of upper mantle peridotites and lower crustal rocks, and sometimes associated with high-

*This project has been supported by the European Union's Horizon 2020 research and innovation programme, GeoERA (Grant Agreement № 731166, project GeoE.171.001).*

temperature hydrothermal venting. The exposure of the ultramafic massifs within the NTOs is favoured by low magmatic supply and low-angle detachment faulting occurring at segment ends.

Side-scan sonar imagery along the MAR in the Azores region has shown that sediment cover is marked by very distinct maxima, mainly restricted to the non-transform discontinuities, and that the volcanic processes are mainly confined to the interior of segments (e.g., Blondel 1996; Parson et al. 2000). Neo-volcanic activity declines with distance from the Azores. In contrast, tectonic activity increases with distance away from the hotspot, but is not restricted to spreading segments. The northern segments are more affected by volcanism, and the southern segments by tectonics. This is explained by the declining influence of the Azores hotspot with distance (Blondel 1996; German et al. 1996).

The northern MAR, between 31°N and the Azores archipelago (~ 40°N), comprises a significant ridge section (~ 1000 km long) in which lavas, more enriched than N-MORB, are extruded because of the interaction of the Azores plume with the (MAR) and mixing of a buoyant thermal plume with the surrounding asthenosphere (e.g., Dosso et al. 1999). This interaction is geochemically evidenced by the first order enrichment in incompatible trace elements, steep, decreasing geochemical gradient towards 37°N; low $He_3/He_4$ ratios; highly enriched radiogenic Sr and Pb signatures; and high (La/Sm)N ratios (Schilling 1975; Schilling et al. 1983; Dosso et al. 1999). The geochemical gradients are often systematically coupled with bathymetry, for example the MAR shoals by several thousand meters from 33°N to the Azores archipelago (e.g., Ridley et al. 1974; Detrick et al. 1995). Associated with this bathymetric anomaly, a regional, long-wavelength, gradient away from the Azores characterizes the mantle Bouguer anomaly. Gravity-derived crustal thickness estimates (e.g., Cochran & Talwani 1978) together with seismic refraction data obtained along the MAR in the Azores region (e.g., Searl 1980) show a gradual increase in the average crustal thickness with proximity to the Azores, suggesting an increase in melt supply. The resulting overall crustal thickening from 33°N toward the Azores archipelago region was estimated to be ~ 3.5 – 4 km.

More exhaustive rock sampling along the MAR during the last three decades has added further information about the characteristics of the geochemical and geophysical gradients across the Azores region. One of the main geochemical outcomes was that some ridge segments have produced lavas that present a higher degree of enrichment in incompatible elements than what is expected from the regional variation alone. Moreover, this local enrichment is also recognized in the Sr-Nd-Pb isotopic signatures. When plotting these geochemical parameters against latitude, the elemental enrichment produces local peaks that are detached from the regional trend (Dosso et al. 1999).

Several active sites of hydrothermal venting have been found and sampled on the MAR in the Azores region including the most important, from north to south, “Menez Gwen” (Fouquet et al. 1994, 1995; Ondréas et al. 1997), “Lucky Strike” (Langmuir et al. 1993, 1997; Fouquet et al. 1994, 1995; Humphries et al. 2002), “Rainbow” (German et al. 1996) and “Saldanha” (Bougault et al. 1997; Barriga et al, 1998) that are described in a subsequent chapter.

From the Azores Islands, the MAR strikes north and bend northwest to meet the east-west striking Charlie Gibbs Fracture Zone at about 52°N. North of the fracture zone, the MAR continues as the Reykjanes Ridge until the ridge goes ashore on Iceland. The Reykjanes Ridge is considered slow with a spreading rate of 2 cm per year. Iceland is a topographic expression of increased magmatic activity caused by a mantle hotspot positioned close to the MAR under Iceland. The ridge can be

*This project has been supported by the European Union's Horizon 2020 research and innovation programme, GeoERA (Grant Agreement № 731166, project GeoE.171.001).*

followed along the neovolcanic zones across Iceland from south to north, and Iceland represents the only place on Earth where a mid-oceanic rift can be followed above sea level.

From the northern shelf of Iceland, at about 66°N the MAR continues as the Arctic Mid-Ocean Ridge into the Norwegian-Greenland Sea, through the narrow gateway of the Fram Strait, and across the Eurasia Basin. The Arctic Mid-Ocean Ridge is divided from south to north into six segments separated by three major fracture zones and two major ridge cusps: The Kolbeinsey Ridge strikes north from Iceland and terminates at the island of Jan Mayen, from where the Jan Mayen Fracture Zone offsets the ridge to the Mohn's Ridge. The Mohn's Ridge is about 550 km long, striking northeast, and terminates in a marked bend in the rift zone. From here the ridge continues for 500 km straight north as the Knipovich Ridge. Across the Spitsbergen and Molloy Fracture Zones on either side of the Molloy Ridge, the ridge follows the Lena Trough to the Gakkel Ridge, the latter two separated by another sharp bend in the ridge axis (Figure 4) (Pedersen et al. 2010).

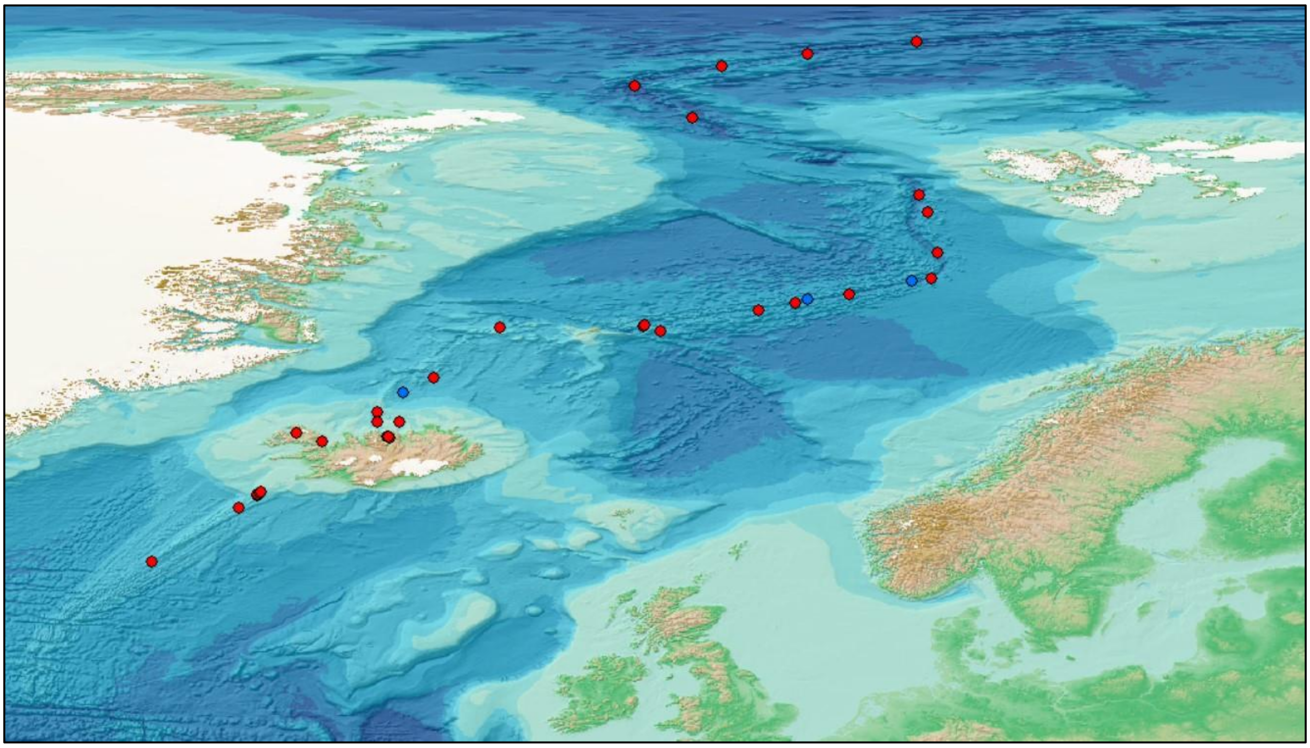

*Figure 4. Northern Mid-Atlantic Ridge with vent sites and seabed mineral deposits as recorded by the MINDeSEA data library. Red colours are inferred or confirmed active vent sites; blue colours are mineral occurrences at inactive sites. Bathymetric imagery reproduced from the GEBCO_2020 Grid, GEBCO Compilation Group (2020) GEBCO 2020 Grid (doi:10.5285/a29c5465-b138-234d-e053-6c86abc040b9).*

The Arctic Mid-Ocean Ridge has a highly diverse architecture with spreading rates gradually decreasing from around 20 mm/year on the Kolbeinsey Ridge to 6 mm/year on the Gakkel Ridge. Spreading varies between the segments from orthogonal to oblique, and towards south, the Iceland hotspot heavily influences a gradually shallowing ridge with increased magma supply and a thickened oceanic crust (Pedersen et al. 2010). The attention towards the potential for massive sulphide deposits in the Arctic Mid-Ocean Ridge has been substantial, partly because of the ultra-

*This project has been supported by the European Union's Horizon 2020 research and innovation programme, GeoERA (Grant Agreement № 731166, project GeoE.171.001).*

slow spreading rates and the existence of oceanic core complexes, but also due to the ridges' proximity to continental margins and large accumulation of sediment in parts of the ridges (Pedersen and Bjerkgård 2016). Vent sites along the ridge are hosted by basalts or ultramafic rocks.

## 4.2. Macaronesia: Canary Islands

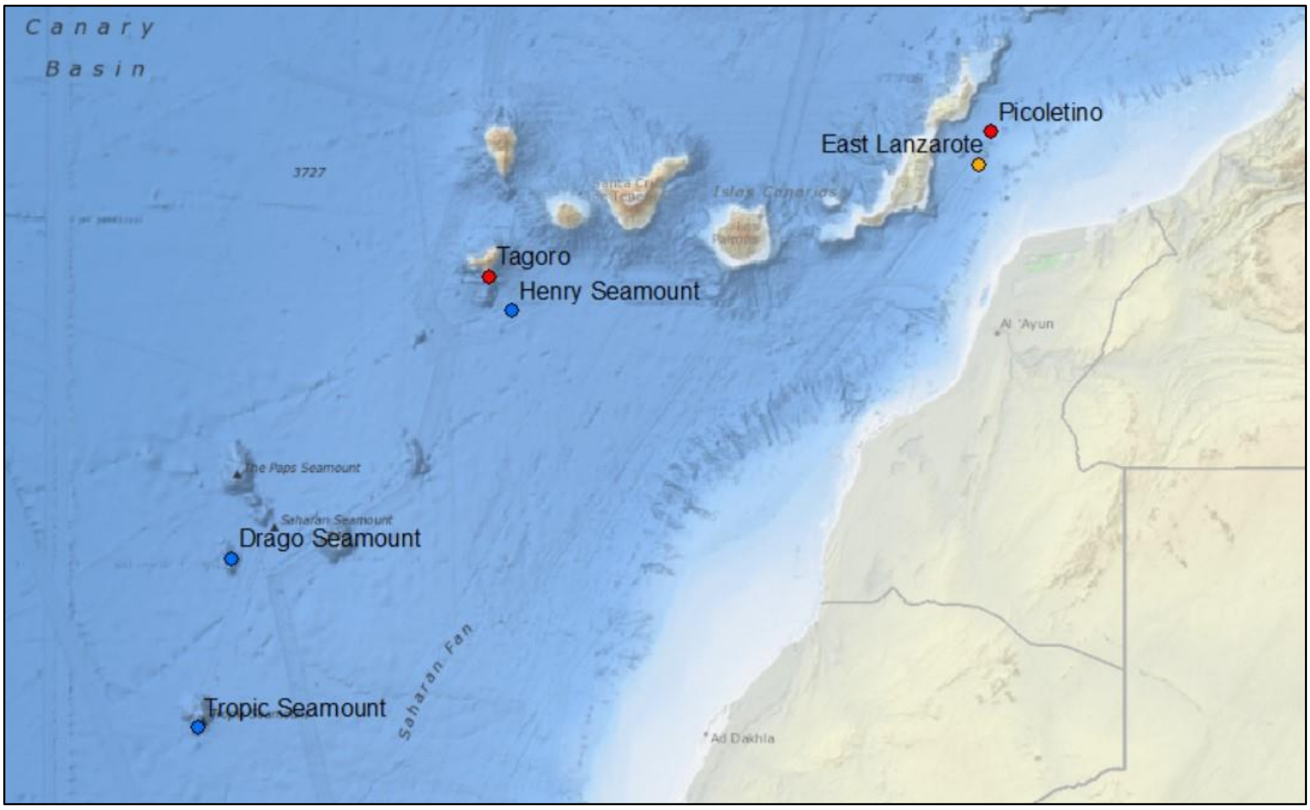


*Figure 5. The Canary Islands with vent sites recorded in the MINDeSEA library. Red: active; blue: inactive; orange: activity unconfirmed. Bathymetric imagery from the EMODnet WMS service ([https://www.emodnet-bathymetry.eu](https://www.emodnet-bathymetry.eu))*

The Canary Archipelago off-shore Northwest Africa represents a geological setting controlled by intra-plate volcanism associated with the Canary hotspot (Carracedo et al., 2002; Ancochea, 2004). The Canary Islands form an approximately 400 km long train of volcanic islands on the African plate, generally getting younger from east to west, and reflecting the slow movement of the African plate above the Canary Hotspot. El Hierro is the westernmost and youngest island along the chain and located near the present Canary Hotspot. The Canary Island Seamount Province, islands and seamount cluster form one of the most important volcanic provinces in the Atlantic Ocean, with recurrent volcanism from the Early Cretaceous to the present day (van den Bogaard, 2013). Hydrothermal activity has been recorded both in the eastern (Picoletino Seamount) and western (Tagoro Volcano) part of the island chain, with scattered inactive hydrothermal sites recorded also south of the Canary Islands (Figure 5)

*This project has been supported by the European Union's Horizon 2020 research and innovation programme, GeoERA (Grant Agreement Nº 731166, project GeoE.171.001).*

## 4.3. The Mediterranean Sea

The geodynamics of the Mediterranean Sea is ultimately controlled by the collision of the African and Eurasian tectonic plates, resulting in a complex faulting and subduction pattern involving a number of microplates along the length of the basin. Tectonism gives rise to earthquakes and volcanism, and seafloor hydrothermal activity is found both in the Tyrrhenian Sea, in the Aegean Sea and on the Eratosthenes Seamount south of Cyprus in the Levantine Basin.

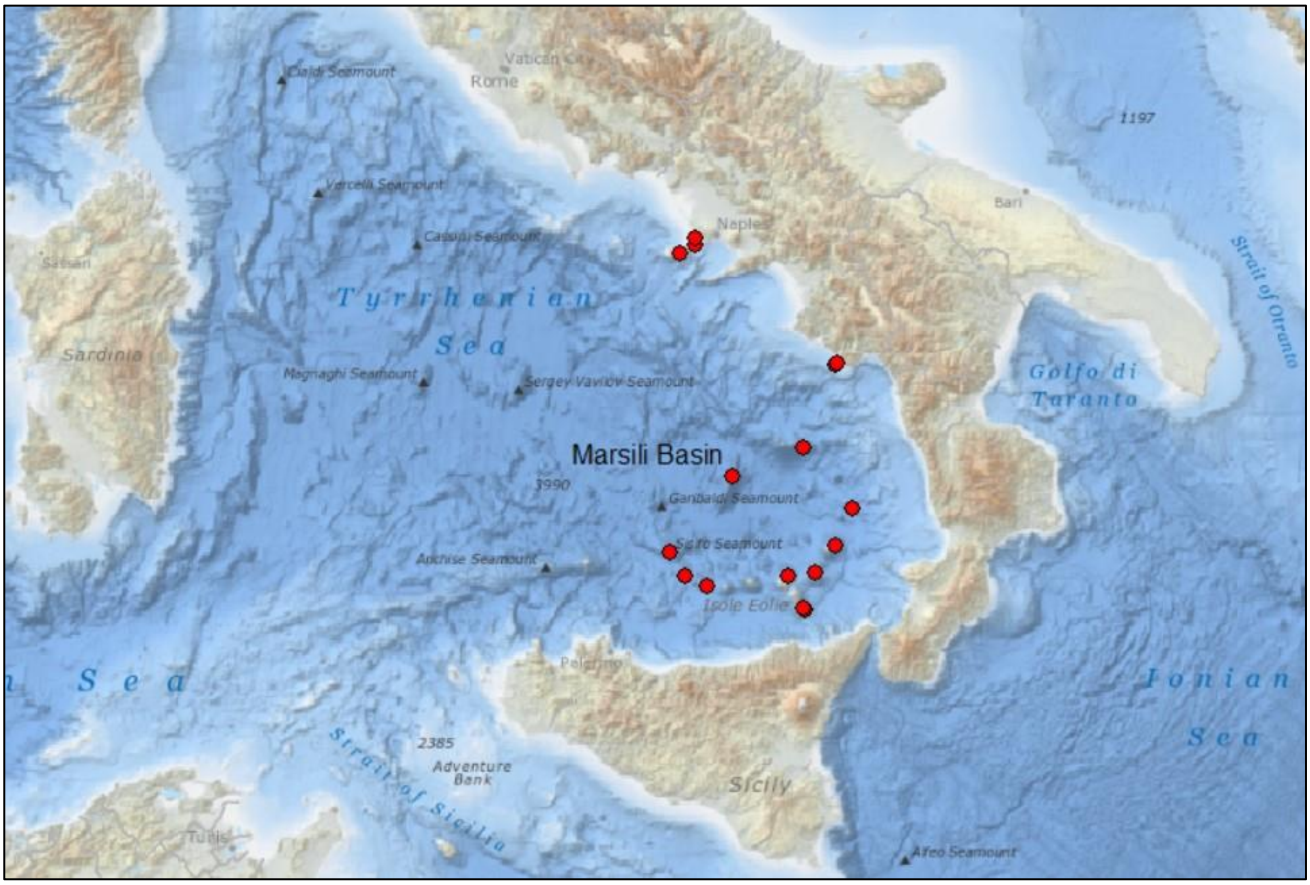


*Figure 6. Hydrothermal activity in the Tyrrhenian Sea as recorded in the MINDeSEA library. Bathymetric imagery from the EMODnet WMS service ([https://www.emodnet-bathymetry.eu](https://www.emodnet-bathymetry.eu))*

The Tyrrhenian Sea is a back-arc basin in the Mediterranean Sea which formed within the general framework of the convergence between Africa and Eurasia. Current hydrothermal activity is most prominent in association with seamounts in the Aeolian Arc in the southern part of the Tyrrhenian Sea, where activity defines a horseshoe-like pattern surrounding the Marsili seamount and basin (Figure 6). Hydrothermal activity is also present further north on the Central Tyrrhenian Sea floor. The volcanic activity in the central/northern and south Tyrrhenian Sea is controlled by roll-back of the Adriatic and Ionian plates subducting under the Eurasian plate (Greve et al., 2014; Alagna et al. 2010).

In the Aegean area, subduction of the African plate takes place south of the island of Crete, which constitute a part of the Hellenic Arc (Figure 7). Hydrothermal activity in the Aegean Sea is caused by back arc spreading along the Inner Hellenic Volcanic Arc which is located about 120 km north of the

This project has been supported by the European Union's Horizon 2020 research and innovation programme, GeoERA (Grant Agreement Nº 731166, project GeoE.171.001).

subduction zone. Several active volcanic centres are present along the Active Volcanic Arc, including Methana, Santorini, Nisyros and the Bodrum Peninsula.

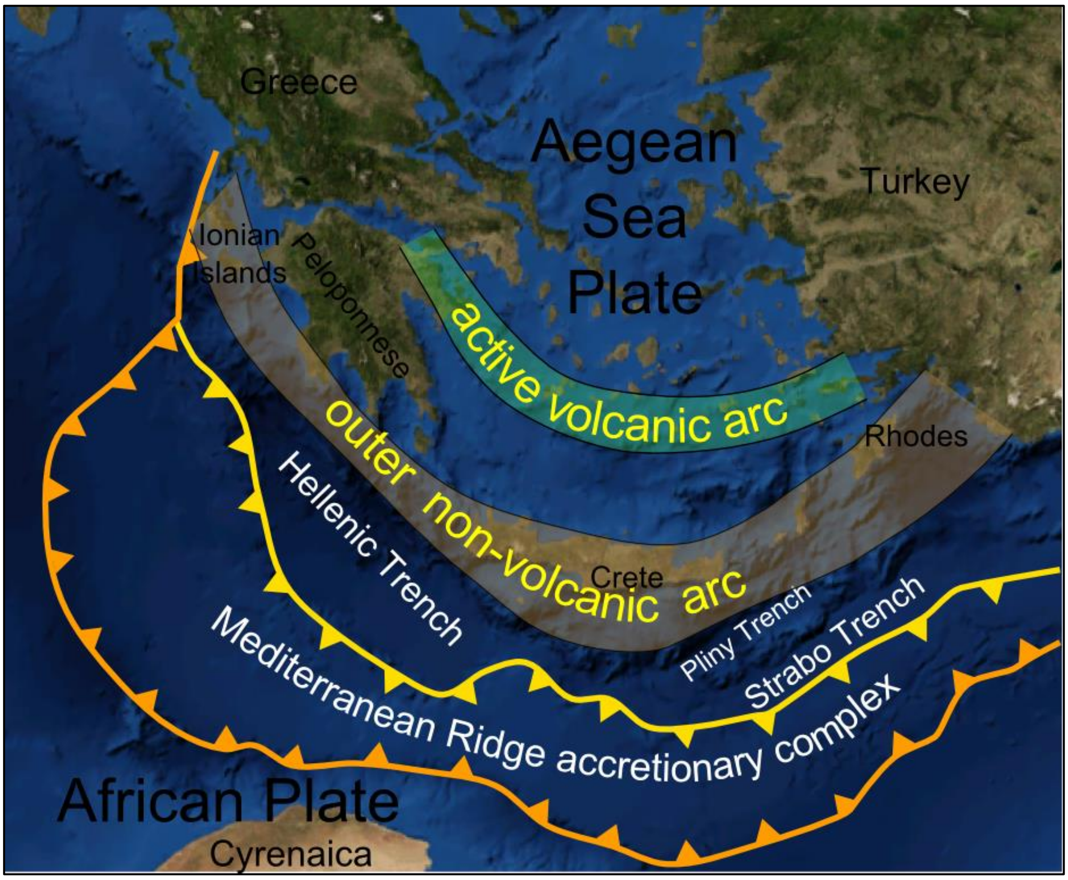


*Figure 7. The Hellenic Arc with the active volcanic arc in the Aegean Sea. Cred. Mike Norton, https://upload.wikimedia.org/wikipedia/commons/d/da/Hellenic_arc.png*

## 5. THE MINDESEA DATABASE

The MINDeSEA data library for marine hydrothermal deposits has been compiled from a range of resources, including scientific papers, reports and thesis's, and cruise reports. The most important dataset is the InterRidge vent site compilation (https://vents-data.interridge.org/maps) containing data for more than 700 vent sides around the World. Data have been correlated with the EMODnet database (https://www.emodnet-geology.eu/) and synergies between the two European portals should be exploited further. A major compilation of chemistry related to black smoker deposits has been assembled by Toffolo et al. (2019), and whereas the PetDB hosted by EarthChem (https://search.earthchem.org/) contains a large library of sea floor samples, there are currently few references to metallic ores and deposits.

The main purpose of the MINDeSEA database is to provide a more comprehensive dataset to the European resource data portals. The collection scheme has therefore been designed to merge marine data with terrestrial data following INSPIRE terminology as strictly as possible. The collection Scheme is shown in Figure 8.

*This project has been supported by the European Union's Horizon 2020 research and innovation programme, GeoERA (Grant Agreement № 731166, project GeoE.171.001).*

| | Data | FIELDNAME | Format | Information |
|---|---|---|---|---|
| | **OBJECTID** | FID | Number | Feature ID. An internally generated identification number for each feature. Aut |
| | **Shape** | SHAPE | Geometry | Point |
| | **Latitude** | LATITUDE | Number (Double) (11,4) | Degrees N |
| | **Longitude** | LONGITUDE | Number (Double) (11,4) | Degrees W/ Degrees E |
| | **Country Code** | CODE | Text (2) | Two letter country code (see INSPIRE CODE: CountryType) |
| **General Data** | **Administration** | ADM | Text (40) | Legal status following the division of the Law of the Sea Convention: Territorial |
| | **Geographical Area** | GEO_AREA | Text (100) | Atlantic Ocean, Mediterranean Sea, etc |
| | **Sector** | SECTOR | Text (100) | Canary Island Seamount Province, Eolian Islands, Gulf of Bothnia, etc |
| | **Ocurrence/Deposit name** | DEPOS_NAME | Text (40) | Name of occurrence/ deposit |
| | **Mineral Ocurrence Type** | OCURR_TY | Text (40) | see INSPIRE CODES: OcurrenceTypeType |
| | **Year of Discovery** | YEAR_DIS | Short Integer (5) | 2001, 2016, etc |
| | **Year of Database Entry** | YEAR_DB | Short Integer (5) | 2018, 2019, etc |
| | **Date of Database Update** | UPDATE_ | Date | dd/mm/yyyy (Date of last update of attributes) |
| | **Deposit Group** | DEPOSIT_G | Text (100) | **MarineVolcanicAssociation**- this exact wording must be entered in bold type (see INSPIRE CODE: DepositGroupType). Mineral deposits formed in a marine volcanic environment. Magmatic and hydrothermal fluids react with sea water for giving volcanogenic massive sulphides (VMS), which are at the origin stratiform deposits of Cu, Zn, Pb, Ag, Au. |
| | **Deposit Type** | DEPOSIT_TY | Text (40) | Choose between **MaficVolcanismMassiveSulphide** and **BimodalFelsicVolcanism** -this exact wording must be entered in bold type (see INSPIRE CODE: DepositTypeType) |
| | **Hydrothermal activity** | HYDR_ACT | Text (40) | Active, inactive |
| | **Distance from rift or active vent sites** | RIFT-DIST | Number (Double) (11,4) | Distance in km |
| | **Age** | AGE | Text (250) | Age of the mineral deposit and host rock (see INSPIRE CODE: NamedAgeType) |
| | **Host Rock** | HOST_ROCK | Text (250) | Substrate rock or sediment surrounding the ore deposit (see INSPIRE CODE: L |
| **Metallogeny** | **Metallic Commodity** | METAL_COMM | Text (100) | Including precious and non-precious metals (see INSPIRE CODE: CommodityT |
| | **Other Metals** | OTHER_ME | Text (100) | See INSPIRE CODE: CommodityType |
| | **Commodity Group** | COMM_G | Text (100) | Base metals, precious metals, energy metals, technological metals (see INSPIF |
| | **Ore Minerals** | ORE_MIN | Text (250) | Principal minerals/commodities (see INSPIRE CODE: MineralNameType = IMA |
| | **Gangue Minerals** | GANGUE | Text (250) | Non-economic minerals (see INSPIRE CODE: MineralNameType = IMA listing ) |
| | **Ore mineral distribution** | ORE_DISTR | Text (250) | Brecciated, banded, micro-layered, etc (see INSPIRE CODE: ShapeType) |
| | **Alteration** | ALTER_ | Text (250) | Alteration minerals formed during/after the process of mineralization (see INSF |
| | **Structure** | STRUCT | Text (250) | stockwork, chimney, debris flow, etc |
| | **Morphology** | MORPH | Text (250) | Shape and internal structure (thickness) of the mineral deposit (see INSPIRE |
| | **Texture** | TEXT | Text (250) | Banded, columnar, mottled, etc |
| | **Genetic type** | GEN_TY | Text (250) | e.g. Hannington classification |
| | **Geochemistry** | GEOCHEM | Text (100) | Yes or No (link to geochemistry table) |
| | **Number of samples** | N | Short Integer (5) | Number of analysed samples |
| | **$SiO_2$ %** | SiO2__pc | Number (Double) (11,4) | Average concentration, dry wt |
| | **$TiO_2$ %** | TiO2__pc | Number (Double) (11,4) | Average concentration, dry wt |
| | **$Al_2O_3$ %** | Al2O3__pc | Number (Double) (11,4) | Average concentration, dry wt |
| | **$Fe_2O_3$ %** | Fe2O3__pc | Number (Double) (11,4) | Average concentration, dry wt |
| | **MnO %** | MnO__pc | Number (Double) (11,4) | Average concentration, dry wt |
| | **MgO %** | MgO__pc | Number (Double) (11,4) | Average concentration, dry wt |
| | **CaO %** | CaO__pc | Number (Double) (11,4) | Average concentration, dry wt |
| | **$Na_2O$ %** | Na2O__pc | Number (Double) (11,4) | Average concentration, dry wt |
| | **$K_2O$ %** | K2O__pc | Number (Double) (11,4) | Average concentration, dry wt |
| | **$P_2O_5$ %** | P2O5__pc | Number (Double) (11,4) | Average concentration, dry wt |
| | **$SO_2$ %** | $SO_2$__pc | Number (Double) (11,4) | Average concentration, dry wt |
| | **Ag (ppm)** | Ag_ppm | Number (Double) (11,4) | Average concentration, dry wt |
| | **Au (ppm)** | Au_ppm | Number (Double) (11,4) | Average concentration, dry wt |
| | **Ba (ppm)** | Ba_ppm | Number (Double) (11,4) | Average concentration, dry wt |
| | **Bi (ppm)** | Bi_ppm | Number (Double) (11,4) | Average concentration, dry wt |
| | **Co (ppm)** | Co_ppm | Number (Double) (11,4) | Average concentration, dry wt |
| | **Cr (ppm)** | Cr_ppm | Number (Double) (11,4) | Average concentration, dry wt |
| | **Cu (ppm)** | Cu_ppm | Number (Double) (11,4) | Average concentration, dry wt |
| | **Ga (ppm)** | Ga_ppm | Number (Double) (11,4) | Average concentration, dry wt |
| | **Ge (ppm)** | Ge_ppm | Number (Double) (11,4) | Average concentration, dry wt |
| | **In (ppm)** | In_ppm | Number (Double) (11,4) | Average concentration, dry wt |
| | **Li (ppm)** | Li_ppm | Number (Double) (11,4) | Average concentration, dry wt |
| | **Mo (ppm)** | Mo_ppm | Number (Double) (11,4) | Average concentration, dry wt |
| | **Nb (ppm)** | Nb_ppm | Number (Double) (11,4) | Average concentration, dry wt |
| | **Ni (ppm)** | Ni_ppm | Number (Double) (11,4) | Average concentration, dry wt |
| | **Pd (ppm)** | Pd_ppm | Number (Double) (11,4) | Average concentration, dry wt |
| | **Pt (ppm)** | Pt_ppm | Number (Double) (11,4) | Average concentration, dry wt |
| | **Rh (ppm)** | Rh_ppm | Number (Double) (11,4) | Average concentration, dry wt |
| **Chemistry** | **Pb (ppm)** | Pb_ppm | Number (Double) (11,4) | Average concentration, dry wt |
| | **Sb (ppm)** | Sb_ppm | Number (Double) (11,4) | Average concentration, dry wt |
| | **Sc (ppm)** | Sc_ppm | Number (Double) (11,4) | Average concentration, dry wt |
| | **Se (ppm)** | Se_ppm | Number (Double) (11,4) | Average concentration, dry wt |
| | **Sn (ppm)** | Sn_ppm | Number (Double) (11,4) | Average concentration, dry wt |
| | **Ta (ppm)** | Ta_ppm | Number (Double) (11,4) | Average concentration, dry wt |
| | **Te (ppm)** | Te_ppm | Number (Double) (11,4) | Average concentration, dry wt |
| | **Th (ppm)** | Th_ppm | Number (Double) (11,4) | Average concentration, dry wt |
| | **U (ppm)** | U_ppm | Number (Double) (11,4) | Average concentration, dry wt |
| | **V (ppm)** | V_ppm | Number (Double) (11,4) | Average concentration, dry wt |
| | **W (ppm)** | W_ppm | Number (Double) (11,4) | Average concentration, dry wt |
| | **Y (ppm)** | Y_ppm | Number (Double) (11,4) | Average concentration, dry wt |
| | **Zn (ppm)** | Zn_ppm | Number (Double) (11,4) | Average concentration, dry wt |
| | **Zr (ppm)** | Zr_ppm | Number (Double) (11,4) | Average concentration, dry wt |
| | **La (ppm)** | La_ppm | Number (Double) (11,4) | Average concentration, dry wt |
| | **Ce (ppm)** | Ce_ppm | Number (Double) (11,4) | Average concentration, dry wt |
| | **Pr (ppm)** | Pr_ppm | Number (Double) (11,4) | Average concentration, dry wt |
| | **Nd (ppm)** | Nd_ppm | Number (Double) (11,4) | Average concentration, dry wt |
| | **Pm (ppm)** | Pm_ppm | Number (Double) (11,4) | Average concentration, dry wt |
| | **Sm (ppm)** | Sm_ppm | Number (Double) (11,4) | Average concentration, dry wt |
| | **Eu (ppm)** | Eu_ppm | Number (Double) (11,4) | Average concentration, dry wt |
| | **Gd (ppm)** | Gd_ppm | Number (Double) (11,4) | Average concentration, dry wt |
| | **Tb (ppm)** | Tb_ppm | Number (Double) (11,4) | Average concentration, dry wt |
| | **Dy (ppm)** | Dy_ppm | Number (Double) (11,4) | Average concentration, dry wt |
| | **Ho (ppm)** | Ho_ppm | Number (Double) (11,4) | Average concentration, dry wt |
| | **Er (ppm)** | Er_ppm | Number (Double) (11,4) | Average concentration, dry wt |
| | **Tm (ppm)** | Tm_ppm | Number (Double) (11,4) | Average concentration, dry wt |
| | **Yb (ppm)** | Yb_ppm | Number (Double) (11,4) | Average concentration, dry wt |
| | **Lu (ppm)** | Lu_ppm | Number (Double) (11,4) | Average concentration, dry wt |
| | **REY %** | REY_pc | Number (Double) (11,4) | Average concentration, dry wt |
| | **Analytical technique** | TECHNIQUE | Text (50) | Technique used (AAS, ICP-MS, ICP-AES, XRF etc) (see INSPIRE CODE: Analyti |
| | **Mine Status** | STATUS | Text (40) | see INSPIRE CODE: MineStatusType |
| | **Mining Activity Type** | MINING_TY | Text (40) | see INSPIRE CODE: MiningActivityTypeType |
| | **Deposit Size** | SIZE | Text (100) | Magnitude of the mineral deposit calculated according to ProMine (unknowed, c |
| | **Grade** | GRADE | Text (250) | Specify assessments of grade (Mean content of manganese (Mn); iron (Fe); co |
| | **Resources** | RESOURCES | No. Double (11,4) | Resources in Mt |
| | **Reserves** | RESERVES | No. Double (11,4) | Reserves in Mt |
| | **Mined Tonnage** | MIN_T | No. Double (11,4) | in Mt |
| | **Total Tonnage** | TOTAL_T | No. Double (11,4) | in Mt |
| | **Remaining Tonnage** | REM_T | No. Double (11,4) | in Mt |
| **Economic Data** | **Resource Reporting Standard/ compliancy** | RES_REP | Text (100) | PERC, JORC, NI43-101, etc (see INSPIRE CODE: ClassificationMethodUsedType |
| | **Reference for Tonnage Assesment** | REF_T | Text (40) | Company ordering the assesment |
| | **Data Scale** | SCALE | Text (100) | Specify the scale in which the deposit has been mapped and delivered |
| | **Exploration Activity Type** | EXPLOR_TY | Text (250) | see INSPIRE CODE: ExplorationActivityTypeType |
| | **Operator** | OPERATOR | Text (250) | Research, exploration or operating agency/company |
| | **Cruises** | CRUISE | Text (250) | Cruises identification |
| | **Sampling Methods** | SAMPLING_M | Text (250) | Type of method to recover samples (dredge, ROV…) |
| | **Data Provider** | DATA_PROVI | Text (150) | Name of organisation providing data |
| | **Data Provider Contact** | DATA_CONT | Text (150) | The data providing **organisation/institute** contact details – email is required |
| | **Deposit Extent** | DEPOS_KM2 | No. Double (11,4) | Area of deposit **(Sq. Km)** |
| | **Depth to Deposit (m)** | DEPTH_TO_D | No. Double (11,4) | Depth to deposit from sea surface |
| **Environment** | **Fauna** | FAUNA | Text (100) | Type of fauna (e.g. corals,…) |
| | **Description** | DESCRIPT | Text (500) | Deposit summary and metallogenetic model |
| **Other Data** | **Gallery** | GALLERY | Text (100) | Images on the mineralization (geophysical, sampling, textural features, parage |
| | **References** | REFERENCES | Text (500) | Link to bibliographic references (DOI and/or Author, Year & Title if you wish) |
| | **Comments** | COMMENTS | Text (500) | Any additional comments or observations |

*Figure 8. The MINDeSEA data scheme for hydrothermal deposits in European waters.*

Currently the MINDeSEA database contains data for 153 European mineralisations and vent sites. The database relies on a set of almost 600 samples, of which 450 representing 25 sites have chemistry.

Most of the recorded deposits are located along the Mid-Atlantic Ridge, including the Azores Triple Junction and ridge segments affected by the Icelandic hot spot. Number-wise mid-ocean ridge setting therefore must be considered the most important metallogenic setting of the European sea floor hydrothermal deposits. The sulphide deposits within this setting are all considered mafic (or ultramafic) hosted and are potential sources of copper, zinc, lead, silver, and gold. However, the setting also includes shallow or colder vent systems precipitating mainly anhydrite or barite.

Deposits related to intra-plate hotspots are represented by occurrences in the Canary Island archipelago. These precipitations comprise epithermal deposits, volcanogenic massive sulphide deposits (VMS), and exsolved oxyhydroxides, and their main products are copper-zinc sulphides, barite, and iron oxyhydroxides.

Apart from the hydrothermally generated iron and manganese crusts found on the Eratosthenes Sea Mount in the Levantine Basin all venting and precipitations in the Mediterranean Sea are related to back-arc spreading, either in the Central and South Tyrrhenian Sea or the Aegean Sea. These deposits are considered of bimodal to felsic exhalative types, or of epigenetic origin. In both the Aegean and the Tyrrhenian Sea, deposits generally consist of iron and/or manganese with a few occurrences of lead and zinc precipitates around, for instance, the Kolumbo volcano north of Santorini.

In terms of chemistry, the dataset is not in itself sufficient to resolve metallogenic questions related to geodynamic setting, and the dataset primarily illustrates the dependence of metal precipitation on temperature. At the same time, sampling from the sea floor is highly biased towards what can be sampled, and the dataset is primarily based on averages from surface sampling comprising chimneys, mounds and probably also near vent sediments. However, trends are apparent as shown in figures 9-14 below, with the recorded mid-ocean ridge deposits in the database on average being richer in most of the base metals, including copper and zinc, but also in barium. The Mediterranean back-arc deposits, on the other hand, tend to be richer in e.g., silver, lead and antimony as predicted by their setting and bimodal character.

*This project has been supported by the European Union's Horizon 2020 research and innovation programme, GeoERA (Grant Agreement Nº 731166, project GeoE.171.001).*

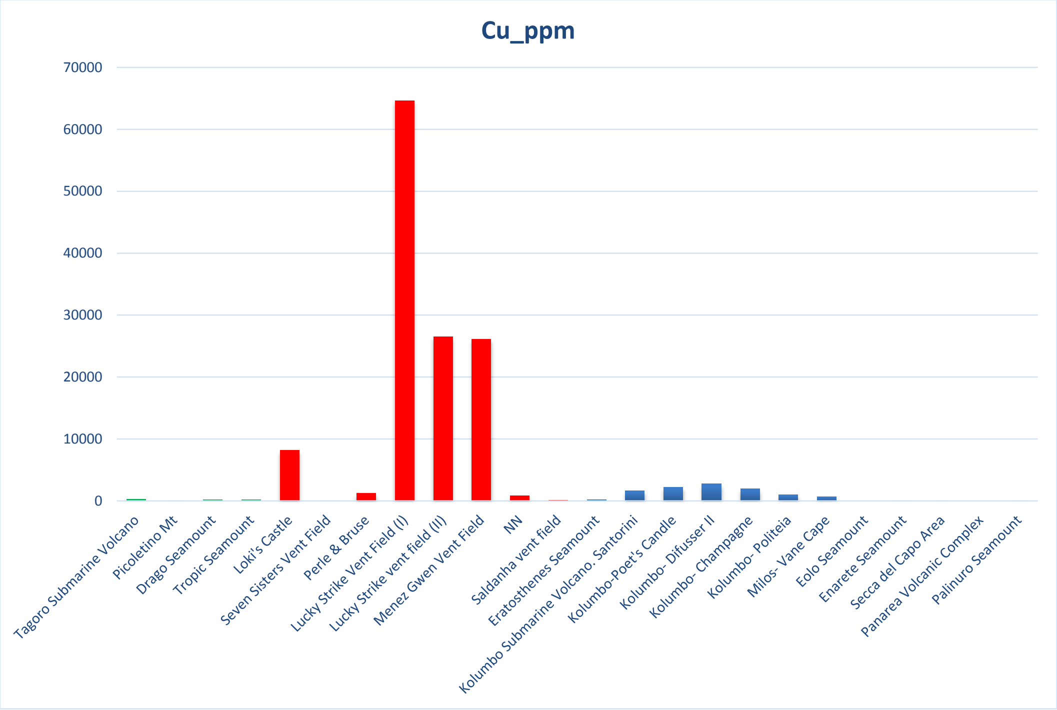


*Figure 9. Average copper concentrations in 25 vent fields in European waters. Intra-plate hotspots in green, mid-ocean ridges in red, and arc/back-arc settings in blue. Data from the MINDeSEA database.*

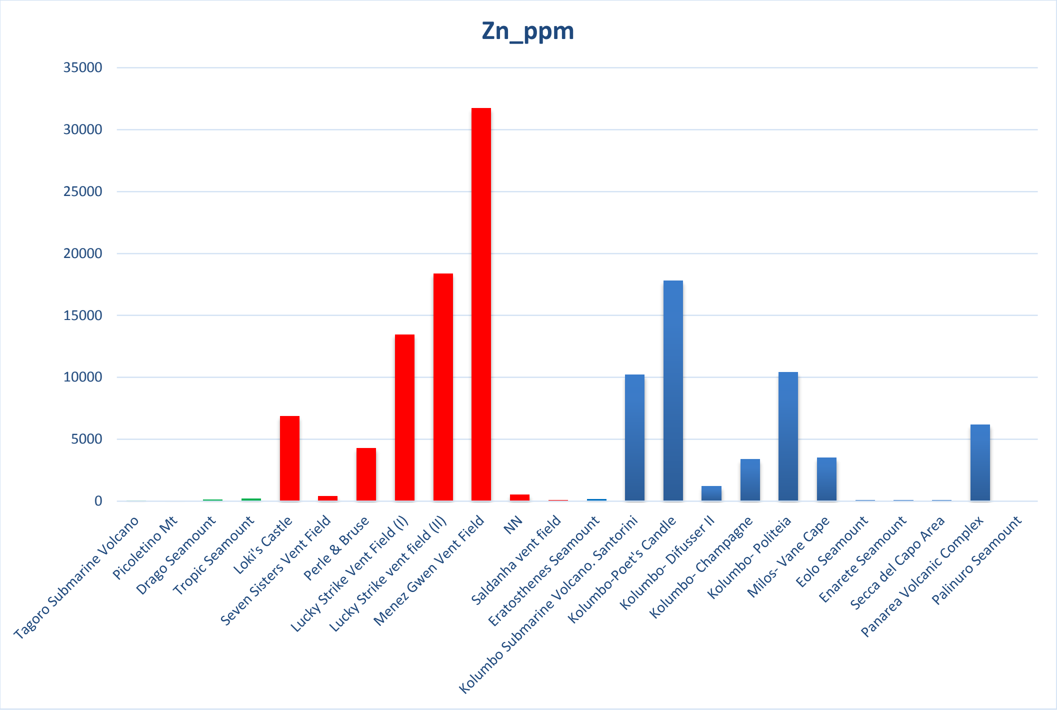


*Figure 10. Average zinc concentrations in 25 vent fields in European waters. Intra-plate hotspots in green, mid-ocean ridges in red, and arc/back-arc settings in blue. Data from the MINDeSEA database.*

*This project has been supported by the European Union's Horizon 2020 research and innovation programme, GeoERA (Grant Agreement Nº 731166, project GeoE.171.001).*

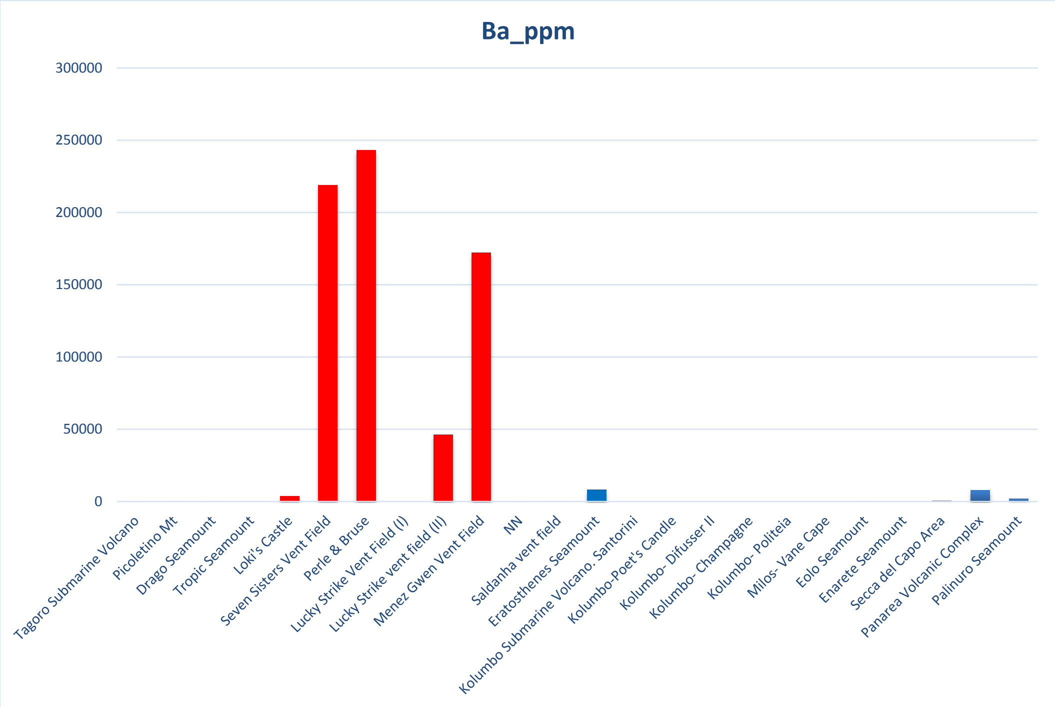


*Figure 11. Average barium concentrations in 25 vent fields in European waters. Intra-plate hotspots in green, mid-ocean ridges in red, and arc/back-arc settings in blue. Data from the MINDeSEA database.*

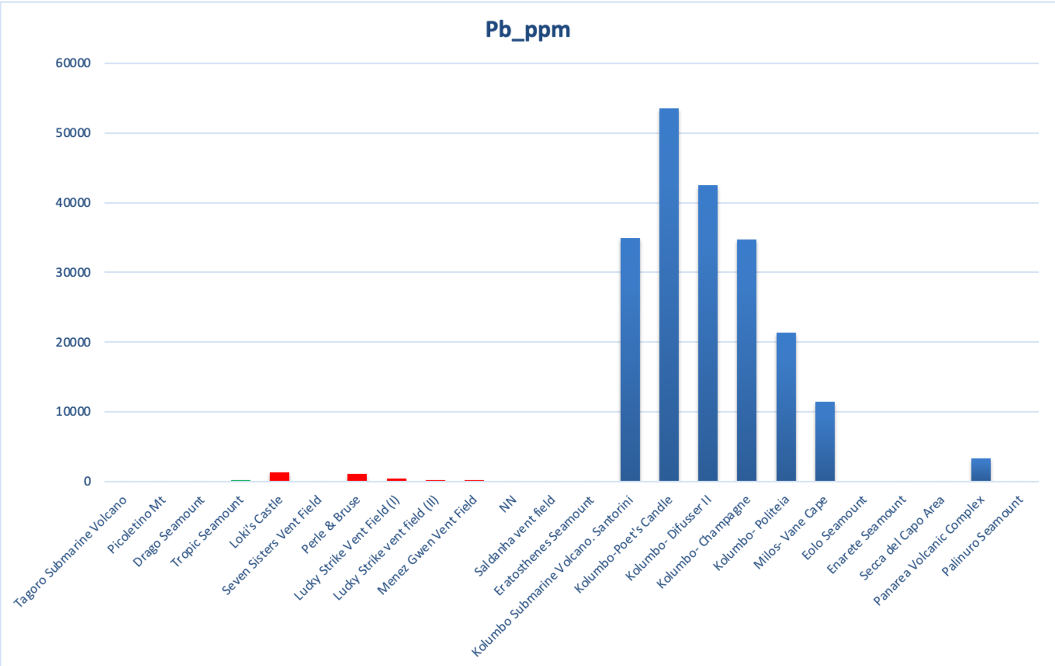


*Figure 12. Average lead concentrations in 25 vent fields in European waters. Intra-plate hotspots in green, mid-ocean ridges in red, and arc/back-arc settings in blue. Data from the MINDeSEA database.*

*This project has been supported by the European Union's Horizon 2020 research and innovation programme, GeoERA (Grant Agreement Nº 731166, project GeoE.171.001).*

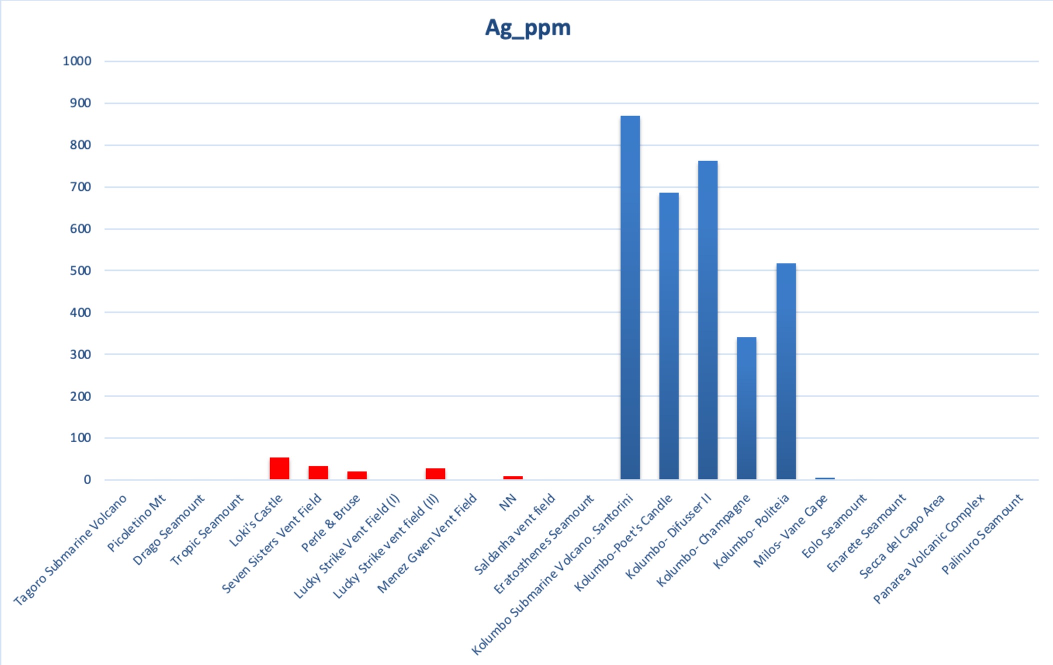


*Figure 13. Average silver concentrations in 25 vent fields in European waters. Intra-plate hotspots in green, mid-ocean ridges in red, and arc/back-arc settings in blue. Data from the MINDeSEA database.*

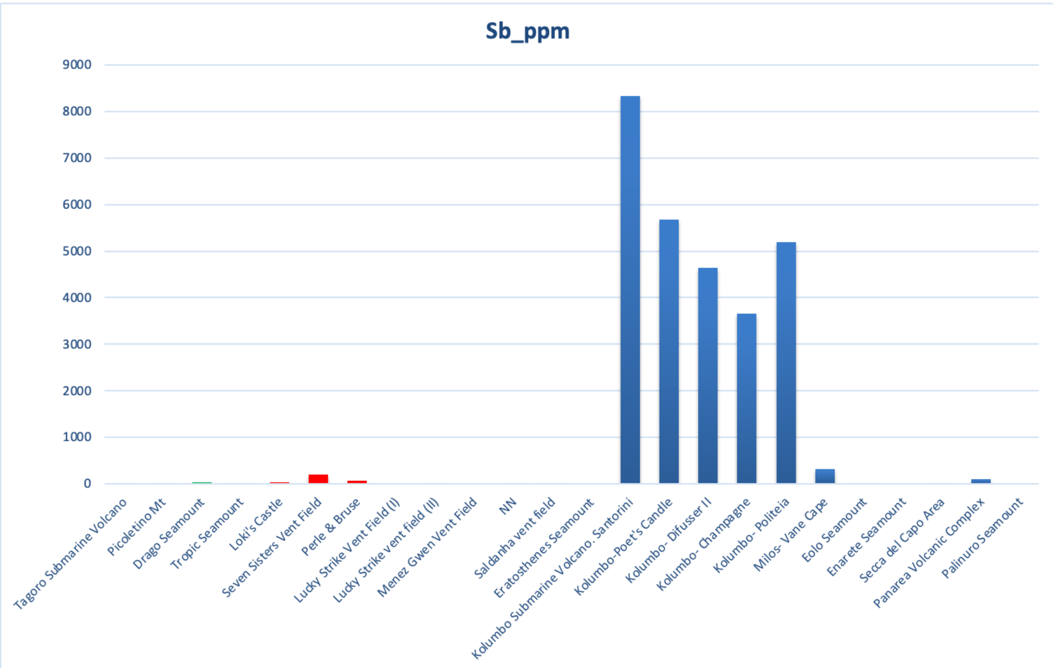


*Figure 14. Average antimony concentrations in 25 vent fields in European waters. Intra-plate hotspots in green, mid-ocean ridges in red, and arc/back-arc settings in blue. Data from the MINDeSEA database.*

*This project has been supported by the European Union's Horizon 2020 research and innovation programme, GeoERA (Grant Agreement № 731166, project GeoE.171.001).*

# 6. HYDROTHERMAL DEPOSITS IN EUROPEAN WATERS

## 6.1. The Mid-Atlantic Ridge – The Reykjanes and Arctic Mid-Ocean Ridge

A number of vent sites have been documented on the Mid-Atlantic Ridge north and south of Iceland (Figure 15). For the submarine hydrothermal systems close to Iceland, reliable data are available from three, which are all located in relatively shallow water. These are the Steinaholl hydrothermal field on the Reykjanes Ridge south of Iceland, and the Grimsey and Kolbeinsey hydrothermal fields on the Kolbeinsey Ridge north of Iceland. The Grimsey and Kolbeinsey fields lie within the maximum extend of the Icelandic Ice Sheet during the last glaciation and may have been eroded (Franzson et al., 2016).

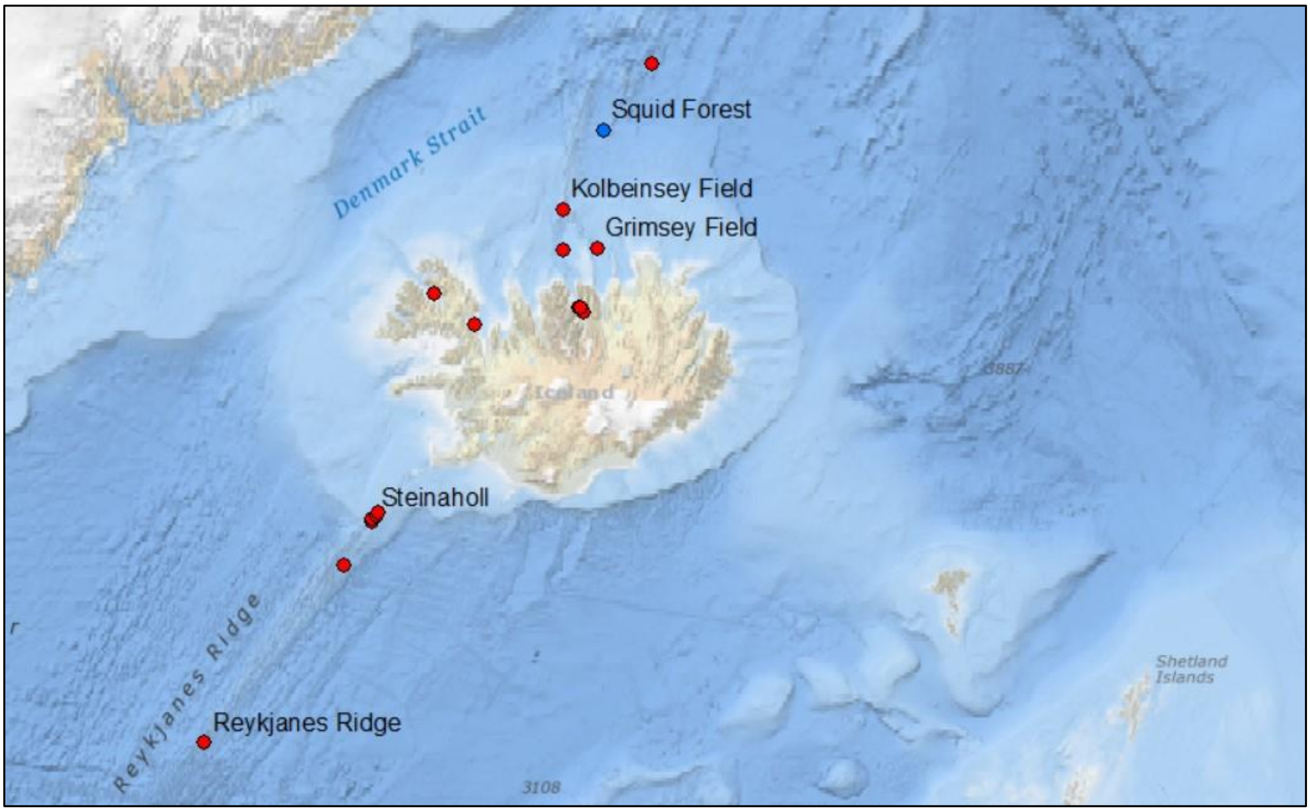


*Figure 15. Active (red) vent systems along the Reykjanes Ridge to the south of Iceland and Kolbeinsey Ridge to the north of Iceland. The inactive (blue) vent site on the Kolbeinsey Ridge is the Squid Forest vent site. Bathymetric imagery from the EMODnet WMS service (https://www.emodnet-bathymetry.eu)*

The Steinaholl hydrothermal field on the Reykjanes Ridge is located about 100 km southwest of the Reykjanes peninsula in Iceland. It is situated in the northern sector of a sequence of en-echelon arranged fissure swarms at 250-300 m water depth. According to Franzson et al. (2016), the field has not been sampled, but bubble-rich plumes indicate an underlying boiling hydrothermal field.

North of Iceland, two well documented vent fields are found close to the islands of Grimsey, 40 km north of Iceland, and Kolbeinsey, 100 km north of Iceland. The Grimsey field is located near the north-eastern edge of a sedimented extensional basin along the Tjörnes Fracture Zone, connecting

This project has been supported by the European Union's Horizon 2020 research and innovation programme, GeoERA (Grant Agreement Nº 731166, project GeoE.171.001).

the neovolcanic zone of North Iceland to the Kolbeinsey Ridge. In the Grimsey field, the vents are divided into three venting areas aligned in a northerly trend about 1 km long and 350 m wide. Again, the observation of bubble plumes indicates boiling conditions in the vent system at 400 m water depth. Of the known hydrothermal fields in Icelandic waters, the Grimsey field shows the largest amount of precipitates, with mounds, 20 m across and 10 m high, and isolated chimneys consisting of anhydrite and minor talc (Franzson et al., 2016; Pedersen and Bjerkgård, 2016). The Kolbeinsey field further north-west is located near the southern end of the Kolbeinsey Ridge. The hydrothermal field is confined to the southern part of a small volcanic ridge which rises from 200 to 90 m below sea level. Mineral deposition seems to be limited and most samples are highly altered and fragmented lava flows (Franzson et al., 2016).

Squid Forest is an extinct field in Icelandic waters at the Kolbeinsey Ridge, located at 900 m water depth at the plateau of a flat-topped semi-circular volcano. The site hosts two sulphide chimney areas, which have been sampled and analysed. A chimney top sample display a porous inner zone composed of sphalerite and pyrrhotite, and an outer part consisting of sphalerite, barite and amorphous silica (Pedersen et al., 2010, Pedersen and Bjerkgård, 2016)

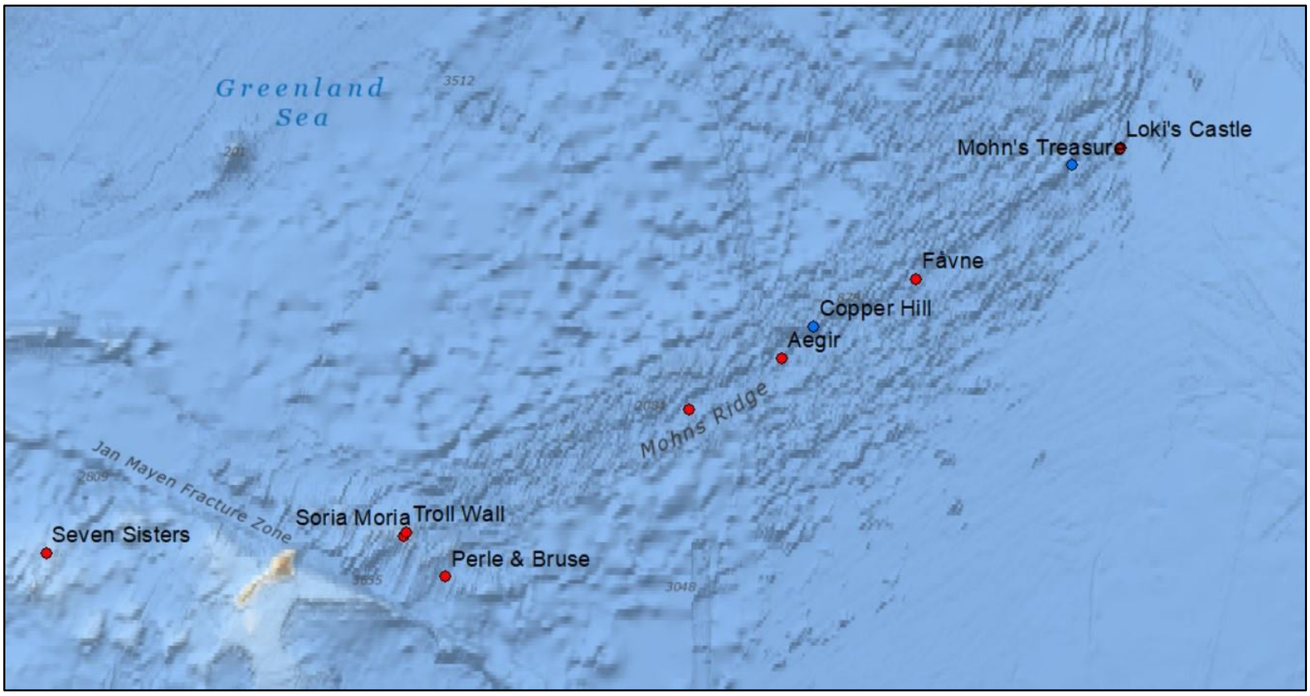


*Figure 16. The Mohn's Ridge with vent sites and seabed mineral deposits as recorded by the MINDeSEA data library. Red colours are inferred or confirmed active vent sites; blue colours are mineral occurrences at inactive sites. Bathymetric imagery from the EMODnet WMS service (https://www.emodnet-bathymetry.eu)*

In the northern extremity of the Kolbeinsey Ridge an especially shallow part of the ridge known as the Eggvin Bank hosts a vent field called the Seven Sisters. The Seven Sisters vent field is located within Norwegian jurisdiction. The shallowest part of the Eggvin Bank is less than 30 m deep and is defined by a large volcanic edifice with a summit caldera (Yeo, 2016). Large, recent lava flows fill the rift valley to the north of the summit caldera. The Seven Sisters vent field is located approximately 20 km north of the summit crater at a depth of 130 m along a chain of flat-topped

This project has been supported by the European Union's Horizon 2020 research and innovation programme, GeoERA (Grant Agreement № 731166, project GeoE.171.001).

central-type volcanic edifices that follow the eastern margin of the rift valley (Marques et al., 2020). Barite and minor anhydrite are the major hydrothermal phases present in collected samples. Sulphides include pyrite and marcasite, sphalerite, chalcopyrite, galena and Ag-sulphosalts, the latter four forming rims on pyrite and barite grains. The precipitates have been interpreted to display hybrid characteristics between exhalative and seawater-buffered epithermal deposits (Marques et al., 2020)

A few tens of km north of the Seven Sisters vent field the Jan Mayen Fracture Zone offsets the Mid-Atlantic Ridge towards east. The Mid-Atlantic Ridge continues east of Jan Mayen Island as the Mohn's Ridge towards east-northeast to meet the Knipovich Ridge. The Mohn's Ridge hosts a string of confirmed active and inactive vent sites along with documented massive sulphide deposits (Figure 16). All deposits along the Mohn's Ridge lie within Norwegian jurisdiction, either in the Norwegian Exclusive Economic Zone or the Extended Continental Shelf. The Mohn's Ridge has been the focus of several studies and cruises and has been a priority for the investigations by the Norwegian Petroleum Directorate as part of an opening process to allow commercial exploration for seabed mineral resources. Regional prospectivity mapping and estimation of undiscovered deposits predicts a total of 11 undiscovered sulphide deposits along the 550 km long Mohn's Ridge (Juliani and Ellefmo, 2018).

The Jan Mayen vent field east of Jan Mayen Island is located on the southernmost segment of the Mohn's Ridge. The field is relatively shallow and influenced by higher magmatic production than the ridge further north. It consists of three discreet subfields, each including a number of vent sites; the Troll Wall, Soria Moria, and Perle & Bruse (Pedersen et al., 2010; Pedersen and Bjerkgård, 2016). The Troll Wall is found at a water depth of 550 m. The deposit contains chimneys dominated by sphalerite as the main sulphide mineral, accompanied by lesser amounts of pyrite and chalcopyrite. Diffuse low-temperature venting in the area results in numerous mounds of iron hydroxide deposits (Pedersen et al., 2010; Pedersen and Bjerkgård, 2016; da Cruz, 2015). The Soria Moria vent field is situated 5 km south of the Troll Wall at a water depth of 700 m. At Soria Moria, 8-9 m high sphalerite-dominated sulphide chimneys occur among edifices composed of barite, silica, and minor pyrite, sphalerite and galena. The hydrothermal deposits at Soria Moria are enriched in silver and gold. Two km east of the Troll Wall, the Perle & Bruse field is located on the flanks of a large central volcano. Active venting primarily takes place at two hydrothermal mounds 300 m apart (Pedersen and Bjerkgård, 2016).

Two inactive sites with sulphide formation are known in the Mohn's Ridge system. In the Copper Hill deposit, samples of sulphide-mineralised breccias have been sampled at a non-venting site, most likely related to an oceanic core complex. The sulphides are dominated by chalcopyrite and it is assumed that the sulphide-bearing breccias were exhumed by faulting. At the Mohn's Treasure in the northernmost section of the Mohn's Ridge, hydrothermal sulphides have been dredged from a site with no accompanying seawater anomalies detected. The sulphides are mainly composed of pyritic chimney fragments (Pedersen and Bjerkgård, 2016). Mohn's Treasure appears to be a fossil sediment-hosted hydrothermal deposit, and a magnetic survey suggests a body of about 150x200 m buried beneath 15 m of sediments (Lim et al., 2019).

The Aegir (Aegirs Kilde) vent field is an active vent site, located at around 2050 m water depth in the central part of the Mohn's Ridge. It is currently undergoing investigations (Stensland, 2019)

Further North-East on the Mohn's Ridge, at 72.8°N, 4.2°E, the Fåvne vent field was recently sampled by the University of Bergen and The Norwegian Petroleum Directorate at 3000 m water depth. Fåvne is hosted by ultramafic rocks, and the vent field consists of both active and inactive

This project has been supported by the European Union's Horizon 2020 research and innovation programme, GeoERA (Grant Agreement № 731166, project GeoE.171.001).

vent sites. The individual vents are composed of isocubanite, pyrrhotite and chalcopyrite, accompanied by various amounts of iron-oxyhydroxides and anhydrite. The Fåvne vent field differs from other known vent fields along the Arctic Mid Ocean Ridges due its high Cu and Co contents as well as a depletion in the vast majority of other metals and metalloids, including Zn, Pb, and Ag (https://www.uib.no/dyphav/134727/geochemistry-sulfide-mineralization-fåvne-vent-field-arctic-mid-ocean-ridges)

One of the best studied sites of active venting on the Mohn's Ridge is the Loki's Castle, almost in the middle of the bend between the Mohn's and Knipovich Ridges. Loki's Castle is located in a setting characterised by ultra-slow spreading in a ridge valley which is impacted by sediments from the Bear Island sediment fan. Venting of 310–320 °C black smoker fluids occur at two sites around 150 m apart. Loki's Castle is basalt-hosted but fluids seem to have interacted with ultramafic rocks, and there is a significant signature of sediment influence (Baumberger et al., 2016). Two 20–30-m high sulphide mounds have developed, each 150–200 m across (Pedersen et al. 2010b). Sulphide mineralisation consists of chalcopyrite, isocubanite, and sphalerite, with pyrite, marcasite, and lesser galena and pyrrhotite. Several samples document gold concentrations at the level of several ppm. (Snook et al. 2018; see also da Cruz 2015)

North, along the Knipovich Ridge (Figure 4), three plume sightings have been recorded but activity has not been confirmed. These are all located within the Norwegian territorial waters.

In the Lena trough (Figure 4) two deposits have been dredged and provided samples of massive sulphides, including chimney fragments, and hydrothermal sediments. For one of the locations an ultramafic substrate was sampled along with the sulphides (Pedersen and Bjerkgård 2016).

A number of hydrothermal plumes have been observed on the Gakkel Ridge between 83 and 87°N (Figure 4) but so far, no sulphide samples have been retrieved (Pedersen and Bjerkgård, 2016). Most of the plumes have been observed in international waters, but the westernmost observations are located within territorial waters of Greenland.

## 6.2. The Mid-Atlantic Ridge – The Azores Triple Junction Area

In the following, vent sites along the Mid Atlantic Ridge around the Azores islands are described from north to south, from the Moytirra deposit in the north to the Saldanha deposit in the south. All deposits here are under Portuguese jurisdiction (Figure 17).

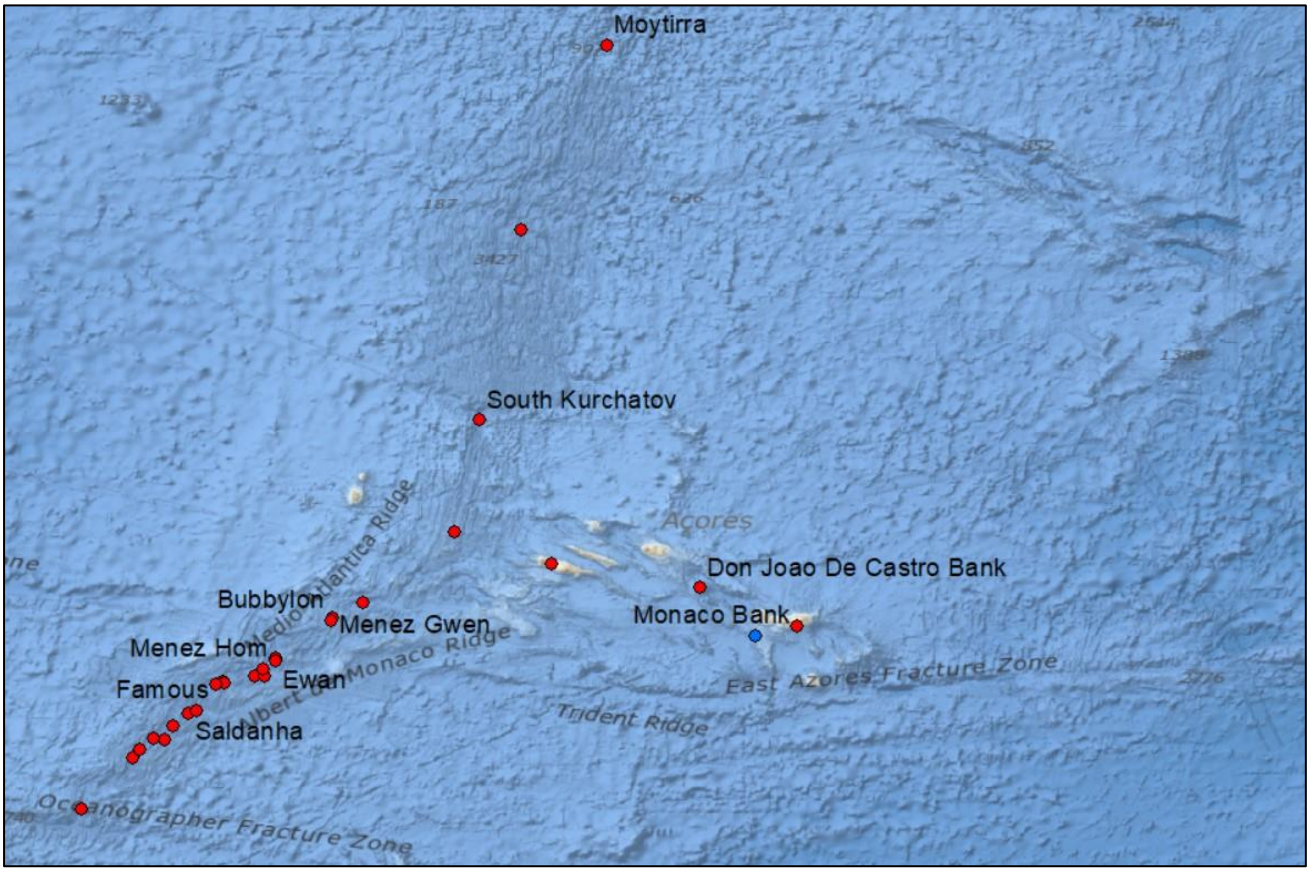


*Figure 17. Active (red) and inactive (blue) vent fields along the Mid-Atlantic Ridge across the Azores Triple Junction. Bathymetric imagery from the EMODnet WMS service (https://www.emodnet-bathymetry.eu)*

### Moytirra

Moytirra is the only high-temperature hydrothermal vent known between the Azores and Iceland in the North Atlantic. It is located on a slow to ultraslow spreading ridge uniquely situated one third of the way up a 300 m high, near-vertical fault scarp forming the eastern median valley wall of the MAR at 45°N. It is about 3.5 km from the axial volcanic ridge crest. Moytirra is located at water depths between 2750 and 3060 m. The Moytirra vent field is clearly tectonically controlled and is the only hydrothermal system known to vent from the steep scarps forming the median valley wall. Moytirra is hosted by basalts and dominated by brecciated pillow lavas and more massive dolerite dykes. It is presumably heated by an off-axis magma chamber. The Moytirra vent field consists of an alignment of four sites of vigorous venting, of which three are actively emitting “black smoke” and producing a complex of chimneys and beehive diffusers (Wheeler et al., 2013).

*This project has been supported by the European Union's Horizon 2020 research and innovation programme, GeoERA (Grant Agreement № 731166, project GeoE.171.001).*

The hydrothermal field is in a second order ridge segment with a 40 km long, and 8 to 12 km wide median valley, that is bound to the east and west by steep-sided walls forming near vertical cliffs up to 500 m high. Rising from the flat median valley floor is an axial volcanic ridge (AVR) that occupies the centre of the ridge segment. The AVR is 400 m high and 2-6 km wide, and extends for 25 km. It is an expression of the most recent volcanic activity (Searle et al., 2010; Yeo et al., 2012).

The vent field is located along the western flank of a detached ridge (Moytirra ridge), which extents 8 km sub-parallel to the direction of the AVR at the intersection of oblique minor faults with a major median valley bounding fault. The vent field is found about 1.5 km from the edge of the neovolcanic AVR and 3.5 km from the AVR crest.

ROV observations show that the active hydrothermal field is composed of an elongated mound of sea-floor polymetallic massive sulphides topped by numerous anhydrite-sulphide chimneys up to 20 m high at 2915- 3000 m water depths. The active hydrothermal field is surrounded by talus extending from 3000 to 3038 m water depths, covering an area of ∼24,000 square meters. The talus is made up by blocks of weathered sulphides, variably covered by hemipelagic and hydrothermal sediments. The chaotic debris resulted from the destruction of active vents. Hydrothermally extinct seafloor massive sulphide deposits forming chimneys and mounds also occur towards west at deeper waters from 3030 to 3040 m. This area is composed of an accumulation of weathered sulphides and iron-rich sediments with a discontinuous pelagic sedimentary cover. The field of hydrothermal chimneys covers an area of around 5580 $m^2$ (Somoza et al. 2020; 2021).

**MAR 43N**

During RRS Discovery Cruise 147 (1984), a detailed hydrographic station was worked over a segment of the median valley of the MAR at 43°N and various water column samples were collected. Measurements of temperature, salinity, dissolved oxygen, and micronutrients showed the water to be well mixed within the valley, with no distinct indication of perturbations of these constituents by hydrothermal activity. However, in the deeper water, anomalously high concentrations of Mn were detected at 3279 m, and this signature was attributed to hydrothermal activity (Hydes et al., 1986). No additional information is available for this inferred vent site.

**South Kurchatov**

During five oceanographic campaigns on the Mid-Atlantic Ridge, seven ridge segments was found to show strong evidence of high-temperature hydrothermal activity (Chin et al. 1998), one being the Kurchatov segment. During the Fazar cruise, covering the MAR between 33° and 41°N, water column anomalies, indicative of high-temperature hydrothermal activity, were detected. Additionally, total dissolved manganese recordings attributed to hydrothermal circulation, were observed south of the Kurchatov segment (Aballéa et al. 1998).

**Luso**

The Luso hydrothermal field was recently discovered during the BlueAzores2018 cruise to the eastern slope of the Gigante seamount. The seamount is located at the Azores latitude on the Mid-Atlantic Ridge (MAR) and associated with the Faial transform fault crossing the MAR. The Gigante

*This project has been supported by the European Union's Horizon 2020 research and innovation programme, GeoERA (Grant Agreement Nº 731166, project GeoE.171.001).*

seamount is situated 98 km WNW of Faial Island and 6 km east from the MAR. It is approximately 16 km long and 6–13 km wide at the 1000 m depth contour. It is a shallow seamount reaching 161 mbsl, and the summit has a small surface area of 0.7 $km^2$ at the 300 m depth contour (Cascão et al. 2017). At a depth of 570 m, low temperature translucent fluids vent through well-developed ochre-coloured chimneys hosted by basaltic rocks (Dias et al. 2019). It occupies an area of about 400 $m^2$ and includes at least 26 chimney structures, having variable dimensions and openings up to 30 cm in diameter. Chimneys are formed by loose and poorly crystalline material dominated by Fe-oxyhydroxides and amorphous Si ($Fe_2O_3$ + $SiO_2$ is around 72 wt%). Concentrations of S, Cu, Zn and Pb are generally negligible, but higher contents in S, Cu and Zn were recorded in the intermediate zone and inner wall. Other trace metals, such as P, V, Cr, Co, Ni, As, Mo and ΣREE, are particularly enriched in the outer wall (Dias et al., 2019).

**D.João de Castro Bank, Espalamaca, Monaco Bank and Ribeira Quente (Azores Archipelago)**

The Azores Archipelago is rich in shallow marine hydrothermal vent sites. A total of ten vent sites have been identified. Some of the sites are characterized by an intense degasification in addition to a moderate to high thermal anomaly. The majority of the hydrothermal vent occurrences are in intertidal areas close to the shores of S. Miguel, Faial, Flores and Graciosa islands, and will not be considered here. The remaining three shallow vent sites are located at (1) the D. João de Castro Bank at 18-45 mbsl; (2) Espalamanca (Faial Island) at 5-50 mbsl; (3) Ribeira Quente (S. Miguel island) at 6-8 mbsl (Couto et al. 2015).

D. João de Castro Bank is one of the best studied sites and represents the remains of an island formed by a submarine eruption in 1720 and which disappeared in 1722. It has an elevation of 1000 m and is located in the hyper-slow spreading Terceira Rift. This is one of the few Azorean vents that is not near an island, lying 36 nautical miles away from Terceira and 40 miles away from São Miguel islands (Santos et al., 2001). D. João de Castro Bank is the only vent with analysed gas compositions: The major component is $CO_2$ (90%), with lesser with lesser $H_2S$, $H_2$ and $CH_4$. Fluid temperatures are between 36 and 63°C at the discharge point (Cardigos et al., 2005).

The vent site Espalamaca is approximately 2.6 km from the town of Horta on the Faial Island. It is a degassing low-temperature hydrothermal field extending for a few tens of meters. Gas can be observed emitting from the sediment as well as through cracked hard ground. Preliminary analyses of the gaseous discharges suggest that they are mainly composed of $CO_2$, with a low concentration of methane, and no sulphur. Temperature may be as high as 35°C, with a pH of 5.7 (Rajasabapathy et al. 2014).

The Ribeira Quente shallow vent field is a small moderately active sulphhydric vent, occupying a circular area of 200 m in diameter, very close to the Ribeira Quente beach. Numerous gas bubbles emerge from the sandy sediments, rich in $CO_2$ and some $H_2S$ (Zuillig et al. 1990).

Monaco Bank is a submarine volcano along a NW-SE-trending 20 km long fissure south of the western tip of Sao Miguel Island, representing a prominent 70 km long bathymetric feature with a maximum width of 25 km. The linear volcano is located along regional tectonic trends connecting the Sete Cidades volcano with Santa María Island, SE of Monaco Bank. The summit of the volcano rises to within 197 mbsl.

**Menez Gwen**

This project has been supported by the European Union's Horizon 2020 research and innovation programme, GeoERA (Grant Agreement Nº 731166, project GeoE.171.001).

The Menez Gwen is one of the northernmost hydrothermal fields in a series of fields that stretches north from the Oceanographer Fracture Zone to the Azores Archipelago. It is in the southernmost segment (KP-5), which extends 55 km in a S-SW to N-NW direction, and is one of five second-order segments between Kurchatov and Pico large discontinuities (Figure 3).

The hydrothermal field resides in the central area of the segment, at water depths of 840–870 m on a young circular on-axis volcano that is 700 m high and about 15 km in diameter (Charlou et al. 2000). The volcano is sediment-free with an axial graben at its top that is 9 km long, 2 km wide and 300 m deep, and floored by fresh lava and volcanic breccia. At the base of the graben there is a lava lake with very fresh lavas and, on both sides of the lava lake, fresh lobate flows (Fouquet et al. 1994; Charlou et al. 2000). At Menez Gwen, intense volcanic activity occurs with extensive sheet flows and locally fissured, robust, and persistently focused magmatic activity (Parson et al. 2000) where outcrops of eruptive lavas alternate with large areas of explosive volcanic ejecta (Ondréas et al. 1997).

The area of active hydrothermal venting covers 200 $m^2$ at the bottom of the graben, and is characterized by small, friable, isolated, <5 m in height, anhydrite+sulphide chimneys growing on top of fresh pillow basalts and barite-rich mounds (Fouquet et al. 1994). Sulphides are not abundant (Marques et al. 2009) and the oxidation of sediments forms slag-like deposits along the mounds. The chimneys' small size is believed to reflect their young age.

Five major sites of hydrothermal activity have been documented at Menez Gwen: Atos 10, Cage Site, Marker 4, White Flames, and Woody (Marcon et al. 2013). This region is dissected by several N-NE-striking fractures that are thought to serve as conduits for hydrothermal flow (Marcon et al. 2013).

Diffuse clear fluids are venting from the small mounds and chimneys, and locally also exiting from small fractures in some localities. The fluids have temperatures up to 281°C (Charlou et al. 2000). Vent fluids have salinities lower than seawater, low metal and $H_2S$ concentrations, indicating that boiling, seawater mixing, and perhaps conductive cooling is taking place in the subsurface (Charlou et al. 2000). The fluids are highly depleted in iron compared to other vent sites along the MAR. These characteristics are believed to reflect low temperatures in the reaction zone and interaction with basaltic rocks that have already undergone extensive hydrothermal alteration (Karson et al. 2015), and may be an indicator of metal sulphide precipitation in the subsurface (Von Damm et al. 1998; Charlou et al. 2000). Isotopic signatures of $CO_2$ and $CH_4$ are consistent with a primary magmatic origin, and the degassing observed in these fluids (increasing towards the Azores) is associated with magmatic degassing processes, leaching of $CO_2$ from enriched basalts or gabbroic bodies, and serpentinization reactions at depth (Charlou et al. 2000). Most other hydrothermal sites on the MAR are located substantially deeper than Menez Gwen, making Menez Gwen unique in terms of possible boiling processes in the subsurface (Karson et al. 2015).

Other bubble plumes were observed during several multibeam surveys, in particular on top of the eastern Menez Gwen graben wall, indicating that more sites with hydrothermal activity exist in the Menez Gwen area (Marcon et al. 2013)

### Bubbylon

The Bubbylon vent field was discovered during the Meteor Cruise No. M82/3 in 2010, when hydrothermal activity was revealed by combining gas bubble detection using R/V METEOR's new EM 122 multibeam echosounder with analyses of water column samples, and in situ sensor data.

*This project has been supported by the European Union's Horizon 2020 research and innovation programme, GeoERA (Grant Agreement № 731166, project GeoE.171.001).*

The hydrothermal field lies at approximately 1000 m water depth, 5 km from the large Menez Gwen vent field. Bubbylon lies on talus material covering an east-facing fault scarp in the southwestern part of the axial graben, which forms part of the inner rift valley cutting through the large axial Menez Gwen volcano. The axial graben wall is a large, deep-rooted fault which is known to redirect fluids to far off-axis areas (e.g., Logatchev, TAG; McCaig et al. 2010; German et al. 2016). Redirection of fluids along the axial graben wall faults from a potential magma body at depth is supported by the detection of many additional hydrothermal bubble flairs along the axial graben walls (Dubilier and the M82/3 scientific party 2012).

The hydrothermal field have vent chimneys as high as one meter and is characterized by variable styles of venting. Tiny chimneys at the western boundary of the field are venting through talus piles masking a fault zone. Four discrete small vent sites (Piquinho West and East, Pico and Pontinho) were observed here. The main area of venting consists of the three mound-style Fontenova sites, and the associated precipitates are mineralogically similar to those of the Menez Gwen hydrothermal field. They appear to consist of sandy and slab-like material, and sampling of one of the slabs has shown that this material is dominated by hydrothermal clays. The presence of larger areas covered with oxidized slabs and small vents associated with cracks, indicate that hydrothermal activity at Fontenova is not only a very recent phenomenon, but that is has also occurred in the past (Dubilier and the M82/3 scientific party 2012). With the exception of a single small volcanic edifice, the surrounding area lacks prominent volcanic features.

The fluid sampled from the Bubbylon field has pH between 3.9 and 5.3, and contain large amounts of methane and hydrogen sulphide. The measured temperature of 253–254°C is below the boiling curve of seawater. Some vent fluids within this new area were observed to be 'flashing', which suggests that hot fluids are present at the site, but no temperature measurements has been made to confirm this (Dubilier and the M82/3 scientific party 2012).

**Lucky Strike**

The Lucky Strike Hydrothermal Field is located approximately 400 km south of the Azores on the Lucky Strike segment of the MAR (Langmuir et al. 1992). Since the identification of the hydrothermal field in the segment centre, this region has been extensively studied. Fundamental geological and geochemical understanding has been obtained through various submersible dives, mainly by French and American scientific teams using the Nautile and Alvin submersibles, respectively.

The Lucky Strike segment (PO-1, Figure 3) is located between 37°00' and 37°35'N and has a total length of about 65 km. It is bound by two second-order non-transform discontinuities. Bathymetry and sidescan sonar imagery show that the segment has a large composite volcanic plateau at its centre (e.g., Fouquet et al. 1994; Langmuir et al. 1997). The segment is also characterized by a typical morphology of a slow-spreading centre having a well-developed rift valley with rectilinear and subparallel axial valley walls, characterised by large fault throws up to 1000 m. The axial valley floor is commonly flat, between 8 and 12 km wide, and up to 950 m deep, and exhibits the greatest relief both across and along axis, of any segment on this part of the MAR (e.g., Scheirer et al. 2000).

The central topographic high is made up of a composite volcano that is 13 km long and 7 km wide, and rises from a mean depth of 2200 m. It is divided into two parts separated by a N-S valley. This is one of the largest axial volcanoes within the rift valley on the MAR. The western part is an elongated narrow ridge (Western Ridge), while the eastern part has a semi-circular shape with

This project has been supported by the European Union's Horizon 2020 research and innovation programme, GeoERA (Grant Agreement № 731166, project GeoE.171.001).

three volcanic cones at its summit, that forms the north-western, north-eastern, and southern limits of the summit. The existence of a lava lake at the central part of the depression between the three summit cones was discovered during the DIVA1 cruise (Fouquet et al. 1995).

Hydrothermal activity at Lucky Strike is mainly focused in and along the sides of the solidified lava lake (Humphris et al. 2002). The most active part is on the eastern side of the lava lake. This structure has a circular shape and is about 300 m in diameter and up to 6 m deep and is found at a water depth of between 1730 m and 1736 m. Very fresh lavas with low vesicularity are present at the bottom of the lake, whereas most of the lavas of the three volcanic cones are composed of older, highly vesicular volcanic breccia. The lava lake exhibits extensive collapse structures and other volcanic features indicative of rapid eruption rates, and relatively low-viscosity lava. This area is considered to have been subjected to a relatively recent emplacement of lava, based on the freshness of the glass and relatively light dusting of sediment. In places, older collapse margins located outside the present boundary of the lava lake suggest that the summit depression has been subjected to multiple eruptions. The lava lake probably constitutes the latest eruption in this area,and seems to be characterized by multiple events (Fouquet et al. 1995).

The seamount is underlain by a 3 to 4 km wide magma chamber at about 3.5 km depth beneath the seafloor; it extends nearly 7 km along the axis (Singh et al. 2006). This magma chamber is thought to provide the heat that drives the hydrothermal flow at this site, with recharge channels most likely focused along steep faults along the axial valley walls.

Active and inactive hydrothermal deposits are distributed over a wide area of about 1 $km^2$ at shallow depths (1630-1730 m), and about 30 vent sites have been identified. Numerous inward-dipping normal faults cut the area. These faults serve as outflow conduits for fluids (Ondreas et al. 2009). Hydrothermal venting is located on extensive deposits of sulphide rubble and hydrothermally cemented hyaloclastite deposits both east and west of the lava lake (Humphris et al. 2002; Ondreas et al. 2009; Barreure et al. 2012; Mittelstaedt et al. 2012).

Hydrothermal discharge occurs as high temperature black smokers, which can reach temperatures of around 325°C. The smokers have anhydrite flange structures rich in barite, and host underlying reflecting pools of hydrothermal fluid, and iron-zinc sulphides (e.g., Langmuir et al. 1997; Von Damm et al. 1998). In the eastern zone, black smoker chimneys can be up to 20 m high, and deposits may have complex morphologies. The active vents are distributed over a wide area and hydrothermal activity appears to be episodic (e.g., Ondréas et al. 1997; Humphries et al. 2002).

The hydrothermal deposits consist of a series of sulphide mounds with numerous inactive chimneys (sulphide rubble) that cover large areas of the summit of the Lucky Strike volcano. These deposits include iron- and copper-rich massive sulphides and a typical hydrothermal slab structure (hydrothermally cemented breccia) which forms flat and layered deposits. The mounds can be up to 20 m in diameter and rise several meters above the surrounding seafloor (Barreyre et al. 2012). The most vigorous high-temperature venting (<300°C) chimneys are dominated by chalcopyrite and anhydrite, with minor iron and zinc sulphide minerals, as well as amorphous silica (Langmuir et al. 1997; Rouxel et al. 2004). Diffuse venting structures with metal-depleted fluids are predominantly composed of iron sulphide minerals and barite, while 180–220°C fluids near the bases of spires consists of barite and zinc sulphide (Rouxel et al. 2004).

Observations from dives, indicate the presence of a N-S trending swath of terrain in which the active vent sites are located. The northern part of the area is dominated by sulphide rubble, while the southern part is composed of hydrothermal slabs (e.g., Fornari et al. 1996).

This project has been supported by the European Union's Horizon 2020 research and innovation programme, GeoERA (Grant Agreement № 731166, project GeoE.171.001).

The spatial distribution and inferred volume of the sulphide rubble suggest that hydrothermal activity has occurred over a long period of time, and that active tectonism, which has clearly influenced the structural development of the central topographic high as it grew, has resulted in a relatively continuous disaggregation of sulphide structures and mass-wasting of the hydrothermal debris.

**Ewan**

The Ewan hydrothermal field was discovered during the Graviluck 2006 cruise and constitutes a new on-axis site with diffuse flow. Ewan is located at the summit of the Lucky Strike central volcano, disecting the axial graben (Escartín et al. 2014). The field is hosted by tectonic depressions about 2 km south of the main Lucky Strike hydrothermal field. The seafloor here displays a complex set of horst and graben, with numerous east- and west-verging normal faults that contain the most recent unsedimented lava flows (Escartín et al. 2014). Ewan, as the Lucky Strike main hydrothermal field, is situated immediately above the 3–3.5 km deep axial magma chamber (Singh et al. 2006)

Bacterial mats occur both along slopes and on flat-lying volcanic seafloor. Detailed observations reveal local shimmering in diffuse outflow areas at the main Lucky Strike hydrothermal field. No active nor fossil high-temperature venting has been found during the observations or in the seafloor photomosaics, suggesting that Ewan hosts only diffuse hydrothermal activity. The distribution and shape of individual bacterial patches also indicates fluid percolation through the seafloor at very slow flow rates.

Ewan may be associated with a recent magmatic event, such as the emplacement of a lava flow or dike propagation in the shallow crust, as suggested by hydrophone data (Dziak et al. 2004).

**Menez Hom**

The hydrothermal field, Menez Hom, is located on an ultramafic dome (1780–1900 mbsl) at the inside corner of the intersection of the MAR with a non-transform discontinuity separating the Lucky Strike and North Famous segments. Serpentinized mantle peridotites on the seafloor are associated with major fault systems, such as ridge axes and transform and non-transform faults. These faults favour deep circulation of seawater, and promote serpentinization of the upper oceanic mantle, and are responsible for the tectonic emplacement of the serpentinites (Costa et al., 2008).

One of the strongest $CH_4$ anomalies known from the MAR was observed in the water column at the top of the Menez Hom dome (Charlou et al. 1997), but venting is diffuse and does not exceed 10°C (Fouquet and IRIS Scientific Party, 2001). Weak $^3He$ signatures also occur in South Lucky Strike in the vicinity of the Menez Hom seepage site.

Diving operations have revealed the outcrop of ultramafic rocks at the top of the dome. No active vents have been seen. However, one small carbonate chimney was sampled and consists of calcite (dominant), aragonite, brucite and traces of quartz. Anomalous, rapid lithification of the sediment covers were observed at the northern side of the dome, near the limit between the ultramafic rocks and the basaltic cover. This may indicate a preferential discharge of diffuse low-temperature $CH_4$-rich fluids at the contact between the ultramafic and the basaltic cover (Fouquet et al. 2010).

*This project has been supported by the European Union's Horizon 2020 research and innovation programme, GeoERA (Grant Agreement № 731166, project GeoE.171.001).*

Carbonate chimneys, carbonates within sediments, and low-temperature carbonatization (aragonite) of ultramafic rocks are common at low-temperature fields, such as Menez Hom. The features are related to high calcium concentrations in fluids due to the release of Ca during serpentinization, when silicates, such as clinopyroxene, react with heated seawater (Costa et al. 2008).

**Lucky Strike Segment, southern end**

In the southern end of the Lucky Strike segment, a second order discontinuity, corresponding to a left lateral non-transform offset (NTO3) is associated with an elevated faulted massif, detached from its segment flanks. It has an irregular acoustic backscatter pattern and is, like some other discontinuities south of 38°N, consistently broader and larger, with complex structural fabrics accommodating the offset. Some of these massifs have been explored in the MAR, south of the Azores and sampled during dives. The surveys reveal that they are composed of upper mantle peridotites and lower crustal rocks, and sometimes associated with high-temperature hydrothermal venting (Grácia et al. 2000).

Water column surveys adjacent to the NTO3 massif over the eastern wall at around 1800 m depth, have revealed high $CH_4$ and total dissolvable manganese (TDM) concentrations, possibly resulting from the serpentinization process (Grácia et al. 2000).

The exposure of the ultramafic massifs within the NTOs is favoured by low magma supply and low-angle detachment faulting occurring at segment ends. The pervasive fracturing and faulting at these discontinuities favour circulation of hydrothermal fluids and occurrence of high-temperature vent sites.

**FAMOUS and North FAMOUS segments**

The Famous segment is located between 36°30’N and 37°00’N and exhibits a morphology typical of a slow spreading ridge. With isobaths reminiscent of the shape of an hourglass, it is made up by a narrow axial valley with 800 m high scarps at its centre, and deep and wide basins at its two extremities (Grácia et al. 2000).

Using transmissometer and nephelometer readings, anomalies indicating hydrothermal activity have been observed in the Famous segment (e.g., German et al. 1996). In addition, elevated dissolved methane concentrations have been observed (Charlou et al. 1993, 1996). Increment in Nephels and TDM concentrations are attributable to hydrothermal circulation in the Famous segment.

Complementary, sub-horizontal nephelo-transmissometer records on TOBI and dynamic hydrocast deployments made during the Heat Cruise detected discrete hydrothermal signals, either from vertical $CH_4$ profiles and nephelo–transmissometer signals or nephelo–transmissometer signals along TOBI profiles. Based on these local signals, dynamic hydrocasts were conducted to map hydrothermal plumes at segment scale which showed anomalies well above the seawater background in the open ocean for both Mn, $CH_4$ and $^3He$ along the FAMOUS segment. These results were interpreted to be the result of time-integrated hydrothermal discharges dispersed and mixed in a closed basin and delineated by the rift valley and the segment ends (German et al. 1996).

This project has been supported by the European Union's Horizon 2020 research and innovation programme, GeoERA (Grant Agreement № 731166, project GeoE.171.001).

A silicate hydrothermal deposit was sampled by the diving saucer Cyana in the transform fault north of the FAMOUS segment near 37°N. No tubeworms, sulphides or black smokers were found (German et al. 1996).

**Saldanha**

The Saldanha hydrothermal field is on the top of a 100 m high semi-circular NNE–SSW trending seamount at 2200–2300 m water depth. It is located about 700 m from the southern tip of the Famous segment in a non-transform offset (NTO5, between Famous and Amar segments) on the MAR (Barriga et al. 1998). This hydrothermal system was first described as a transparent low-temperature fluid discharge site with centimetre-sized vents without formation of chimney structures. The existence was inferred from geochemical anomalies, such as high concentrations of $CH_4$ and $H_2$, and low TDM in the water column (Charlou et al. 1997; Bougault et al. 1998), driven by peridotite–seawater reactions (serpentinization processes). The Saldanha hydrothermal field is hosted by ultramafic and mafic rocks, and the hydrothermal activity occurs essentially as diffuse flow over an area of at least 400 $m^2$, with more focused activity taking place through centimetre sized holes in the sediments (Dias & Barriga 2006).

It is one of the rare sites where direct evidence of low-temperature (7–9°C) hydrothermal activity has been observed. Hydrothermal fluid venting takes place through small orifices in the ocean floor sedimentary cover, which seem to form an impermeable cover blanking the system (Dias et al, 2006). The hydrothermal fluids react not only with the underlying crystalline rocks but also with the sedimentary cover. However, petrographic and geochemical studies of sediments from the vent area, reveal that hydrothermal fluids have reacted with these sediments at temperatures higher than 250 °C (Dias et al. 2010).

Mount Saldanha is a serpentinite protrusion through a section of oceanic crust (Barriga et al. 1998), consisting of a faulted massif detached from its segment flanks, almost parallel to the ridge segment. Geological mapping with direct observations and collected samples, reveals the presence of highly heterogeneous lithologies across the Saldanha massif. At the top of the seamount, there are basalts, metasomatized gabbros and basalts, serpentinites and steatites. Steatites are essentially located at the northern part of the Saldanha dome in a NE–SW elongated area. The occurrence is most probably related to a dominant fault network striking NE–SW, E–W and WNW–ESE, responsible for the exposure of ultramafic rocks. The network seems to play an important role in the hydrothermal circulation at the site (Gràcia et al. 2000). Around the Saldanha seamount fresh basalts are the dominant lithology, except at the base of the SW flank where a significant outcrop of serpentinized peridotite exposed by a NE–SW discontinuity occurs, and on the NE flank where gabbroic rocks also crop out in a scarping fault with the same orientation as the serpentinites (Dias et al. 2010).

This project has been supported by the European Union's Horizon 2020 research and innovation programme, GeoERA (Grant Agreement Nº 731166, project GeoE.171.001).

## 6.3. The Mid-Atlantic Ridge – International waters south of the Azores

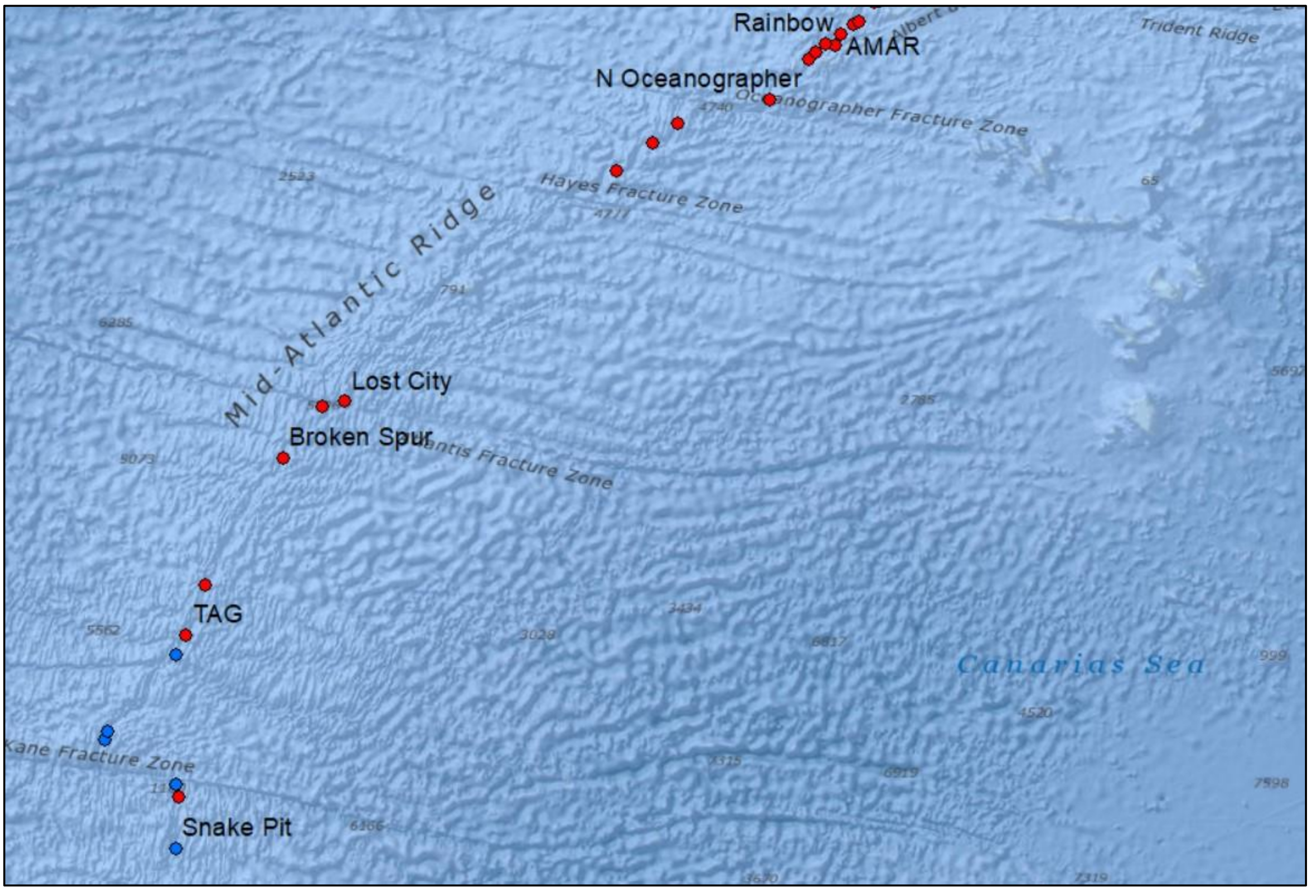


*Figure 18. Active (red) and inactive (blue) vent fields along the Mid-Atlantic Ridge. International waters south of the Azores Triple Junction. Bathymetric imagery from the EMODnet WMS service (https://www.emodnet-bathymetry.eu)*

### AMAR and South AMAR segments (Figure 18)

In contrast to the FAMOUS valley the AMAR valley is broad, U-shaped, but still has the typical shape of a slow spreading rift valley. The axial valley is 3-15 km wide with walls that rise up to 1200 m above the valley floor. The topography here is not dominated by central volcanoes but by four N-S fault-bounded ridges, which are highly fractured and dissected by orthogonal faults. The region of most recent volcanism with the least sediment cover is the symmetrical centre of the valley (Stakes et al., 1984).

Dynamic hydrocast experiments enabled recording of Mn (TDM), $CH_4$ concentrations and $^3He$ ratios through vertical cross-sections of hydrothermal plumes along the southern part of the AMAR segment. The results were well above the seawater background in the open ocean and were interpreted to be the result of time-integrated hydrothermal discharge dispersed and mixed in a closed basin, delineated by the rift valley and the segment ends (Bougault et al. 1998). Additionally, nephelo–transmissometer signals recorded from instruments attached to the side scan sonar TOBI (HEAT cruise) showed the presence of hydrothermal activity in the southern end of the AMAR segment (German et al. 1996). A 550 m thick plume (1800 to 2350 mbsl) was detected in this region during the FAZAR cruise, but the possibility that the Rainbow plume may be the source for the AMAR anomaly cannot be excluded (Chin et al. 1998).

In the South AMAR segment, south of the Rainbow offset, hydrothermal activity was indicated by anomalous nephel and light transmittance signals during the FAZAR cruise. Subsequent work and water column surveys have confirmed the hydrothermal activity. A hydrothermal anomaly was identified in the northern part of the area at 2630 mbsl (36.0830 N, 34.0830 W), isolated from the large Rainbow plume. A second anomaly (35.9670 N, 34.1830 W) showed a plume maximum at a depth of 2240 mbsl, indicating another distinct venting source (Chin et al. 1998).

**Rainbow**

The Rainbow hydrothermal vent field is an ultramafic hosted hydrothermal field located at 36°14′ N; 33°53′ W, at about 2300 m depth. It is located on the western flank of the Rainbow massif, which is a dome-shaped massif in the central part of a non-transform offset, that separates the AMAR and South AMAR second order ridge segments. Rainbow was discovered in 1997 during the French FLORES diving program, based on surveys for $CH_4$ and manganese anomalies (Charlou et al. 2002; Douville et al. 2002). In the Rainbow area, completely serpentinized peridotite outcrops covered by whitish pelagic sediments are often crosscut by normal faults, exposing the serpentinite. Basalt outcrops are found exclusively on the bottom of the South AMAR segment west of the Rainbow massif and at the easternmost section of the vent field area at the summit of the Rainbow massif.

Hydrothermal products include Cu–Zn–(Co)-rich massive sulphides with characteristics comparable to those found in mafic volcanic-hosted massive sulphide deposits. Petrography, mineralogy, and geochemistry of non-mineralized and mineralized rocks in the Rainbow vent field indicate that serpentinized peridotites host the hydrothermal vent system. Serpentinization occurred prior to and independently of the sulphide mineralization event (Marques et al. 2007).

The Rainbow vent area is a site of vigorous high temperature (~360°C, the highest temperature reported for MAR fluids) hydrothermal activity (Charlou et al. 1997; German et al. 1999). The vent area is composed of a group of at least ten black smokers extending over a surface of 200x100 m. The active venting area contains numerous active and inactive sulphide chimneys that lie on top of sulphide mounds built up mostly by the accumulation of collapsed, dead chimneys. High-temperature venting occurs along the rim of a west-facing hanging scarp of a tilted ultramafic block. The rim is cut by a network of intersecting N-S and NE-SW faults. Active venting and relict hydrothermal deposits exhibit tectonic control at a range of scales (Fouquet et al. 2010). On the western limit of the active vent area, a subvertical 25 m normal fault scarp trending N–S, reveals ultramafic rocks with visible networks of sulphide bearing veinlets, corresponding to a well-defined stockwork. All stages of a complete replacement of serpentinites by Cu-rich massive sulphides are observed in dredged samples from Rainbow (Fouquet et al. 1997; Marques et al. 2006; 2007). In the upper part of the scarp, sulphides become more abundant and are found as semi-massive sulphides. The western side of the hydrothermal field is tectonized with only low temperature diffuse discharge, and the eastern side is very active, but only with small chimneys. A second inactive site (Rainbow 2), with 2 to 3 m high chimneys is located near the top of the Rainbow ridge. In many places unusual lithification of the sediments around the active field and near the top of the Rainbow ridge, as well as several areas with dead mussels, may be related to diffusion of low-

This project has been supported by the European Union's Horizon 2020 research and innovation programme, GeoERA (Grant Agreement № 731166, project GeoE.171.001).

temperature methane-rich fluids through the sediment (Fouquet et al. 2010; Marques et al. 2006; 2007).

The vent fluids have a unique chemical composition with high chlorinity, low pH, and very high Fe, Mn, Cu, Zn, Ni and rare earth element (REE) concentrations (Douville et al. 2002). The fluids reflect the high concentrations of copper, zinc, and cobalt within the massive sulphide deposits. The fluids are also highly enriched in dissolved $CO_2$ and $CH_4$, and they have extraordinarily high concentrations of $H_2$ (Charlou et al. 2002), resulting from phase separation at depth (Fouquet et al. 1997; Douville et al. 2002). The Rainbow vent field area has been subjected to extensive surveys of water column chemistry and plume paths and have revealed the strongest thermal and chemical output recorded along the Mid-Atlantic ridge (e.g., German & Parson 1998). The fluid chemistry is also reflected in the surrounding hydrothermal sediments recording significant input of Fe, Mn, Cu and REE (Chavagnac et al. 2005; Dias and Barriga, 2006). The high $CO_2$ concentrations and the elevated temperatures most likely reflect the presence of a high-temperature gabbroic heat source in the subsurface (Marques et al. 2007). The high $CH_4$ and $H_2$ concentrations are now recognized as signatures of venting systems impacted by fluids interacting with ultramafic rocks (Charlou et al. 2002).

**N Oceanographer, S Oceanographer, S OH-1 and S OH-2**

The Mid-Atlantic Ridge between the Hayes and Oceanographer fracture zones is segmented into three major spreading centres (Figure 3) with distinctly different axial morphologies and gravity signatures. All segments are separated by small, 35 km offset, non-transform discontinuities.

Segment OH-1 is a long and robust segment with a wide and shallow axial valley floor. Sidescan sonar data and submersible observations support the inference that this segment is characterized by intense volcanic activity concentrated primarily at the segment centre. Robust off-axis seamount chains have been identified, and the segment is associated with one of the largest mantle Bouguer anomalies (MBA) of the northern MAR (Detrick et al. 1997). The eastern flank of the median ridge is irregular and steep, characterized by recent tectonic activity and fault scarps, and exposed sections of pillow lava and breccia with fresh talus at the base. At mid slope, 1900 mbsl, extinct hydrothermal chimneys and white hydrothermal deposits have been observed (Gracia et al. 1998).

Through vertical hydrocasts made during FAZAR expedition, small anomalies in $CH_4$ concentrations were measured in two non-transform discontinuities. The first between OH-1 and OH-2, in NTO8, and a second between OH-2 and OH-3 in NTO9. Both are at depths over 3000 mbsl. Serpentinites are exposed in the massifs located in the latter non-transform discontinuity (Gracia et al., 1998).

Several water column surveys were conducted in the Oceanographer Fracture Zone region and provide evidence for hydrothermal activity in the North Oceanographer PO-8 segment, and South Oceanographer (OH-1 segment). Very small plumes were measured by the nephelometer at 2200 and 3300 m within this region (Chin et al. 1998).

**Several occurrences in MAR south of 30ºN (“MAR, 30 N”, “MAR, 27 N”, “MAR, 25 50 N’”, “MAR, 22 30’N”, “MAR, 24 20’N”, “MAR, 23 35’N” and “MAR, 24 20’N”)**

A survey along the axis of the slow-spreading MAR between 27 and 30°N using a combination of geophysical imaging and geochemical sensing identified two areas as possible sources for hydrothermal activity. The areas are located in the first-order mid-ocean ridge segment lying between the Kane and Atlantis fracture zones (occurrences referred in InterRidge Vents Database as “MAR, 30°N” and “MAR, 27°N”). During the CD76 cruise (RRS Charles Darwin) the presence of a high-temperature hydrothermal vent field, Broken Spur (see below), was also identified. The anomalies at 30°N were detected in the nodal deep basin at the western ridge-transform intersection of the Atlantis Fracture Zone. Signals were limited to manganese enrichments but without corresponding particulates. Three hypotheses have been proposed to explain these anomalies: (1) an old, or (2) distal hydrothermal plume, or (3) a manganese-rich fluid emission from serpentinization reactions. At 27°N, a weak signal of particulate-rich water was observed 250 m above the axial valley floor. However, no corresponding manganese anomaly was observed (Murton et al., 1994).

Vertical profiles of manganese concentrations in sea water above the rift valley in the Kane FZ region showed the presence of two anomalies: one north of Kane FZ (referred in InterRidge Vents Database as “MAR, 25 50’ N”) and a second further south (“MAR, 22 30’N) (Klinkhammer et al. 1985). In both places, disseminated sulphides and quartz veins were identified in a greenstone breccia in a fault zone between fault blocks of a topographic high (Rona 1984).

At the “MAR, 24 20’” site, in the first segment just north of Kane FZ, dredging on the east wall of the rift valley brought up tholeiitic basalts that have undergone hydrothermal alteration forming chlorites, analcime, calcite, and quartz-rich rocks, as well as disseminated and vein sulphides. The quartz is a late remobilization product occurring in cracks and vugs as massive fillings and euhedral crystals. Oxygen-isotope thermometry indicates that the quartz was deposited from hydrothermal solutions comprising either sea water at 200°C or primary water at 330°C, consistent with a history of intense hydrothermal activity. The selection of the dredge site was based on magnetic and structural characteristics (Rona et al. 1980; Rona 1984).

At “MAR, 23 35’”, greenstone breccias have been recovered. A suite of quartz-cemented, pyrite and chalcopyrite bearing breccias was dredged from the east facing wall in the central graben 10-15 km south of the eastern intersection with the transform fault. Slab-like breccias were also recovered from various adjacent locations, consisting essentially of quartz, sulphides and chlorite, resembling samples from stockwork vein systems subjacent to massive sulphide deposits. These brecciated, quartz-cemented greenstones have been formed along, and are exposed by, zones of movement on the bounding faults of the shallow, active, interior corner of the ridge-transform intersection. Salinities determined from fluid inclusion studies are much higher than those of normal seawater and most likely require subsurface hydrothermal fluid temperatures in the range 400-500°C (Delaney et al. 1987; Rona 1984).

Finally, a vent site, “MAR, 24 20’ N”, has been identified at 3900 mbsl and is considered inactive (e.g. Tivey & Dyment 2010; Rona 1984).

**Lost City**

The Lost City vent field was discovered in 2000 during a cruise to investigate the Atlantis Massif at the intersection of the MAR and the Atlantis Transform Fault. The Atlantis Massif rises nearly 4 km above the surrounding seafloor over a horizontal distance of 20 km. The massif is not formed by volcanic activity but by extreme crustal extension and long-lived faulting and uplift associated with a major detachment fault. Variably metamorphosed peridotite and gabbro rock types are exposed on the seafloor (Kelley et al., 2001).

*This project has been supported by the European Union's Horizon 2020 research and innovation programme, GeoERA (Grant Agreement № 731166, project GeoE.171.001).*

Lost City is distinctly different from all other known seafloor hydrothermal fields in that it is located on 1.5 Myr old crust, nearly 15 km from the spreading axis, and the field may be driven by the heat from exothermic serpentinization reactions between sea water and mantle rocks. Lost City is dominated by steep-sided pinnacles composed entirely of carbonate and magnesium hydroxides that extend for at least 400 m. There are at least 30 active and inactive structures on the site (Kelley et al. 2001).

Located at 750 m depth, the Lost City field resides on a fault bounded promontory on the south face of the Atlantis massif (Kelley et al. 2005). It is underlain by a 100 m thick, mylonitic, low-angle detachment zone composed predominantly of altered ultramafic rocks with lesser gabbroic material (Kelley et al. 2001; 2005; Boschi et al. 2006).

In clear contrast to the high-temperature acidic fluids in black smoker systems, the carbonate chimneys at Lost City vent 50–90°C, high-pH (9–11) fluids, that are particle free. The heat source required to drive the hydrothermal flow is most likely derived from cooling of the crustal rocks that make up the massif, with lesser contributions from exothermic reactions in the underlying mantle rocks (Kelley et al. 2001, 2005; Früh-Green et al. 2003).

**Broken Spur**

Broken Spur is located in a second order segment approximately 100 km south of the Atlantis Fracture Zone at around 3000 mbsl. At least five sulphide mounds occupy the vent field. Two weathered mounds aligned at 110° and expelling low temperature (<50°C) vent fluids, and three mounds, located 150 m to the south, venting high-temperature fluids up to 365°C. The mounds are aligned across an axial summit graben that lies along the crest of a neovolcanic ridge within the axial valley floor. The neovolcanic ridge is parallel to the axis of the MAR and lies along the western side of the axial valley. The largest high-temperature venting sulphide mound, which is up to 40 m high, lies in the centre of the graben. Two further, but smaller, high-temperature sulphide mounds are located to the east and west of the larger mound. All three high-temperature venting mounds lie on an axis that strikes 115°C orthogonal to the trend of the axial summit graben and the neovolcanic ridge. The directions are parallel to the strike of two sets of faults that intersect the vent field and may have controlled the hydrothermal activity (Murton et al., 1994; 1995)

The graben walls are covered by fresh and unbroken pillow lavas, but around the hydrothermal vents the lavas are dominantly lobate, suggesting more rapid or voluminous eruptions. Weathered hydrothermal sediments, first seen within 50 m of the vents, rapidly increase in thickness to at least several tens of centimetres at the base of the sulphide mounds. Weathered sulphide rubble deposits are observed in the vicinity of the vents with shimmering water escaping from between blocks. Anhydrite deposits have been seen in association with flange structures (Murton et al. 1995).

The size, shape, and state of alteration of the sulphide mounds and the extent of their oxyhydroxide sediments and weathered sulphide talus aprons, suggest that hydrothermal activity at the Broken Spur vent field has been long-lived, probably lasting several thousand years. The activity is suggested to be controlled by a combination of recent volcanic and tectonic activity (Murton et al., 1995).

*This project has been supported by the European Union's Horizon 2020 research and innovation programme, GeoERA (Grant Agreement № 731166, project GeoE.171.001).*

**TAG**

TAG is the largest single known vent deposit along the mid ocean ridge system and is located at water depths ranging from 3430 to 3670 m on the eastern and shallowest part of a 75 km long, second order spreading segment. The segment is bounded by two right-lateral non-transform discontinuities. The TAG segment is characteristic of most slow-spreading ridge segments, having a fault-bounded graben, bound by abyssal hills and faults forming a deep axial valley that hosts a neovolcanic zone comprising young lavas, hummocky volcanic ridges, and isolated volcanoes (White et al. 1998). TAG is one of the best studied hydrothermal systems on the MAR and is one of only a handful of hydrothermal sites drilled by the Ocean Drilling Program (ODP Leg 158).

TAG hosts both low- and high-temperature zones of venting, and also two major areas of extinct sulphide deposits, which have been mapped in a 5 km by 5 km area (Rona et al. 1984; 1993; Humphris & Tivey 2000). Four main areas of hydrothermal deposits have been mapped. These include:

(1) the active TAG mound hosting numerous high-temperature chimneys; (2) the Alvin Zone, composed predominantly of isolated sulphide outcrops, relict sulphide mounds, and an active mound, 150 m in diameter and 68 m high, venting low-temperature fluids (Humphris & Tivey 2000); (3) a low-temperature zone on the eastern medial valley wall approximately 4 km east of the active TAG mound (Rona et al. 1993; Humphris & Tivey 2000); (4) the MIR zone, located on the lower portion of the eastern valley wall c. 2 km E-NE of the active TAG mound (Humphris & Tivey 2000). The MIR zone includes discontinuous sulphides and low-temperature deposits.

The TAG mound is 200 m in diameter and 50 m high and was probably formed by individual venting structures that combined into one deposit over time. Most of the mound is composed of massive sulphide blocks and debris from black and white smokers that is variably cemented and hydrothermally recrystallized (Hannington et al. 1998; Humphris & Tivey 2000). The combination of faulting, deep-seated intense seismicity, and perhaps a magma reservoir at more than 7 km below the ocean floor, may have led to the development of the immense TAG sulphide deposit (Canales et al. 2007).

Active venting occurs in a black smoker complex at the mound summit with spire-shaped chimneys that vent copper-rich fluids at temperatures up to 363°C. Abundant zinc-rich white smokers are also present discharging fluids that range in temperature from 265°C to 300°C (Charlou et al. 1996). In addition to these sites, diffuse venting fluids locally percolate through the top and sides of the mound. Steep-sided ramparts of variably oxidized sulphide blocks and hydrothermal sediment form the sides of the mound (Murton et al. 2019).

TAG is one of the few sites on the MAR where information is available about the subsurface geometry of the upflow zone. Results from Ocean Drilling Program Leg 158, indicate that the deposit is underlain by a cylindrical pipe or silicified-pyritized stockwork system that is 80 to 100 m in diameter (Hannington et al. 1998). The mound and its underlying network of channels are believed to contain about 3.9 million tons of massive sulphide (Hannington et al. 1998). The large intersecting faults are inferred to have channelled flow to the hydrothermal mound episodically over a 40,000 - 50,000-year period (Humphris & Kleinrock 1996). The long history of venting at TAG and the acidic nature of the fluids has led to a mineralogically zoned deposit and remobilization of many of the metals.

*This project has been supported by the European Union's Horizon 2020 research and innovation programme, GeoERA (Grant Agreement № 731166, project GeoE.171.001).*

**Snake Pit**

The Snake Pit Hydrothermal Site lies on the axis of the MAR at 23.3683°N, about 30 km south of the Kane Fracture Zone. Active black smokers and a surrounding field of hydrothermal sediments occur at the crest of a local peak of a volcanic constructional ridge at a depth of 3450 m. The vent field is at least 600 m long and up to 200 m wide and is covered by a thick blanket of stained hydrothermal sediments and basalts. Both active and extinct vents are located along the crests of steep-sided up to 40 m high sulphide mounds composed of massive sulphide blocks derived from collapsed chimneys. High-temperature (350°C) fluids are venting from black smoker chimneys, and low-temperature (226°C) fluids seep from sulphide domes and subordinate anhydrite constructions. Polymetallic sulphides have been recovered from the black smokers and consists of chalcopyrite, sphalerite, pyrite with paragenetic isocubanite, minor pyrrhotite and marcasite. Some of the sulphides are altered and contain bornite and covellite. Zinc sulphide occurs at the lower temperature vents. The inactive vents have been subject to weathering and diagenesis and have developed smooth coatings of amorphous iron oxides (Karson & Brown 1988).

The mounds are surrounded by what appears to be a continuous blanket of hydrothermal sediments with a distinctive mottled orange to green surface. They are very fine grained and form a smooth surface. Identified minerals include pyrrhotite, chalcopyrite, marcasite, pyrite and minor amounts of sphalerite (Karson & Brown, 1988).

## 6.4. Intra-plate hotspots: Canary Islands

Hydrothermal mineral deposits related to an intra-plate hotspot are present in the Canary Islands Seamounts Province (Figure 5). In this area three different hydrothermal deposits have been identified, each of them linked to a different mineral commodity and genetic process: Authigenic sulphates, hydrothermal sulphides and hydrothermally derived iron oxyhydroxides.

On the Henry Seamount summit, authigenic barite precipitated during hydrothermal emissions at different vents. Dredging on the summit of the seamount retrieved shells of a bivalve (Abyssogena) that is known to live in symbiosis with sulphide-oxidizing bacteria and are found exclusively in habitats around hydrothermal vents and cold seeps (Krylova et al. 2010; Klügel et al. 2011). Mineralogical and chemical analyses of the barites show a purity exceeding 98 % with some replacements of barium by strontium (3–4 mole%) (Klügel et al. 2011). The isotopic ages obtained for the deposit suggest a Quaternary age for the barite, which was later covered by a thin patina of sediments and a coral system (Klügel et al. 2011).

On the Tagoro Volcano, formed after the 2011 eruption at the El Hierro Island, different sulphides (essentially pyrite and chalcopyrite) have been identified filling vesicles and fractures in the basanite rock, and Fe oxyhydroxides precipitated during the hydrothermal venting (Somoza et al. 2017; González et al. 2020). Pyrite grains and filled fractures have been analysed with electron probe microanalyzer (EPMA), and the results show that pyrites are enriched in Nickel, Cobalt, and Bismuth (averages of 2600, 2100 and 1700 ppm resp.). Nickel concentrations up to 3.3 wt.% have been obtained in individual points (González et al. 2020). The iron oxyhydroxides show a significant enrichment in iron (28-58 wt. %), with less silicon (up to 11.3 wt. %) and $P_2O_5$ (1.4–5.1 wt.%). These hydrothermal iron oxyhydroxides have low contents of valuable metals, and the most enriched sample has concentrations of V, Cu, Sr, As, Ba, and Ni of 737, 584, 334, 318, 147 and 102 ppm resp. (González et al., 2020). The REY concentrations in these minerals are very low (15-57 ppm) and the

This project has been supported by the European Union's Horizon 2020 research and innovation programme, GeoERA (Grant Agreement № 731166, project GeoE.171.001).

presence of a slightly positive europium anomaly with a negative Ce anomaly, when compared to the PAAS standard, is typical for hydrothermally precipitated oxyhydroxides.

Similar hydrothermal iron oxyhydroxides have been found in several samples recovered from the Drago and Tropic seamounts (Figure 5). These deposits have iron contents similar to the Tagoro Volcano, with high iron (56 and 38 wt. % resp.), less silicon (3 and 2 wt. %), and the Tropic sample has a slightly elevated concentration of $P_2O_5$ reaching 4 wt. %. The iron oxyhydroxides from the Drago and Tropic sites also show low concentrations of trace metals, but with slight enrichments the Tropic sample and concentrations of Co, Ni, Mo, and REY of 490, 400, 50 and 450 ppm resp. (Marino et al. 2019; Marino 2020).

Finally, in the seamounts East of Lanzarote (Picoletino and East Lanzarote seamounts) hydrothermal deposits were found during the SUBVENT2 survey (Somoza et al. 2014). These deposits are essentially metalliferous sediments and mineralised basalts discovered and dredged from the flanks of the seamounts. One of the samples from the Picoletino Seamount was analysed and probably represents debris from a hydrothermal mound with magnetite and sulphides, the latter containing sphalerite, covellite and bornite. Geochemical analyses reveal high contents of Si (15 wt. %), Fe (12 wt. %) and S (2 wt. %), with also high Ca and Mg (7.5 and 7 wt. % respectively) probably linked to the presence of carbonates (MINDeSEA, 2021). The sample is relatively poor in trace metals, with the highest contents represented by V, Co, Cu, Ni and REY (110, 70, 40, 45, 70 ppm resp.) (MINDeSEA, 2021).

## 6.5. Mediterranean arc/back-arc deposits: Aeolian and south Tyrrhenian Seamounts

In the Aeolian archipelago and south Tyrrhenian Sea (Figure 19) several seamounts have been discovered related to the subduction-induced magmatic activity in the SE Tyrrhenian Sea (Dekov et al., 2004). Two main deposit types are found in the South Tyrrhenian Sea, linked to past and ongoing hydrothermal activity: hydrothermal oxyhydroxides and sulphides.

Hydrothermal oxyhydroxides can be divided into metalliferous sediments, crusts, nodules, and veins within the sediments.

This project has been supported by the European Union's Horizon 2020 research and innovation programme, GeoERA (Grant Agreement № 731166, project GeoE.171.001).

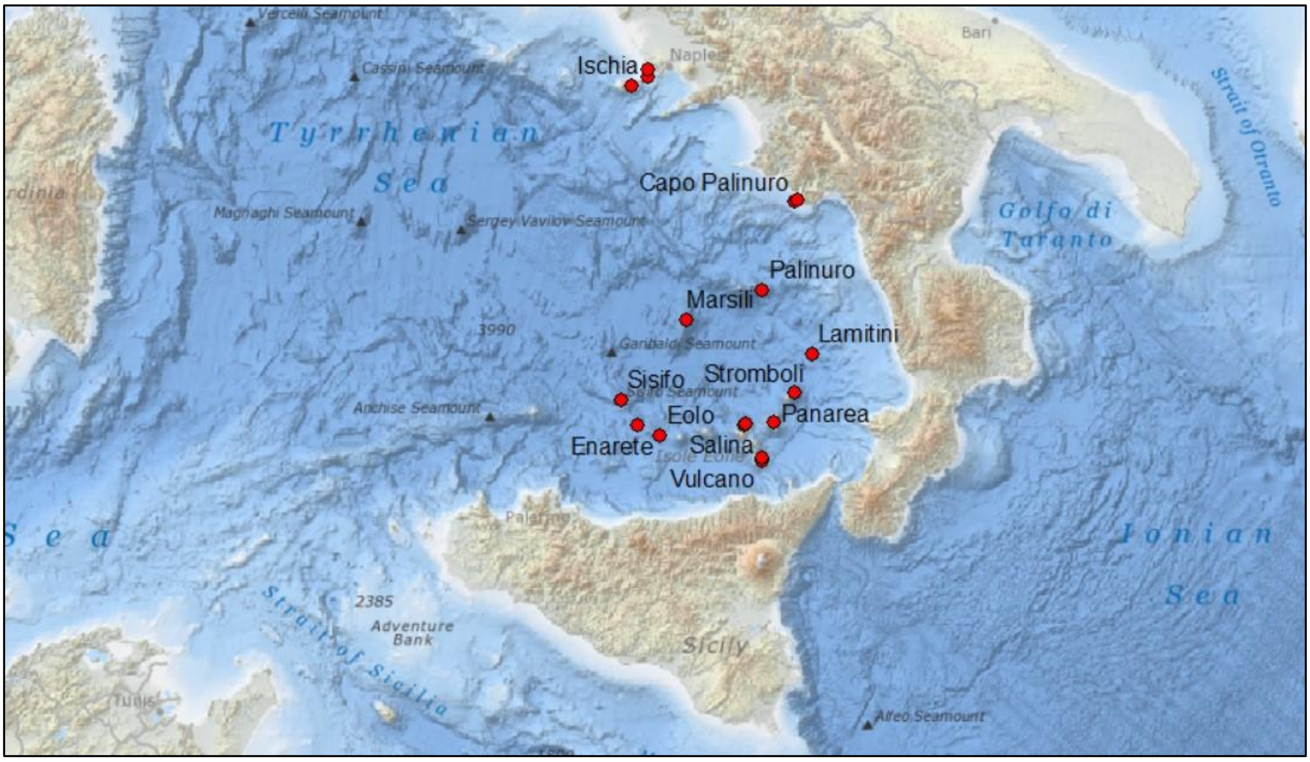


*(Figure 19). Hydrothermal deposits in the South Tyrrhenian Sea. Bathymetric imagery from the EMODnet WMS service (https://www.emodnet-bathymetry.eu)*

*Metalliferous sediments*

Deposits of metalliferous sediments have been discovered at different sites around the Aeolian archipelago and on the Marsili seamount slightly north of the Aeolian Arc (Figure 18). Samples were dredged on the flank and summits of number of seamounts (Eolo, Palinuro, and Marsili seamounts), but also in the submarine portion of the Stromboli, Panarea and Salina complexes. All deposits of metalliferous sediments are linked to the hydrothermal discharge of metals rich fluids (Dekov and Savelli 2004). South Tyrrhenian metalliferous sediments can be found as loose to semi-lithified, sometimes layered and rarely massive deposits, forming yellow reddish to brown patches on the seafloor. The main mineral phase is amorphous goethite (FeOOH), with amorphous silica, todorokite, birnessite, and iron-rich phyllosilicates (Fe-montmorillonite) (Dekov and Savelli 2004). Minor minerals include calcite, quartz, volcanic glass, and various micas. The sediments range from almost pure iron endmembers (Mn/Fe = 0.01) to manganese sands (Mn/Fe = 44) with a mean Mn/Fe value of 3.2 which reflect that the ore forming hydrothermal fluids were mostly manganese dominated. The concentrations of trace metals, such as Cu, Ni, Co, V, Pb and REY in the sediments, are very low (90, 177, 125, 200, 50 and 100 ppm resp.) essentially due to the rapid deposition of these sediments, and the precipitation of certain elements as sulphides (e.g., PbS and ZnS). Plotting the geochemistry of the sediments in the Mn-Fe-(Co+Ni+Cu) X 10 ternary diagram of Bonatti et al. (1972) confirms their hydrothermal origin (Dekov and Savelli 2004).

*This project has been supported by the European Union's Horizon 2020 research and innovation programme, GeoERA (Grant Agreement Nº 731166, project GeoE.171.001).*

*Iron-manganese crusts*

Hydrogenetic-hydrothermal iron-manganese crusts have been found covering flanks and summits of several seamounts in the Aeolian archipelago (Lametini, Eolo, Enarete, and Palinuro seamounts), as well as on the submarine volcanic complex of Panarea and Secca del Capo. Apparently, sedimentation rates have been low enough to allow the accretion of these deposits, generally found on hard substrates or forming thin crusts covering sediments (Dekov and Savelli 2004). Fe-Mn crusts are dark brown to black deposits with thicknesses up to 80 mm and a botryoidal surface. The main mineralogy consists of manganese oxides (essentially todorokite, birnessite and vernadite) and goethite and other amorphous FeOOH-minerals, with minor amounts of quartz, calcite, plagioclase, and clays. The geochemistry is dominated by iron and manganese (15 and 12 wt. % in average resp.), with a mean Mn/Fe value of 127. However, the two elements show a large spread in concentrations from 0.01 to 50 wt. %, varying from purely iron endmembers to purely manganese endmembers (Dekov and Savelli 2004). The average manganese enrichment could be product of diagenetic processes, but the low contents of typical diagenetic elements, such as Ni, Cu and Co (185, 99 and 84 ppm average resp.) does not support this origin. The high Mn/Fe ratio, even if partially due to local diagenetic laminae, reflects the manganese enrichment of the hydrothermal fluids (Lowell et al. 1995; Dekov and Savelli 2004). Other trace elements, such as V, Pb, Ba, Zn, and REY are also present in small concentrations (169, 28, 900 and 75 and 200 ppm average resp.). REYs confirm the predominantly hydrothermal origin of the crusts, with no or a weakly positive Ce anomaly and a slightly positive Eu anomaly, which suggest hydrothermal precipitation with a subsequent hydrogenetic accretion. Similar characteristics have also been seen in the Canary Island seamounts (von Damm 1995; Dekov and Savelli 2004; Marino et al. 2019).

*Iron-manganese nodules*

Deposits of iron-manganese nodules have been found on the summit of the Palinuro, Eolo, and Enarete seamounts, and also near the volcanic complex around Panarea Island. These nodules vary both in size, shape and color, from greenish to yellow-brown spheroidal micro-nodules to well-formed macro-nodules, with an average diameter of 2 cm but with sizes up to 10 cm (Dekov and Savelli 2004). The internal structure is usually seen as fine concentric layers around a calcareous or volcanic nucleus. Mineralogically, the nodules are divided into two major groups: Manganese-rich dark brown to dark green nodules, made up essentially of todorokite, birnessite and vernadite with minor amorphous FeOOH and goethite, quartz, calcite, and clays; iron-rich green yellowish to red-brown nodules, composed mainly of amorphous FeOOH, goethite and smectite, with low contents of the manganese oxides vernadite, todorokite, and birnessite. Nodule geochemistry is dominated by manganese (31 wt. %) with minor iron (5 wt. %), and slightly elevated Si, Ca, and Mg (5, 4.5 and 2.5 % resp.), the latter three probably due to different nuclei. Trace metals are low, except for Ba, Mo and Zr which reach 2400, 370 and 900 ppm resp., whereas concentrations of Co, Ni, and Cu are two orders of magnitude lower than what is found in open ocean hydrogenetic-diagenetic nodules (average of 86, 390 and 220 ppm resp.), even if Cu and Ni may reach concentrations of 1250 and 3400 ppm resp. (Dekov and Savelli 2004). When plotted in the Bonatti et al. (1972) diagram, South Tyrrhenian nodules primarily fall in the hydrothermal field, but on the Mn side, there is an overlap with diagenetic origins. There is no doubt that these nodules formed by early remobilization of elements within the sediments, but their composition is clearly different from the hydrogenetic-diagenetic nodules. The compositional data therefore supports a hydrothermal-diagenetic origin.

*This project has been supported by the European Union's Horizon 2020 research and innovation programme, GeoERA (Grant Agreement № 731166, project GeoE.171.001).*

REY are also low, with mean concentrations of 60 ppm, negative Ce and slightly positive Eu anomalies, which also confirm their hydrothermal origin (Dekov and Savelli 2004).

*Sulphides*

Hydrothermal sulphides are linked to the presence of vents on the summits of seamounts, such as the Palinuro and Marsili, but also in the submerged basal complex around the island Vulcano, and in the area between Panarea and Basiluzzo islet (Dekov and Savelli 2004). Samples consist of sand sized (0.25 to 2 mm) sulphide and sulphate grains within the sediments, and porous and layered decimeter sized pieces. The main sulphides in both deposit types are pyrite and marcasite, which can be found with several morphologies: colloform masses, replacements of grains, well-formed crystals, infilling cement, and spherules with different morphologies (radial, framboidal and massive). Other sulphides are dominated by zinc sulphides (primarily sphalerite, schalenblende, and rarely wurtzite), and galena is a major component in the Palinuro Seamount and in the area close to Panarea. Zinc sulfides form euhedral crystals, aggregates or colloform masses intergrown with other sulphides. Galena form perfect single crystals but also aggregates, colloform masses and rhythmic alternations with other sulphides. Chalcopyrite may also be present (Dekov and Savelli 2004).

A wide spectrum of sulfosalts and selenides are found with the sulphides, which are not common in sulphides along mid ocean ridges. The most important are tetrahedrite-tennantite, enargite, covellite, stibnite, bismuthinite, and proustite. Tyrrhenian massive sulphides are rich in several base and critical elements, such as Zn, Pb, Ba, As, Sb, Hg, Ag and Au, (11.5, 6.7, 15.8, wt. % and 3000, 1300, 1500, 280, 3 ppm resp.) but poor in Cu and Fe (4800 ppm and 16 wt. % resp.) (Dekov and Savelli 2004).

## 6.6. Mediterranean arc/back-arc deposits: Cyprus and Greece

In the Greek and Cypriot archipelagos several submarine volcanoes and seamounts have been found hosting occurrences of hydrothermal iron-manganese oxyhydroxides and sulphides (Hein and Mizzel 2013).

*This project has been supported by the European Union's Horizon 2020 research and innovation programme, GeoERA (Grant Agreement № 731166, project GeoE.171.001).*

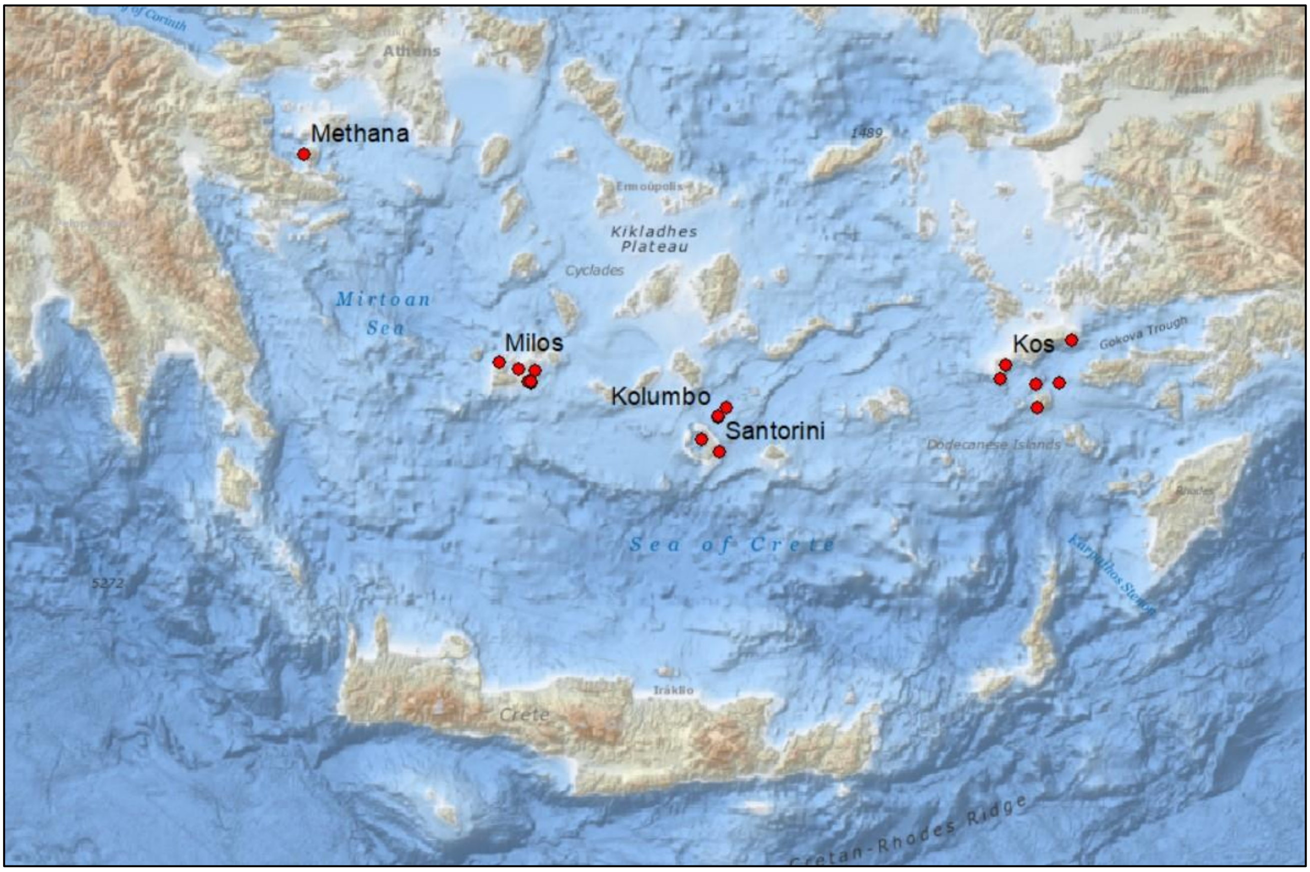


*Figure 20. Active vent fields along the active volcanic arc in the Aegean Sea. Bathymetric imagery from the EMODnet WMS service (https://www.emodnet-bathymetry.eu)*

Several occurrences of hydrothermal mineralisations have been found around the Kolumbo Volcano near the island of Santorini (Figure 20). These deposits form chimneys and iron-rich sediments covering the summit of the volcano (Kilias et al. 2013). Sampled chimneys display an inner sulphide and sulphate layer covered by a few mm thick layer rich in iron oxyhydroxide. Iron oxyhydroxides are made up primarily by biogenic ferrihydrite, jarosite, and goethite. Sulphides are generally pyrite, galena, and sphalerite, with elemental concentrations of 1 wt. % Zn (max: 6 wt. %), 0.16 wt. % Cu (max: 0.37 wt. %), and 3.4 wt. % Pb (max: 6.7 wt. %). The total iron content in sulphides and iron oxyhydroxides varies from 9 to 31 wt. % (Kilias et al. 2013). The sum of Zn, Cu and Pb is on average less than 4.5 wt. % and lower than most marine sulphide deposits, which probably indicates lower temperature venting. The Kolumbo deposit has interesting concentrations of Sb, Ag and Au (averages of 5000, 630 and 10 ppm resp.) (Kilias et al. 2013).

A similar sulphide deposit has been found on the Milos Island. This deposit has an epithermal origin and the studied mineralization is actually located around 500 m above sea level (Naden et al. 2005). The main mineralogy consists of altered rhyolitic tuffs containing pyrite, chalcopyrite, sphalerite, galena, marcasite, tetrahedrite, native gold and electrum. The gold is found in the upper part near the boiling zone (Naden et al. 2005). The Milos deposit is part of a two-component active geothermal system containing a high-enthalpy, high-salinity system 1-2 km below sea level, with temperatures of 250-300 °C and an average 9 wt. % salts, and a shallow reservoir with lower temperatures (100-175 °C) located near the sea level. The fluids are essentially seawater which are enriched in Fe, Mn, Si and Ba in the shallow system (Hein et al., 2000; Naden et al. 2005).

A fossil hydrothermal manganese deposit is present at Vani Cape on Milos. The deposit is close to the sea with its basal part under water and the upper part reaching a height of 35 m a.s.l. The Vani Cape deposit is a fossil, Upper Pliocene (3.5-2 Ma), stratabound hydrothermal deposit formed in volcanic sandstone, which was mined in the past (Hein et al., 2000; Glasbi et al. 2001; 2005). The main manganese mineralogy is made up by romanechite, pyrolusite, ramsdellite, cryptomelane, hollandite and coronadite. The geochemistry is dominated by manganese (16 to 45 wt. % with an average of 26 wt. %) and high contents of Zn and Pb (max. 1.2 and 5.1 wt. % resp.). Cu, Sr, As, and W have average concentrations of 1000, 1200, 900 and 500 ppm resp., whereas REY are low with concentrations around 100 ppm (Glasbi et al. 2005).

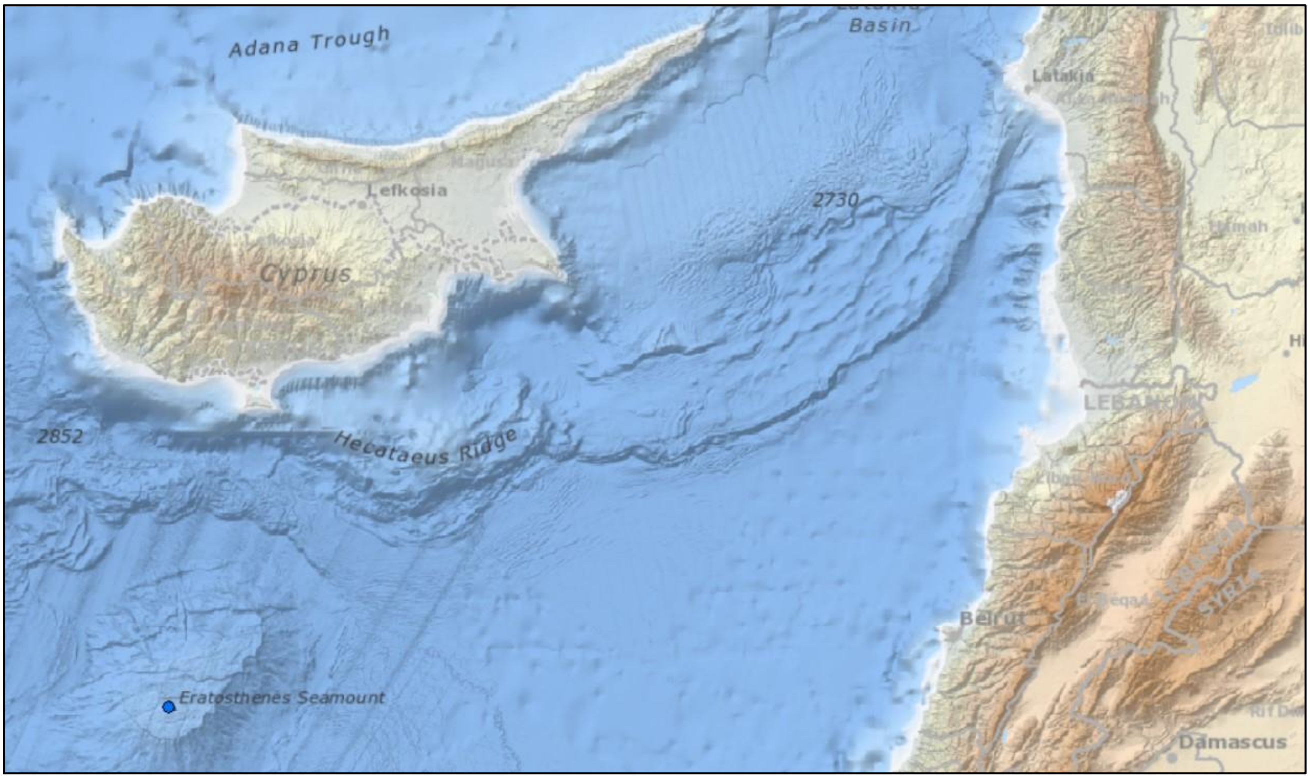


*Figure 21. Map of the Eastern Mediterranean with Cyprus and the location of Eratosthenes iron-manganese oxyhydroxide crusts on the Eratosthenes Seamount south of Cyprus. Bathymetric imagery from the EMODnet WMS service (https://www.emodnet-bathymetry.eu)*

Iron-manganese oxyhydroxide crusts forming a dark continuous deposit within marl sediments have been found around the Eratosthenes seamount (Figure 21). The iron-manganese crusts have a highly porous and layered internal structure with large quantities of granular brown iron-rich sediments within the structure. Spherules of manganese oxides (primarily birnessite) with remains of biogenic carbonates (coccoliths) have also been identified (Varnavas et al. 1988). The geochemistry is dominated by Ca (22 wt. %) derived from sediments, with subsidiary amounts of Mn, Al and Fe (9, 7.5 and 5 wt. % resp.). The crusts are characterised by high Ba and Sr (7862 and 1384 ppm resp.), whereas Co, Ni, Cu, V, and Mo, commonly enriched in Fe-Mn crusts, are low (52, 135, 167, 180 and 89 ppm resp.). The geochemical signature reflects a hydrothermal origin (Varnavas et al. 1988).

This project has been supported by the European Union's Horizon 2020 research and innovation programme, GeoERA (Grant Agreement № 731166, project GeoE.171.001).

# 7. CONCLUSIONS

Exhalative deposits have been important mining targets since pre-historic times, and also today these deposits contribute significant amounts of copper, zinc, lead, silver and gold to the global metal production. Seafloor hydrothermal or massive sulphide (SMS) deposits are analogues to the terrestrial VMS deposits and provide an emerging environment for possible future metal production. For Europe, marine hydrothermal deposits may increase self-sufficiency and provide security against disrupted supply chains affecting European production and industrial development. In addition, exhalative mineral deposits, whether on land or on the seabed, contain companion metals which are highly critical to decarbonization and future green technologies.

As marine mineral targets are being more clearly identified, characterised, and delineated, it is important to include the marine mineral potentials and identified resources in the European mineral resource inventories. Through the project, data have been collected from 153 sites under European national jurisdictions. Deposit data are collected from numerous sources and the current MINDeSEA library is based on more than 600 samples from 25 individual sites.

The current report identifies three main geodynamic settings for hydrothermal deposits in European waters:

- Mid-ocean ridge deposits related to mafic volcanism and hosted by mafic or ultramafic rocks. The most important commodities associated with this setting are copper, zinc and gold. This type of deposits is found in European jurisdictions along the Mid Atlantic Ridge from south of the Azores archipelago to the Arctic Ocean. Due to the slow spreading rate, major discoveries have been made and further discoveries may be expected.
- Intra-plate hotspot-related volcanism drives hydrothermal systems around the Canary Island archipelago. Six different deposits are recorded in the MINDeSEA library representing a large spread in mineralisation characteristics. Mineral deposits include both sulphides, sulphates and oxyhydroxides but metal content in the deposits investigated so far tend to be low.
- Hydrothermal deposits in arc/back-arc geodynamic settings are found in the Mediterranean Sea. The dominant metal commodities in deposits in the Aeolian, Tyrrhenian, and Aegean Arcs are zinc, lead, and silver, but mineralisations include also sulphates and hydrothermally generated crusts and nodules consisting of iron-manganese oxyhydroxides. The Mediterranean deposits are considered related to bimodal or felsic volcanism.

Several European countries are strongly engaged in locating and surveying for hydrothermal mineralisations on the sea floor under their national jurisdictions, and several more countries are involved in similar exploration in the high seas. Very few seabed discoveries have been characterised in any detail, and whereas the seabed is currently immature as a mining target, at least for massive sulphides, the understanding of the marine mineral potential is likely to undergo significant improvement during the coming decades. It is also important to acknowledge that better understanding of marine hydrothermal deposits has a clear potential to improve exploration models for equivalent deposits on land.

*This project has been supported by the European Union's Horizon 2020 research and innovation programme, GeoERA (Grant Agreement № 731166, project GeoE.171.001).*

# 8. REFERENCES

Aballéa, M., Radford-Knoery, J., Appriou, P., Bougault, H., Charlou, J.L., Donval, J.P., Etoubleau, J., Fouquet, Y., German, C.R., Miranda, M. 1998. Manganese distribution in the water column near the Azores Triple Junction along the Mid-Atlantic Ridge and in the Azores domain. Deep Sea Research Part I: Oceanographic Research Papers 45, 8, 1319-1338. doi: 10.1016/S0967-0637(98)80012-5.

Alagna, K.E., Peccerillo, A., Martin, S., Donati, C. 2010. Tertiary to Present Evolution of Orogenic Magmatism in Italy. Journal of the Virtual Explorer 36, paper 18. doi:10.3809/jvirtex.2010.00233

Ancochea, E., 2004. Evolución de la actividad volcánica. In: Vera, J.A. (Ed.), Geología de España. SGE-IGME, Madrid, pp. 639–641.

Barreyre, T., Escartín, J., Garcia, R., Cannat, M., Mittelstaedt, E., & Prados, R. 2012. Structure, temporal evolution, and heat flux estimates from the Lucky Strike deep-sea hydrothermal field derived from seafloor image mosaics. Geochemistry, Geophysics, Geosystems 13(4). doi: 10.1029/2011GC003990

Barriga, F.J.A.S., et al., 1998. Discovery of the Saldanha hydrothermal field on the FAMOUS segment of the MAR (36° 30’N). Eos, Transactions, American Geophysical Union 79 (45), F67.

Baumberger, T., Früh-Green, G.L., Thorseth, I.H., Lilley, M.D., Hamelin, C., Bernasconi, S.M., Okland, I.E., Pedersen, R.B. 2016. Fluid composition of the sediment-influenced Loki’s Castle vent field at the ultra-slow spreading Arctic Mid-Ocean Ridge

Beaulieu, S.E., Szafrański, K.M. 2020. InterRidge Global Database of Active Submarine Hydrothermal Vent Fields Version 3.4. PANGAEA, https://doi.org/10.1594/PANGAEA.917894

Blondel, P.h. 1996. Segmentation of the Mid-Atlantic Ridge south of the Azores, based on acoustic classification of TOBI data, in: MacLeod C.J. et al. (Eds.), Tectonic, Magmatic, Hydrothermal and Biological Segmentation of Mid-Ocean Ridge. Geological Society Special Publication 118, 17-28.

Bonatti, E., Kraemer, T., Rydell, H., 1972. Classification and genesis of submarine ironmanganese deposits. In: Horn, D.R. (Ed.) Ferromanganese Deposits of the Ocean Floor. Arden House, New York, pp. 149–165

Boschi, C., Früh-Green, G.L., Delacour, A., Karson, J.A. and Kelley, D.S. 2006. Mass transfer and fluid flow during detachment faulting and development of an oceanic core complex. Geochemistry, Geophysics, Geosystems 7(1), doi:10.1029/2005GC001074.

Bougault, H., Aballéa, M., Radford-Knoery, J., Charlou, J. L., Jean Baptiste, P., Appriou, P., … Miranda, M. 1998. FAMOUS and AMAR segments on the Mid-Atlantic Ridge: Ubiquitous hydrothermal Mn, $CH_4$, δ3He signals along the rift valley walls and rift offsets. Earth and Planetary Science Letters 161(1–4), 1–17. doi: 10.1016/s0012-821x(98)00094-6.

Canales, J. P., Sohn, R. A. and deMartin, B. J. 2007. Crustal structure of the Trans-Atlantic Geotraverse (TAG) segment (Mid-Atlantic Ridge, 26º10’N): Implications for the nature of hydrothermal circulation and detachment faulting at slow spreading ridges. Geochemistry, Geophysics, Geosystems 8(8). doi:10.1029/2007G C001629.

*This project has been supported by the European Union's Horizon 2020 research and innovation programme, GeoERA (Grant Agreement № 731166, project GeoE.171.001).*

Cardigos, F., Colaço, A., Dando, P.R., Ávila, S.P., Sarradin, P.M., Tempera, F., Conceição, P., Pascoal, A., Santos, R.S. 2005. Shallow water hydrothermal vent field fluids and communities of the D. João de Castro Seamount (Azores). Chemical Geology, 224:153-168. DOI: 10.1016/j.chemgeo.2005.07.019.

Cascão, I., Domokos, R., Lammers, M., Marques, V., Domínguez, R., Santos, R., Silva, M. 2017. Persistent enhancement of micronekton backscatter at the summits of seamounts in the Azores. Frontiers in Marine Science. doi: 10.3389/FMARS.2017.00025.

Cathles, L.M. 2011. What processes at mid-ocean ridges tell us about volcanogenic massive sulfide deposits. Mineraleum Deposita, 46, 639–657. doi:10.1007/s00126-010-0292-9

Charlou, J.L., Donval, J.P. 1993. Hydrothermal methane venting from 12ºN to 26ºN along the Mid-Atlantic ridge, Journal Geophysical Research 98, 9625–9642.

Charlou, J.L., Bougault, H., Fouquet, Y., Donval, J.P., Douville, E., Radford-Knoery, J., Aballea, M., Needham, H.D., Jean-Baptiste, P., Rona, P., Langmuir, C.H., German, C.R. 1996. Methane degassing, hydrothermal activity and serpentinization between the Fifteen- Twenty fracture zone area and the Azores Triple Junction area (Mid-Atlantic Ridge). Journal of Conference Abstracts 1, 771-772.

Charlou, J.L., J.P. Donval, E. Douville, J. Knoery, Y. Fouquet, H. Bougault, B.P. Jean, M. Stievenard, and C. R. German 1997. High methane flux between 15° N and the Azores triple junction, Mid-Atlantic Ridge; hydrothermal and serpentinization processes. Eos Trans. AGU, 78(46), Fall Meet. Suppl., F831.

Charlou, J.-L., Donval, J.-P., Douville, E., Jean-Baptiste, P., Radford-Knoery, J., Fouquet, Y., Dapoigny, A., Stievenard, M., 2000. Compared geochemical signatures and the evolution of Menez Gwen (37°50'N) and Lucky Strike (37°17'N) hydrothermal fluids, south of the Azores Triple Junction on the Mid-Atlantic Ridge. Chemical Geology 171, 49–75.

Charlou, J.-L., Donval, J.P., Fouquet, Y., Jean-Baptiste, P., Holm, N. 2002. Geochemistry of high H2 and CH4 vent fluids issuing from ultramafic rocks at the Rainbow hydrothermal field (36°14′N, MAR). Chemical Geology 191 (4), 345–359.

Charlou, J. L., Donval, J. P., Jean-Baptiste, P. Dapoigny, A. 1996. Gases and helium isotopes in high temperature solutions sampled before and after ODP Leg 158 drilling a TAG hydrothermal field (26ºN, MAR). Geophysical Research Letters 23, 3491–3494.

Chavagnac, V., German, C.R., Milton, J.A., Palmer, M.R. 2005. Sources of REE in sediment cores from the Rainbow vent site (36°14′N, MAR). Chemical Geology 216 (3–4), 329–352.

Cherkashov, G. 2017. Seafloor Massive Sulfide Deposits: Distribution and Prospecting. In: R. Sharma (ed.) Deep-Sea Mining, Springer International Publishing AG, pp 143-164. Doi:10.1007/978-3-319-52557-0_4

Chin, C.S., Klinkhammer, G.P., Wilson, C. 1998. Detection of hydrothermal plumes on the northern Mid-Atlantic Ridge: results from optical measurements. Earth and Planetary Science Letters 162(1-4), 1-13. 10.1016/S0012-821X(98)00141-1.

Cochran, J.R., Talwani, M. 1978. Gravity anomalies, regional elevation, and the deep structure of the North Atlantic. Journal of Geophysical Research 83, 4907-4924.

Costa, I.R., Barriga, F.J.A.S.V., Mellini, M., & Wicks, F. J. 2008. Antigorite in deformed serpentinites from the Mid-Atlantic Ridge. European Journal of Mineralogy 20(4), 563–572. doi: 10.1127/0935-1221/2008/0020-1808.

Couto, P.C., Rodrigues, A.S., Neto, A.I. 2015. Shallow-water hydrothermal vents in the Azores (Portugal). Journal of Integrated Coastal Zone Management, 15(4). DOI: 10.5894/rgci584.da Cruz, M.I.F.S. 2015. Mineralogy and Geochemistry of contrasting hydrothermal systems on the Arctic Mid Ocean Ridge (AMOR): The Jan Mayen and Loki's Castle vent fields. PhD thesis, University of Lisboa, 785p.

von Damm, K.L., 1995. Controls on the chemistry and temporal variability of seafloor hydrothermal fluids. In: Humphris, S., Lupton, J., Mullineaux, L., Zierenberg, R., (Eds.), Physical, Chemical, Biological, and Geological Interactions within Seafloor Hydrothermal Systems, AGU Monogr. 91, 222-247.

von Damm, K L., Bray, A.M., Buttermore, L.G., Oosting, S.E. 1998. The geochemical controls on vent fluids from the Lucky Strike vent field, Mid-Atlantic Ridge. Earth and Planetary Science Letters 160(3–4), 521–536. doi: 10.1016/S0012-821X(98)00108-3.

Dekov, V.M., Savelli, C. 2004. Hydrothermal activity in the SE Tyrrhenian Sea: an overview of 30 years of research. Marine Geology, 204(1-2), 161–185. doi:10.1016/s0025-3227(03)00355-4.

Delaney, J.R., Mogk, D.W., Mottl, M.J. 1987. Quartz-cemented breccias from the Mid- Atlantic Ridge: samples of a high-salinity hydrothermal upflow zone. Journal of Geophysical Research 92(B9), 9175–9192. doi: 10.1029/JB092iB09p09175.

Detrick, R.S., Needham, H.D. & Renard, V. 1995. Gravity anomalies and crustal thickness variations along the Mid-Atlantic Ridge between 33º and 40ºN. Journal of Geophysical Research 100, 3767-3787.

Detrick, R.S., Collins, J., Kent, G. et al. 1997. Mid- Atlantic Ridge Bull's Eye experiment: A seismic investigation of segment-scale crustal heterogeneity at a slow spreading ridge. Inter-Ridge News 6(1), 27 32.

Dias, A., Barriga, F. 2006. Mineralogy and geochemistry of hydrothermal sediments from the serpentinite-hosted Saldanha hydrothermal field (36°34’N; 33°26’W) at MAR. Marine Geology 225, 157–175.

Dias, Á.S., Mills, R.A., Ribeiro da Costa, I., Costa, R., Taylor, R.N., Cooper, M.J. 2010. Tracing fluid–rock reaction and hydrothermal circulation at the Saldanha hydrothermal field. Chemical Geology 273 (3–4), 168–179.

Dias, Á.S., Früh-Green, G.L., Bernasconi, S.M., & Barriga, F.J.A.S. 2011. Geochemistry and stable isotope constraints on high-temperature activity from sediment cores of the Saldanha hydrothermal field. Marine Geology 279(1–4), 128–140. Doi:10.1016/j.margeo.2010.10.017.

Dias, Á.A., Costa, P., Marques, A.F.A., Ribeiro, L., Madureira, P., Calado, A., Gonçalves, E., Morato, T. 2019. Geochemistry of Fe-Si-(Mn) chimneys from Luso vent field, MAR. Goldschmidt2019 Abstract 795.

Dosso, L., Bougault, H., Langmuir, C.H., Bollinger, C., Bonnier, O. & Etoubleau, J. 1999. The age and distribution of mantle heterogeneity along the Mid-Atlantic Ridge (31 - 41º N). Earth and Planetary Science Letters 170, 269-286.

Douville, E., Charlou, J.-L., Oelkers, E.H., Bienvenu, P., Jove Colon, C.F., Donval, J.-P., Fouquet, Y., Prieur, D., Appriou, P. 2002. The Rainbow vent fluids (36°14′ N, MAR): the influence of ultramafic rocks and phase separation on trace metal content in Mid-Atlantic Ridge hydrothermal fluids. Chemical Geology 184, 37–48.

Dubilier, N., and the M82/3 scientific party, 2012. Interdisciplinary Geological, Chemical and Biological Studies at the Menez Gwen Hydrothermal Vent Field Mid-Atlantic Ridge, at 37°50’N. Meteor-reports, No. 82, Leg 3, 1–73.

Dziak, R.P., Smith, D.K., Bohnenstiehl, D.R., Fox, C.G., Desbruyères, D., Matsumoto, H., Tolstoy, M., Fornari, D.J., 2004. Evidence of a recent magma dike intrusion at the slow spreading Lucky Strike segment, Mid-Atlantic Ridge. Journal Geophysical Research 109, B12102. doi: 10.1029/2004JB003141.

Escartín, J., Soule, S.A., Cannat, M., Fornari, D.J., Dü¸sünür, D., Garcia, R., 2014. Lucky Strike seamount: implications for the emplacement and rifting of segment-centered volcanoes at slow spreading mid-ocean ridges. Geochemistry, Geophysics, Geosystems 15 (11), 4157–4179. doi:10.1002/2014GC005477.

Escartin, J., Barreyre, T., Cannat, M., Garcia, R., Gracias, N., Deschamps, A., … Ballu, V. 2015. Hydrothermal activity along the slow-spreading Lucky Strike ridge segment (Mid-Atlantic Ridge): Distribution, heatflux, and geological controls. Earth and Planetary Science Letters, 431, 173–185. doi: 10.1016/j.epsl.2015.09.025.

Fornari, D., et al. 1996. Detailed studies of the Lucky Strike Seamount based on DSL-120 sonar, ARGO II and ROV Jason studies, Eos Trans. AGU., 77(46), Fall Meet. Suppl., F699.

Fouquet, Y., Charlou, J.-L., Costa, I.A., Donval, J.-P., Radford-Knoery, J., Pellé, H., Ondreas, H., Lourenço, N., Ségonzac, M., Tivey, M.K., 1994. A detailed study of the Lucky Strike hydrothermal site and discovery of a new hydrothermal site: Menez Gwen; preliminary results of the DIVA1 cruise (5–29 May,1994). InterRidge News 3, 14–17.

Fouquet, Y., Ondreas, H., Charlou, J.L., Donval, J.P., Radfort- Knoery, J., Costa, I., Lourenço, N., Tivey, M.K. 1995. Atlantic lava lakes and hot vents, Nature 377, 201. doi:10.1038/377201a0.

Fouquet, Y., Charlou, J-L., Ondréas, H., Radford-Knoery, J., Donval, J-P., Douville, E., Apprioual, R., Cambon, P., Pell, H., Landur, J.Y., Normand, A., Ponseveras, E., German, C., Parson, L., Barriga, F. J.A.S., Costa, I., Relvas, J.M.R., Ribeiro, A. 1997. Discovery and First Submersible Investigations on

*This project has been supported by the European Union's Horizon 2020 research and innovation programme, GeoERA (Grant Agreement Nº 731166, project GeoE.171.001).*

the Rainbow Hydrothermal Field on the MAR (36°14′ N). Eos, Trans. - Am. Geophys. Union 78 (46), 832.

Fouquet, Y., IRIS Scientific Party, 2001. IRIS Cruise Report. IFREMER.

Fouquet, Y., Cambon, P., Etoubleau, J., Charlou, J.L., Ondréas, H., Barriga, F.J.A.S., … Rouxel, O. 2010. Geodiversity of hydrothermal processes along the mid-atlantic ridge and ultramafic-hosted mineralization: A new type of oceanic Cu-Zn-Co-Au volcanogenic massive sulfide deposit. Geophysical Monograph Series 188, 321–367. doi: 10.1029/2008GM000746.

Franklin, J.M., Gibson, H.L., Jonasson, I.R., Galley, A.G. 2005. Volcanogenic Massive Sulfide Deposits. Economic Geology 100th Anniversary Volume, 523-560

Franzson, H., Robertsdottir, B.G., Fridleifsson, G.O., Hardardottir, V. 2016. Iceland. In: Boyd et al. (Eds.) Mineral Resources in the Arctic, Geological Survey of Norway, 190-207. https://www.ngu.no/upload/Aktuelt/CircumArtic/Mineral_Resources_Arctic_Mainbook.pdf

Früh-Green, G.L., Kelley, D.S., Bernasconi, S.M. et al. 2003. 30,000 years of hydrothermal activity at the Lost City Vent Field. Science 302, 495–498

German, C.R., Parson, L.M., HEAT Scienti¢c Team, 1996. Hydrothermal exploration near the Azores Triple Junction: tectonic control of venting at slow-spreading ridges? Earth Planetary Science Letters 138, 93-104.

German, C., Klinkhammer, C.P., Rudnicki, M.D. 1996. The Rainbow hydrothermal plume, 36°15′ N, MARine Geophysical Research Letters 23 (21), 2979–2982.

German, C., Parson, L. 1998. Distributions of hydrothermal activity along the Mid-Atlantic Ridge: interplay of magmatic and tectonic controls. Earth Planetary Science Letters 160, 327–341.

German, C.R., Petersen, S., Hannington, M.D. 2016. Hydrothermal exploration of mid-ocean ridges: Where might the largest sulfide deposits be forming? Chemical Geology 420, 114-126 http://dx.doi.org/10.1016/j.chemgeo.2015.11.006

Glasby, G.P., Papavassiliou, C.T., Liakopoulos, A., Galanopoulos, V. 2001. Past mining of the Vani manganese deposit, Milos Island, Greece. Proceedings of the 5th International Mining History Congress, which was held 12-15 September 2000 in Milos Island, Greece, pp 93-105

Glasby, G.P., Papavassiliou, C.T., Mitsis, J., Valsami-Jones, E., Liakopoulos, A., Renner, R.M. 2005. The Vani manganese deposit, Milos island, Greece: A fossil stratabound Mn−Ba−Pb− Zn−As−Sb−W-rich hydrothermal deposit. Developments in Volcanology 7, 255–291. doi:10.1016/s1871-644x(05)80045-2.

González, F. J., Rincón-Tomás, B., Somoza, L., Santofimia, E., Medialdea, T., Madureira, P., López-Pamo, E., Hein, J.R., Marino, E., de Ignacio, C., Reyes, J., Hoppert, M., Reitner, J. 2020. Low-temperature, shallow-water hydrothermal vent mineralization following the recent submarine eruption of Tagoro volcano (El Hierro, Canary Islands). Marine Geology 430, 106333. doi:10.1016/j.margeo.2020.106333

Goslin, J., Benoit, M., Blanchard, D., Bohn, M., Dosso, L., Dreher, S., Gente, P., Gloaguen, R., Maia, M., Oldra, J.-P., Ravilly, M. & Thirot, J.-L. 1999. Extent of Azores plume influence on the Mid-Atlantic Ridge north of the hotspot. Geology 27, 991-994.

Gràcia, E., Parson, L. M., Bideau, D., & Hekinian, R. 1998. Volcano-tectonic variability along segments of the Mid-Atlantic Ridge between Azores platform and Hayes fracture zone: Evidence from submersible and high-resolution sidescan sonar data. Geological Society Special Publication, 148, 1–15. doi: 10.1144/GSL.SP.1998.148.01.01.

Gràcia, E., Charlou, J.L., Radford-Knoery, J., & Parson, L.M. 2000. Non-transform offsets along the Mid-Atlantic Ridge south of the Azores (38°N-34°N): Ultramafic exposures and hosting of hydrothermal vents. Earth and Planetary Science Letters, 177(1–2), 89–103. doi: 10.1016/S0012-821X(00)00034-0.

Greve, S., Paulssen H., Goes, S., van Bergen, M. 2014. Shear-velocity structure of the Tyrrhenian Sea: Tectonics, volcanism and mantle (de)hydration of a back-arc basin. Earth and Planetary Science Letters 400, 45-53. http://dx.doi.org/10.1016/j.epsl.2014.05.028

Grindlay, N.R., Fox, P.J. & MacDonald, K.C. 1991. Second-order ridge axis discontinuities in the South Atlantic: Morphology, structure, and evolution. Marine Geophysical Research 13, 21-49.

Hannington, M.D., Galley, A.D., Herzig, P.M., Petersen, S. 1998. Comparison of the TAG mound and stockwork complex with Cyprus-type massive sulphide deposits. In: Herzig, P.M., Humphris, S.E., Miller, D.J., Zierenberg, R.A. (Eds.), Proceedings of the Ocean Drilling Program-Scientific Results. Texas A&M University, College Station, Texas, pp. 389–415.

Hannington, M.D., de Ronde, C.E.J., Petersen, S. 2005. Sea-Floor Tectonics and Submarine Hydrothermal Systems. Economic Geology 100th Anniversary Volume, 111–141

Hannington, M.D., Jamieson, J., Monecke, T., Petersen, S., Beaulieu, S. 2011. The abundance of seafloor massive sulfide deposits. Geology 39, 1155–1158. doi:10.1130/G32468.1;

Hannington, M.D. and Petersen, S. 2016. A Discussion Paper on Marine Minerals. National Ocean Exploration Forum October 20-21, 2016. https://oceanexplorer.noaa.gov/national-forum/media/noef2016-hannington-petersen.pdf

Hein, J.R., Stamatakis M.G., Dowling, J.S. 2000. Trace metal-rich Quaternary hydrothermal manganese oxide and barite, Milos Island, Greece. Applied Earth Science, V. 109 p. 67-76.

Hein, J.R., Mizzel, K. 2013. Hydrothermal systems and mineralization of volcanic arcs: Comparison of West Pacific and Mediterranean arcs. Geological Setting, Mineral Resources and ancient works of Samos and adjacent islands of the Aegean Sea, 26-30 August 2013, Karlovassi, Samos Island, Greece. Abstracts Book: pp 216-225.

Humphris, S.E., Kleinrock, M.C. 1996. Detailed morphology of the TAG active hydrothermal mound: Insights into its formation and growth. Geophysical Research Letters 23, 3443–3446.

Humphris, S.E., Tivey, M.K. 2000. A synthesis of geological and geochemical investigations of the TAG hydrothermal fluid: insights into fluid flow and mixing processes in a hydrothermal system. In: Dilek, Y., Moores, E., Elthon, D., Nicolas, A. (Eds.), Ophiolites and Oceanic Crust: New Insights from Field Studies and the Ocean Drilling Program. Geological Society of America, Boulder, Special Paper, pp. 213–235.

*This project has been supported by the European Union's Horizon 2020 research and innovation programme, GeoERA (Grant Agreement № 731166, project GeoE.171.001).*

Humphris, S.E., Fornari, D.J., Scheirer, D.S., German, C.R., Parson, L.M. 2002. Geotectonic setting of hydrothermal activity on the summit of Lucky Strike Seamount (37°17′N, Mid-Atlantic Ridge). Geochemistry, Geophysics, Geosystems 3(8), 1–25. doi:10.1029/ 2001gc000284

Hydes, D.J., Statham, P.J., Burton, J.D. 1986. A vertical profile of dissolved trace metals (Al, Cd, Cu, Mn, Ni) over the median valley of the mid Atlantic ridge, 43°N: Implications for Hydrothermal activity. Science of The Total Environment, 49, 133-145. doi: 10.1016/0048-9697(86)90236-6.

Ito, G. & Lin, J. 1995. Oceanic spreading center-hotspot inter-actions: constraints from along-isochron bathymetric and gravity anomalies. Geology 23, 657–660.

Juliani, C., Ellefmo, S. 2018. Probabilistic estimates of permissive areas for undiscovered seafloor massive sulfide deposits on an Arctic Mid-Ocean Ridge. Ore Geology Reviews 95, 917-930. https://doi.org/10.1016/j.oregeorev.2018.04.003

Karson, J. A., Brown, J. R. 1988. Geologic setting of the Snake Pit hydrothermal site: An active vent field on the Mid-Atlantic Ridge. Marine Geophysical Researches 10(1–2), 91–107. doi: 10.1007/BF02424662.

Karson, J.A., Kelley, D.S., Fornari, D.J., Perfit, M.R., & Shank, T.M. 2015. Discovering the deep: A photographic atlas of the seafloor and ocean crust. Discovering the Deep: A Photographic Atlas of the Seafloor and Ocean Crust. Cambridge University Press, 414 pp.

Kelley, D.S., Karson, J.A., Blackman, D.K. et al. 2001. An off-axis hydrothermal field discovered near the Mid-Atlantic Ridge at 30ºN. Nature 412, 145–149.

Kelley, D.S., Karson, J.A., Früh-Green, G.L. et al. 2005. A serpentinite-hosted ecosystem: The Lost City Hydrothermal Field. Science 307, 1428–1434.

Kilias, S.P., Nomikou, P., Papanikolaou, D., Polymenakou, P.N., Godelitsas, A., Argyraki, A., Carey, S., Gamaletsos, P., Mertzimekis, T.J., Stathopoulou, E., Goettlicher, J., Steininger, R., Betzelou, K., Livanos, I., Christakis, C., Croff Bell, K., Scoullos, M. 2013. New insights into hydrothermal vent processes in the unique shallow-submarine arc-volcano, Kolumbo (Santorini), Greece. Scientific Reports, 3(1). doi:10.1038/srep02421.

Klinkhammer, G., Rona, P., Greaves, M., & Elderfield, H. 1985. Hydrothermal manganese plumes in the Mid-Atlantic Ridge rift valley. Nature 314(6013), 727–731. doi: 10.1038/314727a0.

Klugel, A., Hansteen, T. H., van den Bogaard, P., Strauss, H., Hauff, F. 2011. Holocene fluid venting at an extinct Cretaceous seamount, Canary archipelago. Geology, 39, 855–858. doi:10.1130/g32006.1.

Krause, D.C. & Watkins, N.D. 1970. North Atlantic crustal genesis in the vicinity of the Azores. Geophysical Journal of the Royal Astronomical Society 19, 261-283.

Krylova, E.M., Sahling, H., Janssen, R. 2010. Abyssogena: A new genus of the family Vesicomyidae (bivalvia) from deep-water vents and seeps: Journal of Molluscan Studies, v. 76, p. 107–132, doi:10.1093/mollus/eyp052.

Langmuir, C.H., et al. 1993. Geological Setting and characteristics of the Lucky Strike vent field at 37º17N on the Mid-Atlantic Ridge, Eos Trans. AGU., 74(43), Fall Meet. Suppl., F99.

*This project has been supported by the European Union's Horizon 2020 research and innovation programme, GeoERA (Grant Agreement № 731166, project GeoE.171.001).*

Langmuir, C., Humphris, S., Fornari, D., Van Dover, C., Von Damm, K., Tivey, M. K., Bougault, H. 1997. Hydrothermal vents near a mantle hot spot: The Lucky Strike vent field at 37°N on the Mid-Atlantic Ridge. Earth and Planetary Science Letters 148(1–2), 69–91. doi: 10.1016/ s0012-821x(97)00027-7.

Lim, A., Brönner, M., Johansen, S.E., Dumais, M.A. 2018. Hydrothermal Activity at the Ultraslow-Spreading Mohns Ridge: New Insights From Near-Seafloor Magnetics. Geochemistry, Geophysics, Geosystems 20, 1-19. https://doi.org/10.1029/2019GC008439

Lipton, L., Gleesen, E., Munro, P. 2018. Preliminary Economic Assessment of the Solwara Project, Bismarck Sea, PNG. Technical Report compiled under NI 43-101. 242 p.

Lourenço, N., Miranda, M., Luis, J., Ribeiro, A., Mendes-Victor, L.A., Madeira, J. & Needham, H.D. 1998. Morpho-tectonic analysis of the Azores volcanic plateau from a new bathymetric compilation of the Area. Marine Geophysical Researches 20, 141-156.

Lowell, R.P., Rona, P.A., Von Herzen, R.P., 1995. Seafloor hydrothermal systems. J. Geophys. Res. 100, 327-352.

Madeira, J. & Ribeiro, A. 1990. Geodynamic models for the Azores triple junction; a contribution from tectonics. Tectonophysics 184, 405-415.

Marcon, Y., Sahling, H., Borowski, C., dos Santos Ferreira, C., Thal, J., Bohrmann, G. 2013. Megafaunal distribution and assessment of total methane and sulfide consumption by mussel beds at Menez Gwen hydrothermal vent, based on geo-referenced photomosaics. Deep-Sea Research Part I: Oceanographic Research Papers, 75, 93–109. doi.org/10.1016/ j.dsr.2013.01.008.

Marino, E. 2020. Costras de Ferromanganeso ricas en cobalto de los Montes Submarinos al Suroeste de las Islas Canarias: Mineralogía y Geoquímica de Elementos Estratégicos y Críticos. Ph.D Thesis, 502 pp.

Marino, E., González, F.J., Kuhn, T., Madureira, P., Wegorzewski, A.V., Mirao, J., Medialdea, T., Oeser, M., Miguel, C., Reyes, J., Somoza, L., Lunar, R. 2019. Hydrogenetic, Diagenetic and Hydrothermal Processes Forming Ferromanganese Crusts in the Canary Island Seamounts and Their Influence in the Metal Recovery Rate with Hydrometallurgical Methods. Minerals, 9(7), 439. doi:10.3390/min9070439.

Marques, A F.A., Scott, S.D., Gorton, M.P., Barriga, F.J.A. S., & Fouquet, Y. 2009. Pre-eruption history of enriched MORB from the Menez Gwen (37°50’N) and Lucky Strike (37°17’N) hydrothermal systems, Mid-Atlantic Ridge. Lithos 112(1–2), 18–39. doi:10.1016/ j.lithos.2009.05.026.

Marques, A.F.A., Barriga, F., Chavagnac, V., Fouquet, Y. 2006. Mineralogy, geochemistry, and Nd isotope composition of the Rainbow hydrothermal field, Mid-Atlantic Ridge. Mineralium Deposita 41 (1), 52–67.

Marques, A. F. A., Barriga, F. J. A. S., & Scott, S. D. 2007. Sulfide mineralization in an ultramafic-rock hosted seafloor hydrothermal system: From serpentinization to the formation of Cu-Zn-(Co)-rich massive sulfides. Marine Geology, 245(1–4), 20–39. https://doi.org/10.1016/ j.margeo.2007.05.007

*This project has been supported by the European Union's Horizon 2020 research and innovation programme, GeoERA (Grant Agreement Nº 731166, project GeoE.171.001).*

Marques, A.F.A., Roerdink, D.L., Baumberger, T., de Ronde, C.E.J., Ditchburn, R.G., Denny, A., Thorseth I.H., Okland, I., Lilley, M.D., Whitehouse, M.J., Pedersen, R.B. 2020. The Seven Sisters Hydrothermal System: First Record of Shallow Hybrid Mineralization Hosted in Mafic Volcaniclasts on the Arctic Mid-Ocean Ridge. Minerals 10, 439; doi:10.3390/min10050439

McCaig, A.M., Delacour, A., Fallick, A.E., Castelain, T., Früh-Green, G.L., 2010. Detachment Fault Control on Hydrothermal Circulation Systems: Interpreting the Subsurface Beneath the TAG Hydrothermal Field Using the Isotopic and Geological Evolution of Oceanic Core Complexes in the Atlantic. Geophysical Monograph Series 188. https://doi.org/10.1029/2008GM000729.

MINDeSEA, 2021. Available online at: https://geoeramindesea.wixsite.com/mindesea.

Mittelstaedt, E., Escartín, J., Gracias, N., Olive, J.A., Barreyre, T., Davaille, A., … Garcia, R. 2012. Quantifying diffuse and discrete venting at the Tour Eiffel vent site, Lucky Strike hydrothermal field. Geochemistry, Geophysics, Geosystems 13(4). doi: 10.1029/2011GC003991.

Mosier, D.L., Singer, D.A., Salem, B.B. 1983. Geologic and grade-tonnage information on volcanic-hosted copper-zinc-lead massive sulfide deposits. U.S. Geological Survey Open-File Report 83-89, 78 p.

Murton, B.J., Klinkhammer, G., Becker, K., Briais, A., Edge, D., Hayward, N., … Parson, L. 1994. Direct evidence for the distribution and occurrence of hydrothermal activity between 27°N-30°N on the Mid-Atlantic Ridge. Earth and Planetary Science Letters 125(1–4), 119–128. doi: 10.1016/0012-821X(94)90210-0.

Murton, B.J., Van Dover, C., & Southward, E. 1995. Geological setting and ecology of the Broken Spur hydrothermal vent field: 29°10’N on the Mid-Atlantic Ridge. Geological Society Special Publication 87, 33–41. doi: 10.1144/GSL.SP.1995.087.01.04.

Murton, B.J., Lehrmann, B., Dutrieux, A.M., Martins, S., de la Iglesia, A.G., Stobbs, I.J., … Petersen, S. 2019. Geological fate of seafloor massive sulphides at the TAG hydrothermal field (Mid-Atlantic Ridge). Ore Geology Reviews. doi:10.1016/j.oregeorev.2019.03.005.

Naden, J., Kilias, S.P., Darbyshire, D.P.F. 2005. Active geothermal systems with entrained seawater as modern analogs for transitional volcanic-hosted massive sulfide and continental magmato-hydrothermal mineralization: The example of Milos Island, Greece. Geology 33, 541. doi:10.1130/g21307.1.

Ondréas, H., Fouquet, Y., Voisset, M., Radford-Knoery, J. 1997. Detailed Study of Three Contiguous Segments of the Mid-Atlantic Ridge, South of the Azores (37° N to 38°30’ N), Using Acoustic Imaging Coupled with Submersible Observations. Marine Geophysical Research, 19(3), 231–255. doi:10.1023/A:1004230708943.

Ondréas, H., Cannat, M., Fouquet, Y., Normand, A., Sarradin, P. M., & Sarrazin, J. 2009. Recent volcanic events and the distribution of hydrothermal venting at the Lucky Strike hydrothermal field, Mid-Atlantic Ridge. Geochemistry, Geophysics, Geosystems 10(2). doi:10.1029/ 2008GC002171.

Parson, L., Murton, B.J., Searle, R.C., Booth, D., Evans, J., Field, P., Keeton, J., Laughton, A., McAllister, E., Millard, N., Redbourne, L., Rouse, I., Shor, A., Smith, D., Spencer, S., Summerhayes, C.

*This project has been supported by the European Union's Horizon 2020 research and innovation programme, GeoERA (Grant Agreement № 731166, project GeoE.171.001).*

& Walker, C. 1993. En echelon axial volcanic ridges at the Reykjanes Ridge; a life cycle of volcanism and tectonics. Earth and Planetary Science Letters 117, 73-87.

Parson, L., Grácia, E., Coller, D., German, C., Needham, D., 2000. Second-order segmentation; the relationship between volcanism and tectonism at the MAR, 38°N–35°40'N. Earth and Planetary Science Letters 178, 231–251.

Pedersen, R.B., Thorseth, I.H., Nygård, T.E., Lilley, M.D., Kelley, D.S. 2010. Hydrothermal Activity at the Arctic Mid-Ocean Ridges. In: Peter A. Rona (Ed.) Diversity of Hydrothermal Systems on Slow Spreading Ocean Ridges. Geophysical Monograph Series 188, 67-89. 10.1029/2008GM000783

Pedersen, R.B., Rapp, H.T., Thorseth, I.H., Lilley, M.D., Barriga, F.J.A.S., Baumberger, T., Flesland, K., Fonseca, R., Früh-Green, G.L., Jorgensen, S.L. 2010b. Discovery of a black smoker vent field and vent fauna at the Arctic Mid-Ocean Ridge. Nature Communications 1:126. DOI: 10.1038/ncomms1124

Pedersen, R.B., Bjerkgård, T. 2016. Sea-floor massive sulphides in Arctic Waters. In: Boyd et al. (Eds.) Mineral Resources in the Arctic, Geological Survey of Norway, 208-215. https://www.ngu.no/upload/Aktuelt/CircumArtic/Mineral_Resources_Arctic_Mainbook.pdf

Petersen, S., Krätschell, A., Augustin, N., Jamieson, J., Hein, J.R., Hannington, M.D. 2016. News from the seabed – Geological characteristics and resource potential of deep-sea mineral resources. Marine Policy 70, 175–187. http://dx.doi.org/10.1016/j.marpol.2016.03.012

Petersen, S., Lehrmann, B., Murton, B.J. 2018. Modern Seafloor Hydrothermal Systems: New Perspectives on Ancient Ore-Forming Processes. Elements 14, 307–312. DOI:10.2138/gselements.14.5.307

Rajasabapathy, R., Mohandass, C., Colaco, A., Dastager, S., Santos, R., Meena, R. 2014. Culturable bacterial phylogeny from a shallow water hydrothermal vent of Espalamaca (Faial, Azores) reveals a variety of novel taxa. Current science. 106. 58-69.

Ridley, W.I., Watkins, N.D. & MacFarlane, D.J. 1974. The Ocean basins and margins; Vol. 2, The North Atlantic. Plenum Press, New York, 483 pp.

Rona, P.A., Bostrom, K., Epstein, S. 1980. Hydrothermal quartz vug from the Mid-Atlantic Ridge. Geology 8(12), 569–572. doi:10.1130/0091-7613(1980)8<569:HQVFTM>2.0.CO;2.

Rona, P. A. 1984. Hydrothermal mineralization at seafloor spreading centers. Earth Science Reviews 20(1), 1–104. doi: 10.1016/0012-8252(84)90080-1.

Rona, P.A., Thompson, G., Mottl, M.J., Karson, J.A., Jenkins, W.J., Graham, D., Mallette, M., Von Damm, K., Edmond, J.M. 1984. Hydrothermal activity at the trans-atlantic geotraverse hydrothermal field, Mid-Atlantic Ridge crest at 26°N. Journal Geophysical Research 89, 11365–11377.

Rona, P.A., Hannington, M.D., Raman, C.V., Thompson, G., Tivey, M.K., Humphris, S.E., Lalou, C., Petersen, S. 1993. Active and relict sea-floor hydrothermal mineralization at the TAG hydrothermal field, Mid-Atlantic Ridge. Economic Geology 88, 1989–2017.

*This project has been supported by the European Union's Horizon 2020 research and innovation programme, GeoERA (Grant Agreement Nº 731166, project GeoE.171.001).*

Rouxel, O., Fouquet, Y., Ludden, J. N. 2004. Subsurface processes at the Lucky Strike hydrothermal field, Mid-Atlantic Ridge: Evidence from sulfur, selenium, and iron isotopes. Geochimica et Cosmochimica Acta, 68, 2295–2311.

Scheirer, D.S., Fornari, D.J., Humphris, S.E., Lerner, S. 2000. High-resolution seafloor mapping using the DSL-120 sonar system: Quantitative assessment of sidescan and phase-bathymetry data from the Lucky Strike segment of the Mid-Atlantic Ridge. Marine Geophysical Researches 21(1–2), 121–142. doi: 10.1023/a:1004701429848.

Schilling, J.-G. 1975. Azores mantle blob: rare earth evidence. Earth and Planetary Science Letters 25, 103–115.

Schilling, J.-G. 1985. Upper mantle heterogeneities and dynamics. Nature 314, 62–67.

Schilling, J.-G., Zajac, M.R., Evans, Johnston, T., White, W., Devine, J.D. & Kingsley, R.H. 1983. Petrologic and geochemical variations along the Mid-Atlantic Ridge from 29ºN to 73ºN. American Journal of Science 283, 510–586.

Searle, R. 1980. Tectonic pattern of the Azores spreading centre and triple junction, Earth and Planetary Science Letters 51, 415-434.

Searle, R.C., Murton, B.J., Achenbach, K., LeBas, T., Tivey, M., Yeo, I., Cormier, M.H., Carlut, J., Ferreira, P., Mallows, C., Morris, K., Schroth, N., van Calsteren, P., Waters, C. 2010. Structure and development of an axial volcanic ridge: Mid-Atlantic Ridge, 45°N, Earth Planet. Sciences Letters 299(1–2), 228–241.

Sempéré, J.C., Brown, H.S., Lin, J., Schouten, H. & Purdy, G.M. 1993. Segmentation and morphotectonic variations along a slow-spreading center: The Mid-Atlantic Ridge (24°N and 30°4N). Marine Geophysical Research 15, 153–200.

Singer D.A. 1995. World class base and precious metal deposits—a quantitative analysis. Economic Geology 90, 88–104

Singer, D.A. 2014. Base and precious metal resources in seafloor massive sulfide deposits. Ore Geology Reviews 59, 66–72. http://dx.doi.org/10.1016/j.oregeorev.2013.11.008

Singh, S.C., Crawford, W.C., Carton, H., Seher, T., Combier, V., Cannat, M., Miranda, J.M. 2006. Discovery of a magma chamber and faults beneath a Mid-Atlantic Ridge hydrothermal field. Nature 442, 1029–1032. doi: 10.1038/nature05105.

Somoza, L., Vázquez, J.T., Campos, A., Afonso, A., Calado, A., Fernández Puga, M.C., González Sanz, F.J., Fernández-Salas, L.M., Ferreira, M., Sanchez Guillamón, O., López Pamo, E., Lourenço, N., Luque Gómez, V., Mamouni, A., Medialdea, T., Madureira, P., Palomino, D., Rincón Tomás, B., Roque, C., Santos Bettencourt, R.P., Toyos Simón, M. 2014. Informe Científico-Técnico Campaña SUBVENT-2 (CGL2012-39524-C02). http://info.igme.es /SidPDF/166000/941/166941_0000001.pdf

Somoza, L., González, F.J., Barker, S.J., Madureira, P., Medialdea, T., de Ignacio, C., Lourenço, N., León, R., Vázquez, J.T., Palomino, D. 2017. Evolution of submarine eruptive activity during the 2011-2012 El Hierro event as documented by hydroacoustic images and remotely operated vehicle

*This project has been supported by the European Union's Horizon 2020 research and innovation programme, GeoERA (Grant Agreement Nº 731166, project GeoE.171.001).*

observations. Geochem. Geophys. Geosyst. 18, 3109–3137. https://doi.org /10.1002/2016GC006733.

Somoza, L., Medialdea, T., González, F.J., Calado, A., Afonso, A., Albuquerque, M., Asensio-Ramos, M., Bettencourt, R., Blasco, I., Candón, J.A., Carreiro-Silva, M., Cid, C., De Ignacio, C., López-Pamo, E., Machancoses, S., Ramos, B., Ribeiro, L.P., Rincón-Tomás, B., Santofimia, E., Souto, M., Tojeira, I., Viegas, C., Madureira, P. 2020. Multidisciplinary Scientific Cruise to the Northern Mid-Atlantic Ridge and Azores Archipelago. Front. Mar. Sci. 7:568035, DOI: 10.3389/fmars.2020.568035

Somoza, L., Medialdea, T., González, F.J., Machancoses, S., Candón, J.A., Cid, C., Calado, A., Afonso, A., Pinto Ribeiro, L., Blasco, I., Albuquerque, M., Asensio-Ramos, M., Bettencourt, R., de Ignacio, C., López-Pamo, E., Ramos, B., Rincón-Tomás, B., Santofimia, E., Souto, M., Tojeira, I., Viegas, C., Madureira, P. 2021. High-resolution multibeam bathymetry of the northern Mid-Atlantic Ridge at 45–46° N: the Moytirra hydrothermal field, Journal of Maps, 17:2, 184-196, DOI: 10.1080/17445647.2021.1898485

Stakes, D.S., Shervais, J.W., & Hopson, C.A. 1984. Volcanic-tectonic cycle of the FAMOUS and AMAR valleys, MAR (36º 47'): evidence from basalt glass and phenocryst compositional variations for steady state magma chamber beneath the valley midsections, AMAR 3. Journal of Geophysical Research, 89(B8), 6995–7028. doi: 10.1029/JB089iB08p06995.Snook, B., Drivenes, K., Rollinson, G.K., Aasly, K. 2018. Characterisation of Mineralised Material from the Loki's Castle Hydrothermal Vent on the Mohn's Ridge. Minerals 8, 576; doi:10.3390/min8120576

Stensland, A., Baumbergera, T., Mork, K.A., Lilleye, M.D., Thorseth, I.H., Pedersen, R.B. 2019. 3He along the ultraslow spreading AMOR in the Norwegian-Greenland Seas. Deep Sea Research Part I 147, 1-11. https://doi.org/10.1016/j.dsr.2019.04.004

Tivey, M.A., Dyment, J. 2013. The Magnetic Signature of Hydrothermal Systems in Slow Spreading Environments. In Diversity of Hydrothermal Systems on Slow Spreading Ocean Ridges (pp. 43–66). Wiley. doi:10.1029/2008GM000773.

Toffolo, L., Nimis, P., Tret'yakov, G.A., Melekestseva, I.Y., Beltenev, V.E. 2019. Seafloor massive sulfides from mid-ocean ridges: Exploring the causes of their geochemical variability with multivariate analysis. Earth Science Reviews 201, 102958. https://doi.org/10.1016/j.earscirev.2019.102958

van den Bogaard, P., 2013. The origin of the Canary Island Seamount Province — New Ages of Old Seamounts. Scientific Reports. 3:p. 2107. http://dx.doi.org/10.1038/srep02107. http://www.nature.com/articles/srep02107#supplementary-information

Varnavas, S.P., Papaioannou, J., Catani, J. 1988. A hydrothermal manganese deposit from the Eratosthenes Seamount, Eastern Mediterranean Sea. Marine Geology, 81, 205–214. doi:10.1016/0025-3227(88)90027-8.

Wheeler, A. J., Murton, B., Copley, J., Lim, A., Carlsson, J., Collins, P., et al. 2013. Moytirra: discovery of the first known deep-sea hydrothermal vent field on the slow-spreading Mid-Atlantic Ridge north of the Azores. Geochemistry, Geophysics, Geosystems 14, 4170–4184. doi: 10.1002/ggge.20243.

White, S.N., Humphris, S.E., Kleinrock, M.C., 1998. New observations on the distribution of past and present hydrothermal activity in the TAG area of the Mid-Atlantic Ridge (26°08'N). Marine Geophysical Research 20, 41–56.

*This project has been supported by the European Union's Horizon 2020 research and innovation programme, GeoERA (Grant Agreement № 731166, project GeoE.171.001).*

Wilson, C., Charlou, J.L., Ludford, E., Klinkhammer, G., Chin, C., Bougault, H., German, C., Speer, K., Palmer, M. 1996. Hydrothermal anomalies in the Lucky Strike segment (37º17'N). Earth and Planetary Science Letters 142, 467-477.

Yeo, I.A.L., R.C. Searle, K.L. Achenbach, T.P. Le Bas, Murton, B. 2012. Eruptive hummocks: Building blocks of upper-oceanic crust. Geology 40, 91–94.

Yeo, I.A., Devey, C.W., LeBas, T.P., Augustina, N., Steinführer, A. 2016. Segment-scale volcanic episodicity: Evidence from the North Kolbeinsey Ridge, Atlantic. Earth and Planetary Science Letters 439, 81-87. http://dx.doi.org/10.1016/j.epsl.2016.01.029

Zhang, Y.-S. & Tanimoto, T. 1992. Ridges, hotspots and their inter-action as observed in seismic velocity maps. Nature 355, 45–49.

Zillig, W., Holz, I., Janekovic, D., Klenk, H.-P., Imsel, E., Trent, J., Wunderl, S., Forjaz, V.H., Coutinho, R.M., Ferreira, T. 1990. Hyperthermus butylicus, a Hyperthermophilic Sulfur- reducing Archaebacterium that ferments peptides. Journal of Bacteriology, 172:7:3959-3965.

# 9. APPENDICES

## Summary of occurrences; hydrothermal deposits

| Marine sector | Number of occurrences | Commodity | Principal mineralogy | Genetic model |
|---|---|---|---|---|
| Arctic Ocean | 61 | copper; zinc; gold; silver; lead; cobalt; barite | sulphides; sulphates | mafic volcanism |
| North (Mid) Atlantic Ocean | 42 | copper; zinc; gold; silver; lead; cobalt; barite | Sulphides; sulphates | mafic volcanism |
| Canary Island Seamount Province | 6 | barite; zinc; iron | sulphides; sulphates; oxyhydroxides | Mafic volcanism |
| Iberian Abyssal Plane | 1 | iron; manganese | Fe-Mn oxyhydroxides | Mafic volcanism |
| Tyrrhenian Sea | 17 | iron; manganese | sulphides; sulphates; Fe-Mn oxyhydroxides | bimodal and felsic volcanism |
| Aegean Sea | 25 | lead; zinc; iron; manganese; barite | sulphides; sulphates; Fe-Mn oxyhydroxides | bimodal and felsic volcanism |
| Cyprus Basin | 1 | iron; manganese | Fe-Mn oxyhydroxides | mafic volcanism |

*This project has been supported by the European Union's Horizon 2020 research and innovation programme, GeoERA (Grant Agreement Nº 731166, project GeoE.171.001).*

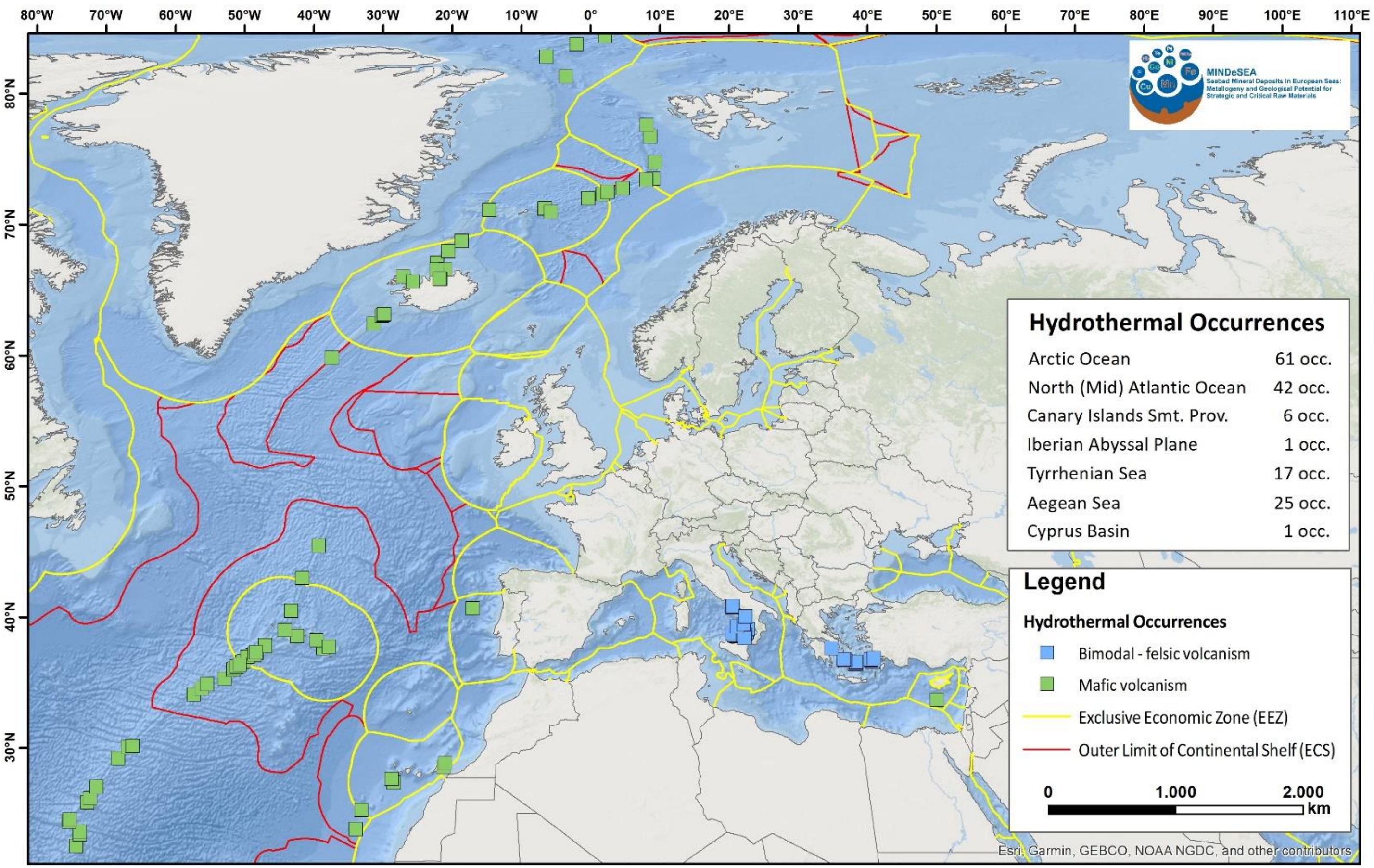



EEZ limits based on: Flanders Marine Institute (2019). Maritime Boundaries and Exclusive Economic Zone (200NM), version 11.
ECF limits based on: http://continentalshelf.org/onestopdatashop/630.aspx

**Pan-European map of seabed hydrothermal occurrences. MINDeSEA dataset and cartography compilation.**

*This project has been supported by the European Union's Horizon 2020 research and innovation programme, GeoERA (Grant Agreement № 731166, project GeoE.171.001).*

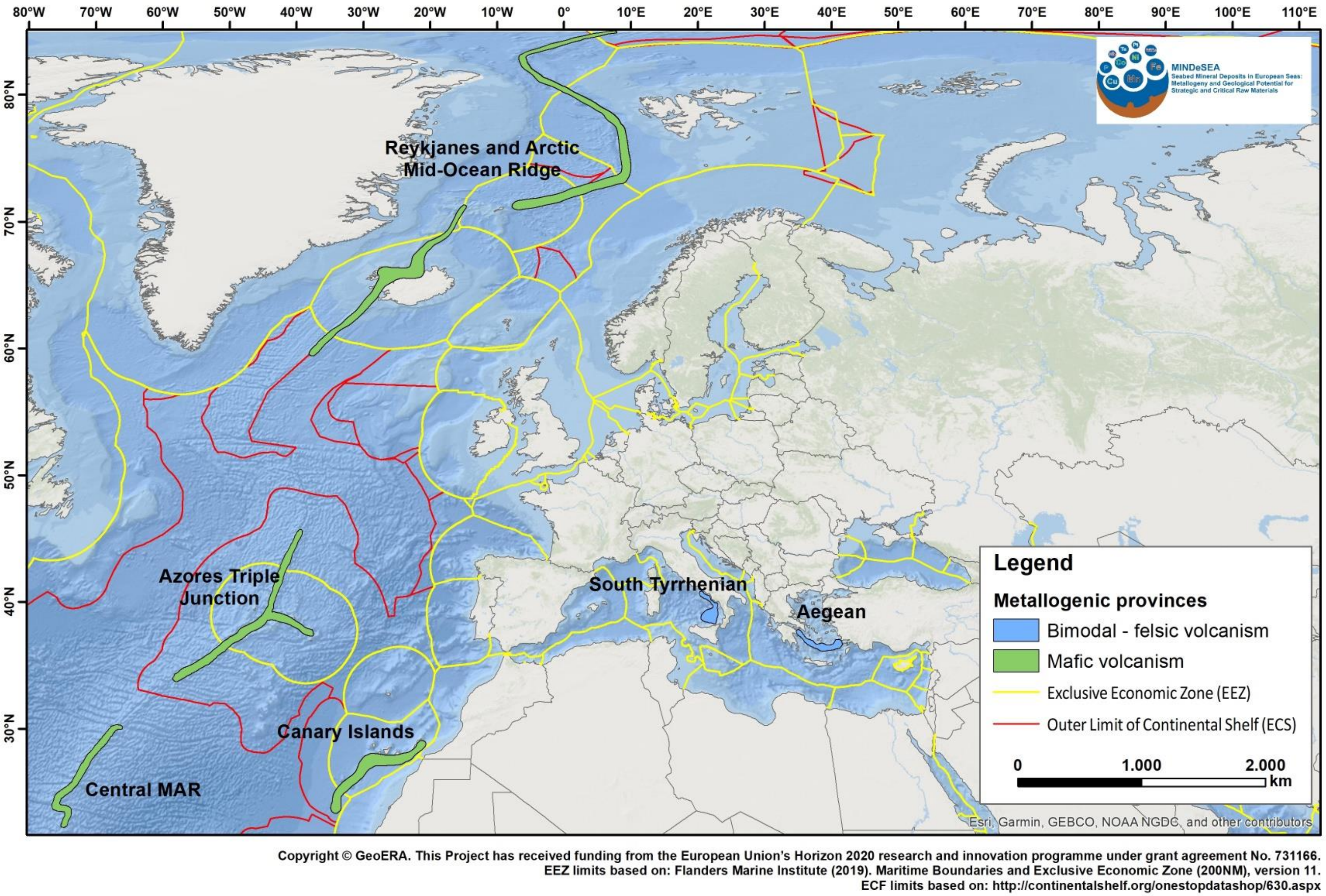


**Metallogenic provinces for hydrothermal deposits defined in pan-European seas.**

*This project has been supported by the European Union's Horizon 2020 research and innovation programme, GeoERA (Grant Agreement Nº 731166, project GeoE.171.001).*